Development and Characterisation of Polyhydroxybutyrate from Selected Bacterial Species

By Soroosh Bagheriasl, MRes.

A thesis submitted to the University of Birmingham
for the degree of

DOCTOR OF PHILOSOPHY

SCHOOL OF METALLURGY AND MATERIALS

UNIVERSITY OF BIRMINGHAM

October 2012

Abstract

Polyhydroxyalkanoates (PHAs) are biodegradable, linear polyesters produced primarily by bacterial fermentation. PHAs have been found to possess similar properties to many non-biodegradable petrochemical plastics. The current cost of PHA production is far greater in comparison to petrochemical plastics. Recent research has focused on developing cost effective production of PHAs from various strains of bacteria. In this study *Serratia* sp. NCIMB 40259 and *R. eutropha* H16 were utilised for the accumulation of Polyhydroxybutyrate (PHB).

Serratia sp. with high phosphatase activity (HPA) or low phosphatase activity (LPA) were fermented for 48, 120, 216 and 320 h and dosed daily with stock solutions in order to accumulate intracellular PHB and biomineralise hydroxyapatite (HA) on the cell surface.

The optimum conditions for the accumulation of PHB, in this study, were found to be 216 h fermentation, producing a PHB yield of 14.6 %w/w and 3.3 %w/w for LPA and HPA respectively. The accumulation of PHB by S*erratia* sp. was found to be directly dependant on the fermentation time. The overall average yields of PHB from LPA *Serratia* cells were consistently higher than that from HPA cells. Phosphatase activity was observed to have an indirect effect on the accumulation of PHB. The molecular and thermal properties of PHB were analysed by means of Fourier Transform Infrared Spectroscopy (FTIR), Differential Scanning Calorimetry (DSC) and Gel Permeation Chromatography (GPC) and were observed to be largely unaffected by the phosphatase activity of the cells and appeared to be dependent on the fermentation period.

A correlation was observed between the fermentation periods, Molecular Weight (M_w) and Polydispersity (PD). GPC analysis of PHB from HPA and LPA *Serratia* sp. showed similar M_w and PD values over the range of fermentation periods. The breadth of the melting

endothermic peaks for PHB from LPA and HPA showed the same pattern of peak broadening with increasing fermentation time. This was attributed to the increase in PD and the presence of smaller polymer chain lengths that reach complete melt at varying temperatures. The % crystallinity of PHB from HPA and LPA were highest after 216 h fermentation and correlated with the peak intensities of the endothermic melting peak of the DSC traces. The % crystallinity was in the expected region for PHB.

The mineralisation of HA was observed to be dependent on the fermentation period and phosphatase activity of the cells. A longer fermentation period yielded greater mineralisation of HA. The fermentations of LPA cells showed an initial decrease in HA mineralisation, while fermentations of HPA cells yielded the highest overall average yields of HA. The production of HA alongside PHB by *Serratia* sp. makes the process more economically viable. In order to make the process a viable option for the production of PHB, optimisation of the fermentation conditions for the accumulation of PHB is necessary, whilst still maintaining high yields of HA mineralisation. Th

R. eutropha cells were fermented with the substrates olive oil and rapeseed oil and compared with glucose. Small scale fermentations using 20 g/l of oils (rapeseed or olive) and glucose, as carbon sources, were conducted. The use of either olive oil or rapeseed oil as carbon sources resulted in the greatest accumulation of PHB at 36 %w/v compared to 12 %w/v from glucose. The thermal and molecular properties of PHB from the various carbon sources were analysed by means of FTIR, DSC and GPC, and were found to be almost identical.

The diameter of the electrospun nanofibres for PHB obtained from glucose (G-PHB), Olive oil (O-PHB) and Rapeseed oil (R-PHB) were found to be similar. This study shows that the source of carbon used did not have a significant effect on the diameters of electrospun nanofibres, this was attributed to the similar M_w properties of each carbon source. The

electrospun fibres of G-PHB, O-PHB and R-PHB were found to have diameters dependant on their solution concentrations. Lower solution concentrations resulted in smaller diameter fibres.

The use of oils in the production of PHB would make a viable replacement for the use of sugars as substrates. It has been suggested that rapeseed oil is a low cost alternative to other conventional oils and in this study rapeseed oil resulted in an almost identical yield of PHB compared with the more costly olive oil.

By adjusting the electrospinning parameters it may be possible to control the crystallinity and the diameters the PHB fibres. Controlling the crystallinity and fibre diameters of PHB electrospun PHB is essential if they are to be used in biomedical applications.

Acknowledgments

It has been a great experience and honour to have carried out this project at The University of Birmingham. I would like to express my sincere thanks and appreciation to my supervisor, Dr Artemis Stamboulis, for all her inspirational mentorship throughout, from my initial Masters through to the completion of this project. I would also like to extend my gratitude to Dr Mike Jenkins, for his willingness to offer guidance and support.

I would also like to give special thanks to Dr Iza Radecka, from the University of Wolverhampton. She was always willing to provide me with much appreciated guidance, and of course PHB, throughout the project. Additionally, I would like to thank Victor Irorere who contributed much of his time in assisting with the fermentation experiments.

I would like to thank my colleagues within the biomaterials group. The steady friendship and support that they offered, has helped make my time at the University of Birmingham rewarding and memorable. In particular, I would like to thank Mark Blevins, without him the art of electrospinning may well have remained a mystery to me.

By the same token, my family deserve equal accolade. The unwavering encouragement and reassurance that they provided has been integral in my completion of this degree. My amazing girlfriend has always managed to lift my spirit when I was down and I don’t think I would have finished this work without her constant support.

Contents

List of Figures iv
List of Tables viii
Abbreviations x

Chapter 1 : Introduction and Literature Review 1

1.1. Introduction 2
1.2. Waste problems associated with the use of synthetic plastics 3
1.3. Polyhydroxyalkanoates (PHAs) 4
1.4. Physical, mechanical and chemical properties of poly-hydroxy-alkanoates 7
1.4.1. Chemical Structure of PHAs 7
1.4.2. The physical and mechanical properties of PHAs 10
1.4.3. Thermal properties of poly-hydroxy-alkanoates 13
1.4.4. Biodegradability of poly-hydroxy-alkanoates 14
1.4.5. Biocompatibility of poly-hydroxy-alkanoates 16
1.5. Bacteria producing Poly-hydroxy-alkanoates 16
1.5.1. Ralstonia eutropha 18
1.5.2. Serratia sp. 19
1.6. Inclusion body formation 21
1.7. Bacterial synthesis pathway 22
1.8. Applications of Bioplastics 25
1.8.1. Advancements in the bioplastics market 25
1.8.2. Applications of bacterially produced Poly-hydroxy-alkanoates 28
1.9. Bacterially Produced Hydroxyapatite 32
1.9.1. Properties of Hydroxyapatite 33
1.9.2. Structural Characterisation of HA 34
1.9.3. Applications of HA 35
1.10. Aims and Objectives- Justification of work undertaken 38

Chapter 2 : Materials and Methods 42

2.1. Preparation of Serratia cells for the production of PHB and HA 43
2.1.1. Growth of Serratia sp. NCIMB 40259 43
2.1.2. Assay of phosphatase activity 44
2.1.3. Preparation of Serratia sp. for the accumulation of PHB and HA 45
2.1.4. Dosing solutions and volumes for the production of PHB and HA 45
2.2. Fermentation experiments using HPA and LPA Serratia sp. 46
2.2.1. Serratia sp. fermented for 48 h 48
2.2.2. Serratia sp. fermented for 120 h 49
2.2.3. Serratia sp. fermented for 216 h 50
2.2.4. Serratia sp. fermented for 360 h 51

2.3. Preparation of Ralstonia eutropha for the production of PHB 52
2.3.1. Chemicals 52
2.3.2. R. eutropha H16 (NCIMB 10442, ATCC 17699) 52
2.3.3. Media Preparation 52
2.3.4. Carbon Sources 53
2.3.5. Starter culture preparation 53
2.3.6. Fermentations 54
2.3.7. Bacterial Growth 54
2.4. Extraction 55
2.4.1. Extraction of PHB and HA from Serratia sp. 55
2.4.2. Extraction of PHB from R. eutropha 57
2.5. Electrospinning 57
2.5.1. Electrospinning apparatus 57
2.5.2. Processing parameters 59
2.5.3. Experimental protocol 59
2.5.4. Preparation of PHB solutions 60
2.6. Characterisation techniques 60
2.6.1. Fourier transform infrared spectroscopy (FTIR) 60
2.6.2. Differential scanning calorimetry (DSC) 61
2.6.3. Gel permeation chromatography (GPC) 62
2.6.4. Scanning electron microscopy (SEM) 63
2.6.5. Transmission electron microscopy (TEM) 63
2.7. Statistical analysis 66
Chapter 3 : Results and Discussion 68
3.1. Introduction 69
3.2. Experiments with HPA and LPA Serratia sp 69
3.2.1. Recovered yields of PHB and HA after 48 h fermentation 69
3.2.2. Recovered yields of PHB and HA after 120 h fermentation 71
3.2.3. Recovered yields of PHB and HA after 216 h fermentation 73
3.2.4. Recovered yields of PHB and HA after 360 h fermentation 74
3.3. Comparison and discussion of the overall average yields of HA from LPA and HPA Serratia sp. 76
3.4. Comparison of overall mean yields of PHB from LPA and HPA cells 79
3.5. Characterisation of PHB extracted from Serratia sp. 82
3.5.1. Gel Permeation Chromatography 82
3.5.2. FTIR 103
3.6. Characterisation of HA extracted from Serratia sp. 106
3.6.1. FTIR 106

3.6.2. X-ray Diffraction 109
3.7. Optical analysis of Serratia sp. during fermentation 111
3.7.1. SEM 111
3.7.2. Transmission electron microscopy 117
Chapter 4 : Results and Discussion 123
4.1. Introduction 124
4.2. Growth of R. eutropha H16 125
4.3. Yields of PHB produced from R. eutropha 126
4.4. Morphologies of PHB Fibres 129
4.4.1. Morphology of G-PHB nanofibres 129
4.4.2. Morphology of O-PHB nanofibres 133
4.4.3. Morphology of R-PHB nanofibres 135
4.5. Characterisation of PHB from R. eutropha 141
4.5.1. GPC 141
4.5.2. DSC of Electrospun and non-electrospun PHB 142
4.5.3. FTIR 152
Chapter 5 :Conclusions 158
5.1. The production of PHB and HA from Serratia sp. 159
5.2. Development and characterisation of electrospun fibres of PHB from various carbon source synthesised from R eutropha. 163
6. Future work **165**
7. Curriculum Vitae **167**
8. References **168**
Appendix **191**

List of Figures

Figure 1: The structure of Poly-(3)-hydroxyalkanoates. 8
Figure 2: Monomers of PHB and PHV combined to form the co-polymer PHBV [44]. 10
Figure 3: Six membrane ring demonstrating the thermal degradation of PHB [64] 14
Figure 4: An illustration of the time taken for biodegradable plastic to degrade [77]. 15
Figure 5: (A) Environmental scanning Electron Microscopy (ESEM) images of *Serratia* cells with EPS visible on the surface [77]. (**B)** *Serratia* cells viewed under scanning electron microscope (scale 2 µm)[3] 20
Figure 6: Metabolic pathways for PHA synthesis [7] 21
Figure 7: Bacterial synthesis of PHB [64] 23
Figure 8: Cyclic biosynthesis and degradation of PHB [124] 24
Figure 9: Mechanism of HA formation on the surface of *Serratia* sp. 25
Figure 10: Biodegradable ballpoint pen produced by PaperMate [130]. 26
Figure 11: Coca Cola plant bottle launched in 2009 [131]. 27
Figure 12: Thinning of a polymer jet in the electric field during a typical electrospinning experiment [160]. 31
Figure 13: ESEM image of HA forming on surface of *Serratia* sp [77]. 33
Figure 14: The schematic diagram for the hexagonal structure of HA crystals [180]. 34
Figure 15: Projection of monoclinic HA on (001) plane. Small white balls phosphorus, grey balls= oxygen, white balls= hydroxyl oxygen, Light Grey= calcium [181]. 35
Figure 16: Air lift fermenter (2.5 L). 44
Figure 17: Wet biomass left to dry on a pre-weighed watch glass. 56
Figure 18: Electrospinning apparatus set up within a fume cupboard. 58
Figure 19: Resin Block with face trimmed to a trapezium. 65
Figure 20: The edge of the glass knife was placed parallel to the bottom edge of the block face in order to obtain ultra-thin sections. 66
Figure 21: Bar chart accompanied with standard error values for the overall average yields of HA recovered from HPA and LPA cells after 48, 120, 216 and 360 h fermentations. Level of significance: one star (*) for 0.05, two (**) for 0.01, and three (***) for 0.001 or 0.005. 76
Figure 22: Bar chart accompanied with standard error values for the overall average yields of PHB recovered from HPA and LPA cells after 48, 120, 216 and 360 h fermentations. Level of significance: one star (*) for 0.05, two (**) for 0.01, and three (***) for 0.001 or 0.005. 79
Figure 23: DSC scan demonstrating the heating and cooling trace for a powder sample of commercial PHB (Sigma-Aldrich Ltd., UK). 87
Figure 24: DSC traces for the heating of PHB samples from HPA *Serratia* sp. after fermentations of (A) 48 h, (B) 120 h (C) 216 h and (D) 360 h time periods. 88
Figure 25: Line chart representing the onset of melting against M_w for PHB from HPA *Serratia* sp. fermented for 48, 120, 216 and 360 h. 89

Figure 26: Line chart representing the onset of melting against PD for PHB from HPA *Serratia* sp. fermented for 48, 120, 216 and 360 h. 89
Figure 27: Line chart representing the breadth of the melting endothermic peaks against the PD for PHB from HPA *Serratia* sp. fermented for 48, 120, 216 and 360 h. 90
Figure 28: Line chart representing the peak intensities against the % crystallinity for PHB from HPA *Serratia* sp. fermented for 48, 120, 216 and 360 h. The peak intensities (mW) is used as a measure of polymer crystallinity. 91
Figure 29: DSC traces for the cooling of PHB samples from HPA *Serratia* sp. after fermented for various time periods (A) 48 h, (B) 120 h (C) 216 h and (D) 360 h. 93
Figure 30: Line graph representing the T_m and T_c against the M_w for PHB from HPA *Serratia* sp. fermented for 48, 120, 216 and 360 h. 94
Figure 31: DSC traces for heating of PHB samples from LPA *Serratia* sp. after fermentations of (A) 48 h, (B) 120 h (C) 216 h and (D) 360 h time periods. 95
Figure 32: Line chart representing the onset of melting against M_w for PHB from LPA *Serratia* sp. fermented for 48, 120, 216 and 360 h. 96
Figure 33: Line chart representing the onset of melting against PD for PHB from LPA *Serratia* sp. fermented for 48, 120, 216 and 360 h. 96
Figure 34: Line chart representing the breadth of the endothermic melting peaks against PD values for PHB from LPA *Serratia* sp. fermented for 48, 120, 216 and 360 h. 97
Figure 35: Line chart representing the peak intensities and % crystallinity for PHB from LPA *Serratia* sp. against fermentation time. The peak intensities (mW) is used as a measure of polymer crystallinity. 98
Figure 36: DSC traces for the cooling of PHB from LPA *Serratia* sp. after fermentations of (A) 48 h, (B) 120 h (C) 216 h and (D) 360 h. 100
Figure 37: Line chart representing the T_m and T_c against the M_w for PHB from LPA *Serratia* sp. fermented for 48, 120, 216 and 360 h. 100
Figure 38: FTIR spectra of PHB extracted from HPA and LPA *Serratia* sp. after 216 h of fermentation compared to the spectrum of commercial PHB. 103
Figure 39: Line chart demonstrating the correlation between the % crystallinity obtained from DSC traces and the CI obtained from the FTIR spectra. 106
Figure 40: FTIR spectra of HA from HPA *Serratia* sp. fermented for 216 h time period. 107
Figure 41: XRD pattern for commercial HA and *Serratia* HA from HPA cells. 110
Figure 42: SEM images of *Serratia* cells with HA mineralisation on the cell surface after 48 h fermentation (a) HPA *Serratia* cells (b) HA formation on LPA cell. 111
Figure 43: SEM images of *Serratia* cells with HA mineralisation on the cell surface after 120 h fermentation (a) HPA *Serratia* sp. (b) LPA *Serratia* sp, black arrows indicate areas of HA mineralisation. 113
Figure 44: SEM images of *Serratia* cells with HA mineralisation on the cell surface after 216 h fermentation (a) HPA *Serratia* cells (b) LPA *Serratia* cells, black arrows indicate areas of high HA mineralisation. 114

Figure 45: SEM images of *Serratia* sp. with HA mineralisation occurring on the cell surface after 360 h fermentation (a) HPA *Serratia* sp. (b) LPA *Serratia* cells. 115
Figure 46: SEM images of HPA *Serratia* sp. with HA mineralisation occurring on the cell surface after 360 h fermentation. 116
Figure 47: TEM images of inclusion bodies accumulated within the cells after 48 h fermentation. (a) LPA *Serratia* sp. (b) HPA *Serratia* sp. 118
Figure 48: TEM images of inclusion bodies developed within the cells after 120 h fermentation. (a) LPA *Serratia* cells (b) HPA *Serratia* cell. 119
Figure 49: TEM images of inclusion bodies developed within the cells after 216 h fermentation. (a) LPA *Serratia* cells showing PHB inclusion bodies (b) HPA *Serratia* cells showing PHB inclusions. 120
Figure 50: TEM images of inclusion bodies developed within the cells after 360 h fermentation. (a) LPA *Serratia* cells (b) HPA *Serratia* cells. 121
Figure 51: Growth curve of *R. eutropha* NCMBI 10442 grown in BSM at 30 °C using glucose, olive oil and rapeseed oil as the carbon sources. 126
Figure 52: SEM images alongside respective histograms demonstrating the effect of G-PHB solution concentration on the morphology and the fibre diameter distribution of electrospun fibres. (1a) Solution concentration of 1.5 %w/v. (1b) Solution concentration of 2 %w/v. (1c) Solution concentration of 2.5 %w/v. 131
Figure 53: Bar chart of the average fibre diameters for the electrospun samples of G-PHB at solution concentrations of 1.5, 2 and 2.5 %w/v. The values are accompanied by their respective error bars. Level of significance: Three (***) for 0.001 or 0.005. 132
Figure 54: SEM images alongside respective histograms demonstrating the effect of O-PHB solution concentration on the morphology and the fibre diameter distribution of electrospun fibres (2a) Solution concentration of 1.5 %w/v. (2b) Solution concentration of 2 %w/v. (2c) Solution concentration of 2.5 %w/v. 134
Figure 55: Bar chart of the average fibre diameters for electrospun sample of O-PHB at solution concentrations of 1.5, 2 and 2.5 %w/v. The values are accompanied by their respective error bars. Level of significance: Three (***) for 0.001 or 0.005 135
Figure 56: SEM images alongside respective histograms demonstrating the effect of R-PHB solution concentration on the morphology and the fibre diameter distribution of electrospun fibres (3a) Solution concentration of 1.5 %w/v. (3b) Solution concentration of 2 %w/v. (3c) Solution concentration of 2.5 %w/v. 137
Figure 57: Bar chart of the average fibre diameters for electrospun sample of R-PHB at solution concentrations of 1.5, 2 and 2.5 %w/v. The values are accompanied by their respective error bars. 138

Figure 58: DSC trace for heating 2(a) and cooling 2(b) of electrospun and non-electrospun samples of G-PHB. 144
Figure 59: Bar chart representing the peak intensities against the % crystallinity for non-electrospun and electrospun samples of G-PHB. 146
Figure 60: DSC trace for heating 2(a) and cooling 2(b) of electrospun and non-electrospun samples of O-PHB. 147
Figure 61: Bar chart representing the peak intensities and % crystallinity for non-electrospun and electrospun samples of O-PHB. 148
Figure 62: DSC traces for heating 3(a) and cooling 3(b) of electrospun and non-electrospun samples of R-PHB. 150
Figure 63: Bar chart representing the peak intensities against the % crystallinity for non-electrospun and electrospun samples of R-PHB. 151
Figure 64: FTIR spectra of electrospun (2 %w/v) and non-electrospun G-PHB. 153
Figure 65: FTIR spectra of electrospun (2 %w/v) and non-electrospun O-PHB. 153
Figure 66: FTIR spectra of electrospun (2 %w/v) and non-electrospun R-PHB. 154
Figure 67: Histogram demonstrating the correlation between the % crystallinity obtaied from DSC traces and the CI obtained from the FTIR spectra of O-PHB, R-PHB and G-PHB (2 %w/v). 155

List of Tables

Table 1: Substrate cost per metric tonne (m.t.) of PHB production [27].....6
Table 2: The corresponding R-groups of PHAs. 8
Table 3: The physical and mechanical properties of PHB, PHV and PP [55].....12
Table 4: An overview of PHAs produced by various bacterial species and carbon sources. 17
Table 5: The quantity and concentrations of reagents required for the stock solutions**.** 46
Table 6: Concentration and volume of dosing solutions. 46
Table 7: Experiments conducted with HPA and LPA *Serratia* sp. at varying fermentation periods.....48
Table 8: Experimental conditions for the production of PHB and HA from HPA *Serratia* sp. fermented for 48 h. 49
Table 9: Experimental conditions for the production of PHB and HA from LPA *Serratia* sp. fermented for 48 h. 49
Table 10: Experimental conditions for the production of PHB and HA from HPA *Serratia* sp. fermented for 120 h. 50
Table 11: Experimental conditions for the production of PHB and HA from LPA *Serratia* sp. fermented for 120 h. 50
Table 12: Experimental conditions for the production of PHB and HA from HPA *Serratia* sp. fermented for 216 h. 50
Table 13: Experimental conditions for the production of PHB and HA from LPA *Serratia* sp fermented for 216 h. 51
Table 14: Experimental conditions for the production of PHB and HA from HPA *Serratia* sp fermented for 360 h. 51
Table 15: Experimental conditions for the production of PHB and HA from LPA *Serratia* sp fermented for 360 h. 51
Table 16: Types of fat contained in 100 ml of the different oils used as carbon sources for the production of PHB (data obtained from product information labels for the respective oil). 53
Table 17: Average yields of PHB and HA from HPA cells recovered after 48 h fermentation. 70
Table 18: Average yields of PHB and HA from LPA cells recovered after 48 h of fermentation 71
Table 19: Yields of PHB and HA from HPA cells recovered after 120 h fermentation. 72
Table 20: Yields of PHB and HA from LPA cells recovered after 120 h fermentation. 72
Table 21: Average yields of PHB and HA from HPA cells recovered after 216 h of fermentation. 73
Table 22: Average yields of PHB and HA from LPA cells recovered after 216 h fermentation. 74
Table 23: Average yields of PHB and HA recovered from HPA cells after 360 h of fermentation. 74

Table 24: Average yields of PHB and HA recovered from LPA cells after 360 h of fermentation. 75
Table 25: M_w, M_n and PD results for PHB from LPA *Serratia* sp. after various fermentations, the results for commercial PHB were obtained from Sigma-Aldrich. 83
Table 26: M_w, M_n and PD results for PHB from HPA *Serratia* sp. after various fermentations, the results for commercial PHB were obtained from Sigma-Aldrich. 84
Table 27: Thermal characterisation of commercial PHB compared to PHB from HPA *Serratia* sp. fermented for 48, 120, 216 and 360 h time periods. 88
Table 28: Thermal characterisation of commercial PHB compared with recovered PHB from LPA *Serratia* sp. fermented for: 48, 120, 216 and 360 h time periods. 95
Table 29: Description of the main FTIR peaks in the spectra of PHB from HPA and LPA *Serratia* sp. compared to that of commercial PHB. 104
Table 30: Description of the main FTIR peaks in the FTIR spectra of *Serratia* HA from HPA compared to that of commercial HA [190]. 108
Table 31: The CDW, average PHB (n=3) and the PHB produced (%w/w) from the different carbon sources after 48 h fermentation. 127
Table 32: The M_w, M_n and PD of electrospun and non-electrospun PHB from olive oil, rapeseed oil and glucose (M_w = weight average molecular weight, M_n = number average molecular weight and PD = Polydispersity. PD = M_w/M_n. 142
Table 33: Thermal properties of non-electrospurn PHB produced by *R. eutropha* grown in BSM at 30 ^oC and 150rpm using olive oil, rapeseed oil or glucose as sources of carbon. T_m = melting temperature and T_c = crystallisation temperature on cooling and C = crystallinity. 143
Table 34: Thermal properties of electrospurn fibres of G-PHB with solution concentrations of 1.5, 2 and 2.5 %, T_m = melting temperature and T_c = crystallisation temperature on cooling and C = cystallinity. 144
Table 35: Thermal properties of electrospurn fibres of O-PHB with solution concentrations of 1.5, 2 and 2.5 %w/v. T_m = melting temperature and T_c = crystallisation temperature on cooling and C = crystallinity. 147
Table 36: Thermal properties of electrospurn fibres of PHB from R-PHB with solution concentrations of 1.5, 2 and 2.5 %w/v. 149
Table 37: FT-IR peaks assignment of PHB. 152

Abbreviations

ATP	Adenosine Triphosphate
ATR	Attenuated Total Reflectance
BSM	Basal Salt Medium
C_6H_{14}	n-Hexane
$CaCL_2$	Calcium Chloride
$CHCl_3$	Chloroform
CH_2	Methylene
CH_3	Methyl
CI	Crystallinity Index
CoA	Coenzyme A
CPI	Citrobacter Phosphatase I
DC	Direct Current
Dnase	Deoxyribonuclease
DNA	Deoxyribonucleic Acid
DWC	Dry Weight of Cells
E.Coli	Escherichia Coli
ECM	Extracellular Matrix
EDS or EDX	Energy Dispersive X-ray Spectroscopy
EPS	Extracellular Polymeric Substance
ESEM	Environmental Scanning Electron Microscopy
FTIR	Fourier Transform Infrared Spectroscopy
GPC	Gel Permeation Chromatography
G2P	Glycerol 2 Phosphate
HA	Hydroxyapatite

HPA	High Phosphatase Activity
HPO_4^{2-}	Hydrogen Phosphate
LCL	Long Chain Length
LPA	Low Phosphatase Activity
Mn	Molecular Mass
mRNA	Messenger Ribonucleic Acid
$Na_3C_6H_5O_7$	Sodium Citrate
OD	Optical Density
O-PHB	PHB from Olive oil
PEG	Polyethylene Glycol
PHA	Polyhydroxyalkanoates
PHB or P3HB	Polyhydroxybutyrate
PHBV	poly (3-hydroxybutyrae-co-hydroxyvalerate)
PHD	Poly(3-hydroxydecanoate)
PHDD	Poly(3-hydroxydodecanoate)
PHN	Poly(3-hydroxynonanoate)
PHHx	Poly(3-hydroxypropionate)
PHH	Poly(3-hydroxyheptanoate)
PHO or P3HO	Polyhydroxyoctanoate
PHP	Poly(3-hydroxypropionate)
PHV	Poly(3-hydroxyvalerate)
PLA	Poly-Lactic Acid
PD	Polydispersity (M_w/M_n)
PP	Polypropylene
*p*NP	p-nitrophenol

*p*NPP	p-nitrophenol Phosphate
RI	Refractive Index
RNA	Ribonucleic Acid
rRNA	Ribosomal Ribonucleic Acid
RPM	Rotation s per Minute
SEM	Scanning Electron Microscope
SCL	Short Chain Length
Sp.	Species
TEM	Transmission Electron Microscopy
TSA	Tryptone Soya Agar
TSB	Tryptone Soya Broth
T_c	Crystallisation Temperature
T_g	Glass Transition Temperature
T_m	Melting Temperature
w/w	Weight by weight
w/v	Weight by volume

Chapter 1 : Introduction and Literature Review

1.1. *Introduction*

Environmental pollution by the disposal of synthetic polymers (i.e. conventional plastics) e.g Polypropylene (PP) is a growing problem. Since the 1940s plastics have been replacing glass, wood, metal and other constructional materials in numerous applications [1].

The use of plastics is widespread within our society, this is primarily due to the favourable thermal and mechanical properties of plastics making it a stable and durable material [1]. The extensive global use of plastics has contributed heavily to environmental pollution; as plastics are not always properly discarded or recycled and consequently persist within the environment. The manufacturing processes required to produce plastic also creates large quantities of chemical pollutants. In recent years there has been a shift in public opinion, with people becoming more ecologically aware. The shift in public opinion and political influence combined with the increasing price of oil, has driven industries to investigate biodegradable alternatives to plastic, which are not manufactured using petrochemical methods. Materials produced from synthetic polymers are widely used for a diverse range of applications in modern society. The production of biodegradable alternatives with greater compatibility in the environment is necessary if the applications continue to grow [2].

Bioplastics have been researched for many years as an alternative to synthetic plastics. Some of the major naturally occurring bioplastics are cellulose, starch, poly (lactic acid) and polyhydroxyalkanoates (PHAs). These materials hold further advantages over synthetic plastics as they are biodegradable and are produced from renewable sources. Unfortunately, in the past the high cost associated with the production of bioplastics compared to the low cost of synthetic polymers has resulted in a loss of interest in bioplastic research [3].

The production of PHAs by bacteria was discovered in 1926 by Lemoigne, who reported the formation of poly 3-hydroxybutyrate (PHB), a member of the PHA family, inside bacteria [3,

4]. This discovery encouraged new research aimed at investigating the production of PHAs produced entirely from bacterial fermentation, whilst also focusing on methods to reduce the cost of production. The cost can be reduced through the implementation of better recovery/purification methods and the use of low cost substrates such as waste oil [5-7].

1.2. *Waste problems associated with the use of synthetic plastics*

Three million tonnes of plastic waste is estimated to be generated annually within the UK [8]. An estimated 56 % of all plastics waste is used as packaging, three-quarters of which originates from households [8]. It is estimated that only 7 % of total plastic waste is currently being recycled [8]. The remaining un-recycled plastic accumulates within landfills sites and oceans [8]. The overall environmental impact varies according to the type of plastic and the production method employed.

Plastic production also involves the use of potentially harmful chemicals, added as stabilisers or colorants. Many of these chemicals have not undergone environmental risk assessment and their impact on human health and the environment is currently uncertain [8, 9].

Synthetic plastics have become integral to people's way of life. Yet the environmental implications of disposing large quantities of synthetic plastics are not well publicised. However, the UK is slowly adopting a similar mentality to China and parts of the United States of America, where retailers are banned from providing customers with free non-biodegradable plastic bags [10]. It was reported within the UK that the number of plastic bags dispensed fell from 13.4 billion in 2007 to 9.9 billion in 2008 [8]. These figures halted the threat of a government ban on free carrier bags [11]. However, UK supermarkets handed out 8 billion single-use plastic bags in 2011, up 5.4 % on 2010 [12].

An ideal solution for combating the impact of plastic waste within the environment is to replace the use of synthetic plastics with bioplastics, such as PHAs which have the ability to biodegrade within the environment after one year [13].

1.3. *Polyhydroxyalkanoates (PHAs)*

PHAs are linear polyesters that are naturally synthesised by the bacterial fermentation of sugars and lipids [7].

The PHA family consists of more than 150 monomers that can be combined to produce versatile biomaterials with a wide range of properties [7]. PHAs have been shown to occur in over 90 genera of bacteria, encompassing both gram negative and positive species [14]. The synthesis of PHAs by bacteria was the first natural method used for PHA production and preparation [15]. Bacterial cells accumulate PHAs as intracellular food and energy reserve as a response to nutrient limitation or imbalance in the environment as a means of preventing starvation when essential nutrients are limited [16]. PHAs accumulate when the bacterial cells are limited for nitrogen, phosphorous, iron, ammonium or sulphate and supplied with an excess supply of carbon [17]. Bacterial cells such as *R. eutropha* are capable of accumulating up to 90 % weight by weight (w/w) of PHAs [18].

PHA production in bacterial cells was initially described by Beijerinck *et al*. [15]. PHA inclusions within the cells were first described as lipids by biochemists, however in 1925 Lemoigne determined the inclusion bodies to be PHB [4]. Lemoigne first reported the discovery of PHB as a component of the bacterium *Bacillus megaterium* in 1926 [4]. The newly discovered PHA was identified as possessing similar properties to those of the synthetic plastic PP and was seen as a potential viable replacement [2]. The wide spread popularity of synthetic plastics and the low cost associated with their production meant that the potential of PHAs were widely ignored. The high production cost associated with PHAs is

primarily a result of the substrate cost, which is a principal reason for PHAs becoming ignored in favour of synthetic plastics [3].

Still to this day there is a high cost associated with PHA production compared to that of synthetic plastics [7]. However the new trend for environmentally friendly products and the growing concerns relating to the effects of synthetic plastic within our environment has sparked significant interest in the use of PHAs. The similarities of PHAs to synthetic plastics have resulted in them becoming highly researched as a substitute for non-polluting synthetic polymers in our environment [19].

The current research into PHA is predominately focused on making the process economically attractive. Recombinant microbial strains are currently being researched in order to achieve close packing of the PHA granules within the host cell and a high substrate conversion rate [3, 20-23]. An improved fermentation process [24, 25], a more efficient recovery/purification process and the use of inexpensive carbon sources for the production of PHB have also been found to substantially reduce the cost of production [6]. Other areas in need of development are the extraction and purification methods that are currently used. A low cost extraction method would significantly reduce the cost of PHAs [26].The carbon sources commonly used for the accumulation of PHB and their relative cost are outlined in Table 1, outlining the high cost associated with the production PHA.

Table 1: Substrate cost per metric tonne (m.t.) of PHB production [27]

Carbon sources	Approximate cost ($ US/ m.t.)	Yield of PHB/substrate (g)
Methanol	184	0.18
Ethanol	502	0.5
Acetic acid	705	0.33
Glucose	493	0.33
Fructose	617	0.33
Cane molasses	220	0.42
Hemicellulose hydrolysate	69	0.2
Fermented cheese whey	173	0.33

Another method of reducing the cost of producing PHAs currently under research is the use of *Serratia* sp. NCIMB 40259 Genus of bacteria that are capable of accumulating Hydroxyapatite (HA) as a second high value product in conjunction with PHB as reported by Lugg *et al*.[28]. This method will not reduce the cost of production but make the fermentation process more economical and hence more desirable.

Many bacterial strains have the ability to produce PHA by utilising plant oils. Plant oils have more carbon atoms per gram in comparison to other substrates commonly used for the production of PHB [29], many species of bacteria are also capable of higher theoretical PHB yield of 0.98 g/g [30] in comparison to 0.48 g/g from glucose [31]. For this reason oils are a potentially superior substrates for the production of PHB. Alias and Tan reported an accumulation of 57.4 %w/w of PHA with palm-oil-utilising bacteria. *Cupriavidus necator* were fermented with various oils to achieve PHA concentrations ranging from 3 to 6 g/l after 25 h fermentation [32]. Fernandez *et al*. reported the production of 66 %w/w PHA from *Pseudonomas aeruginosa* using fatty acids and frying oil as substrates [33].

The bacterial synthesis of PHAs is currently the main candidate for PHA production on a large scale. In recent years the synthesis of PHA by genetically modified plants has gained much attention. Genetic modification is being used to shift the metabolism of plants towards the production of PHAs [34]. PHA synthesis by plants is not yet commercially viable scale. The use of genetically modified crops within the European Union (EU) is currently restricted making the process less attractive.

The use of transgenic plants containing cloned biosynthetic genes is a novel method of synthesising PHAs. If PHA production by this method were to become economically feasible, then it would be possible to produce PHAs using standard agricultural methods. Currently plant cells are only capable of producing a PHA yield of ~10 %w/w. Furthermore, high yields of PHA production by plant cells (10-40 %w/w) have found to stunt the growth of plant cells [35].

1.4. *Physical, mechanical and chemical properties of poly-hydroxy-alkanoates*

1.4.1. *Chemical Structure of PHAs*

The length of the PHA polymer (n value) can exceed values of 3000 monomers. The length is dependent on the species of bacteria and the length of the (R)-pending group [36]. The structure of a PHA monomer is presented in Figure 1 along with the (R)-pending group. The mechanical properties of PHAs are highly dependent on the constituting monomer unit. To date, over 120 monomer units with different (R)-pending group have been reported. The carboxyl group of the monomer forms an ester bond with an available hydroxyl group from a nearby monomer to form a polymer chain [7, 36]. PHAs that consist of one type of monomer are known as homopolymers.

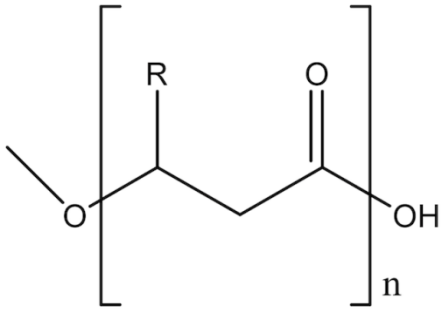

Figure 1: The structure of Poly-(3)-hydroxyalkanoates.

The majority of PHAs are composed of (R)-3-hydroxyalkanoic acid where the (R)-pending group can vary greatly as shown in Table 2 from (C_1) methyl to (C_8) tridecyl. The large degree of variation in the functional group, chain length and number of unsaturated bonds allows PHAs to be tailored towards a large number of applications [37].

Table 2: The corresponding R-groups of PHAs.

Polymer name	**R-Group**	**Sort name**
Poly(3-hydroxypropionate)	Hydrogen = H	PHP
Poly(3-hydroxybutyrate)	Methyl = CH_3	PHB
Poly(3-hydroxyvalerate)	Ethyl = CH_2CH_3	PHV
Poly(3-hydroxyhexanoate)	Propyl = $(CH_2)_2CH_3$	PHHx
Poly(3-hydroxyheptanoate)	Butyl = $(CH_2)_3CH_3$	PHH
Poly(3-hydroxyoctanoate)	Pentyl = $(CH_2)_4CH_3$	PHO
Poly(3-hydroxynonanoate)	Hexyl = $(CH_2)_5CH_3$	PHN
Poly(3-hydroxydecanoate)	Heptyl = $(CH_2)_6CH_3$	PHD
Poly(3-hydroxyundecanoate)	Octyl = $(CH_2)_7CH_3$	PHUD
Poly(3-hydroxydodecanoate)	Octyl = $(CH_2)7CH_3$	PHDD

Two distinct classes of PHAs have been identified. Short-chain-length PHA (scl-PHA) consisting of C_3 to C_5 3-hydroxy fatty acids and medium-chain-length (mcl-PHAs) consisting of C_6 to C_{16} 3-hydroxy fatty acids. The group of bacterium *R. eutropha* are known to produce scl-PHAs by substrate conversion inside the cells. The species of bacterium *Pseudomonas olevorans* has been reported to synthesize mcl-PHAs [38, 39].

The properties of PHAs can be modified by combining different monomers to form co-polymers. As many as 100 different monomers can be combined within the PHA family to give materials with different properties [7, 37]. The production of co-polymers from bacteria is controlled by manipulation of the carbon source that is supplied to the fermentation media. As an example, the use of a mix substrate consisting of glucose and valerate is known to produce poly (3-hydroxybutyrate-co-hydroxyvalerate) (PHBV) [40]. In this instance the co-polymer produced would consist of a random composition of monomer units and is known as a random co-polymer [41, 42]. The composition of the PHA co-polymers can be manipulated by adjusting the concentration of the substrates [42]. This can result in the production of desired ratios for specific monomers. PHA block co-polymers can also be produced and consist of two or more homo-polymers joined by covalent bonds. Block co-polymers can be formed by adjusting the substrate concentrations over a period of time [43]. Figure 2 demonstrates the monomers of PHB and PHV that combine to form the co-polymer of PHBV [43].

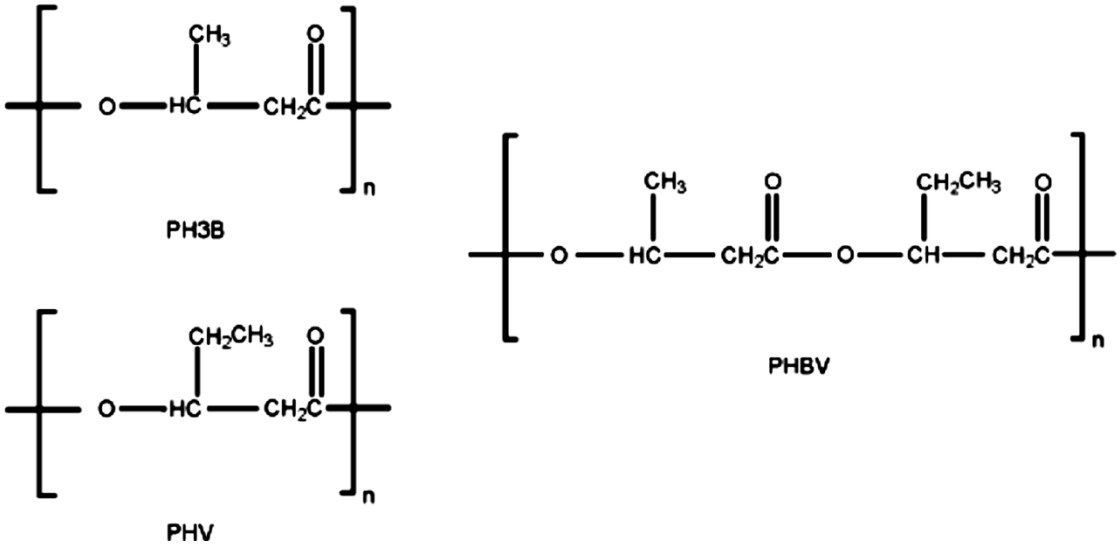

Figure 2: Monomers of PHB and PHV combined to form the co-polymer PHBV [44].

The presence of other types of PHAs besides homopolymers and co-polymers is noteworthy. Labuzek and Radecka reported the production of terco-polymers through the use of gram-positive *Bacillus cereus* UW85 strain. The addition of caprolactone as a carbon source to the fermentation media resulted in the presence of a terco-polymer consisting of 3-hydroxybutyrate (3HB), 3-hydroxyvalerate (3HV) and 6-hydroxyhexanoate (6HHx) units [45].

1.4.2. *The physical and mechanical properties of PHAs*

Polymers usually consist of both crystalline and amorphous regions. An amorphous polymer consists of a random arrangement of linear molecules while a crystalline polymer consists of linear chains. The optical properties of polymers are affected by the degree of crystallinity. Amorphous polymers can be transparent while crystalline polymers consist of a greater refractive index making them opaque [46].

PHA produced from bacteria is a semi crystalline material. The degree of crystallinity can influence many of the polymer properties [47]. PHB homopolymers are known to consist of a

high crystallinity often well in excess of 50 % [48], which is as a result of the strict molecular stereo regularity of PHB produced from biosynthesis [49].

PHAs such as the homopolymer PHB have been reported to be excessively stiff and brittle, as a result of their relatively high crystallinity [50]. PHB displays similar thermal and mechanical properties to the synthetic polymer PP and has been proposed as a substitute for polluting synthetic polymers in our environment [1, 2]. The excessively stiff and brittle nature of PHB homopolymers makes it unsuitable for some commercial applications [51, 52]. Co-polymers of PHB such as PHBV are less brittle and stiff, while maintaining many of the mechanical properties associated with PHB [53]. The mechanical properties of PHB and PHBV are said to be similar to those of isotactic PP, however the ductile and impact strength are much lower and prevent PHB and PHBV from effectively replacing commercial PP [54]. The addition of mcl-3-Hydroxyalkanoate (mcl-3HA) units can control crystallinity, which results in decreased stiffness, increased ductility and strength of the polymer, making it suitable for the replacement of existing plastic resins [53, 54]. The stiffness of PHB is not only a result of the overall polymer crystallinity but also a result of the amorphous region of the polymer. The difference in ductility of the amorphous region for a semi crystalline polymer also effects its overall stiffness [54]. The physical and mechanical properties for PHB, PHV and PP are demonstrated in Table 3.

Table 3: The physical and mechanical properties of PHB, PHV and PP [55].

Parameters	**PP**	**PHB**	**PHV**
Melting temperature (°C)	185	175	145
Glass transition temperature (°C)	-10	2	-1
Tensile strength (Mpa)	38	43	20
Extension to break (%)	400	5	50
Crystallinity (%)	50-60	60	56
Degradation Temperature (°C)	180	185	170

The Molecular weight (M_w) of a polymer can influence many properties, such as degradation rate and mechanical strength [56]. When producing polymers the appropriate M_w based on its application must be considered. PHAs such as PHB have a high M_w that can range anywhere from 200,000 – 3,000,000 Da, although this is dependent on the growth conditions of the bacteria within the medium [57, 58]. The polydispersity (PD) of a polymer can ultimately determine its quality. The PD is portrayed by a value that is always greater than one, the chain lengths of a polymer show greater uniformity as the PD approaches one. Synthetic polymers can be considered to be polydisperse as their chain lengths vary over a wide range of molecular masses. In naturally synthesized polymers such as PHB the PD can be very close to one, suggesting a uniform length of polymer chains is present [57].

The M_w of PHAs can be influenced by the carbon source used during fermentation. Much research has been carried out into the effects of magnesium and phosphate limitations in continuous culture of *A. eutrophus* in order to produce PHB. Research carried out by Asenjo *et al*. showed how the magnesium content was directly linked to the amount of PHB produced. Reducing the magnesium content to below 50 % resulted in a direct decrease in the

M_w of PHB [56]. It has also been reported that no significant M_w changes occur as a result of altering the amount of phosphate in the culture [59]. In the process of producing PHB the mechanism of controlling its M_w is still not well understood.

1.4.3. *Thermal properties of poly-hydroxy-alkanoates*

The homopolymer PHB has a high melting temperature (T_m), which is known to be ~180 °C, close to the polymers thermal decomposition temperature [60]. In an initial attempt to lower the T_m of PHB units of 3-Hydroxyvalerate (3HV) were incorporated into the polymer chain. The addition of 3HV units with randomly dispersed short ethyl side groups along the polymer chain resulted in a decrease in T_m and crystallinity [57, 60].

The glass transition temperature (T_g) of a polymer is the temperature at which reversible transition of the amorphous regions from a hard and relatively brittle state into a molten or rubber-like state [61]. The T_g is linked to the segmental mobility of polymer chains, which play an important role in dictating the toughness of the polymer [54]. PHB has been found to have a T_g of ~2°C [55]. Polymers with a lower T_g are expected to demonstrate greater toughness, however the toughness is compromised by its high degree of crystallinity and limited chain segmental mobility resulting in a highly brittle polymer [54]. The thermal degradation mechanism of PHB is important as it affects the properties of the polymer [62]. The mechanism of thermal degradation is demonstrated in Figure 3 and has been suggested to occur by random chain scission, involving β-elimination through a ring complex [63]. The thermal degradation of PHB is determined by the formation of membrane ring transition.

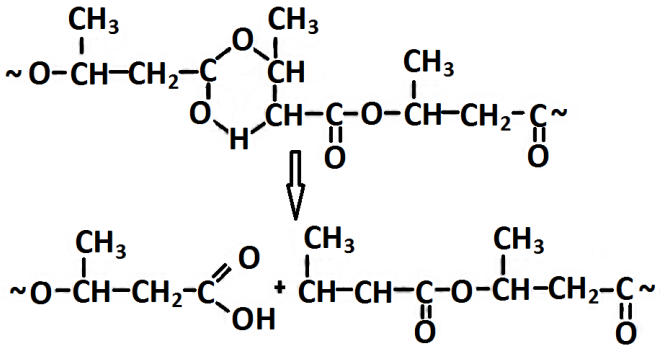

Figure 3: Six membrane ring demonstrating the thermal degradation of PHB [64]

1.4.4. *Biodegradability of poly-hydroxy-alkanoates*

An important property of PHAs is their biodegradability. In nature, enzymes and microorganisms are capable of degrading both natural and synthetic plastics [65]. Microorganisms capable of storing PHAs under conditions of nutrient limitation have the ability to also degrade and metabolize PHA when no other carbon energy source is readily available [14]. Microorganisms are capable of degrading PHAs by the action of PHA depolymerases and PHA hydrolases [14, 66]. Degraded PHA monomers are water soluble and capable of passively diffusing through the bacterial cell wall. Microorganisms are also capable of metabolizing PHA by β-oxidation and the citric acid cycle under aerobic conditions to produce carbon dioxide and water [67, 68].

Extracted PHAs are capable of being fully degraded under composting conditions. Increasing the temperature influences the biodegradability and solubility of PHB [13]. At greater temperatures PHB is amorphous and shows a higher sensitivity to the action of degrading enzymes resulting in rapid degradation [69]. The degradation process of PHAs can be hindered when dry conditions are present [70]. A correlation between the rate of PHB degradation and M_w was reported by Bonartsev *et al*. suggesting that the increase in PHB degradation resulted in a decline in the polymers M_w [71]. Spyros *et al*. also reported initial degradation of PHB occurring primarily in amorphous regions of the polymer. This is as the

amorphous regions are much more susceptible to microbial attack. It is suggested that an increase in PHB degradation results in greater % crystallinity and a decrease in the polymer M_w [72].

The use of UV light has been reported to also accelerate the degradation process of PHAs [73]. The photo-degradability and biodegradability are two separate classes of degradation. Photodegradable plastics will breakdown into small-sized fragments when exposed to UV-light. The UV light activate such bonds to form free radicals, which then react further with oxygen in the atmosphere, producing carbonyl groups in the main chain, however these fragments are unable to degrade any further. Biodegradable plastics are capable of being fully degraded within the environment and have no eco-toxicological impact when degraded [74-76]. The biodegradability of bioplastic over eighty days is demonstrated in Figure 4.

Figure 4: An illustration of the time taken for biodegradable plastic to degrade [77].

Outside the body PHAs are capable of being degraded by enzymatic and non-enzymatic processes. The degradation process that occurs in vivo involves a hydrolysis reaction and the action of tissue enzymes [78]. Pouton *et al.* reported a mass loss of less than 1.6 %w/w after implantation of PHA for a 6 month period. The degradation of PHA in vivo is dependent on many factors including the species, site of implant and the crystallinity of the polymer [79].

1.4.5. *Biocompatibility of poly-hydroxy-alkanoates*

In vivo PHA implants are degraded by a hydrolysis reaction, which breaks down the ester bonds to produce water and carbon dioxide as waste [76]. The high biocompatibility of PHB in vivo is a result of the presence of natural PHB oligomers and 3HB within human blood (intermediate product in the degradation process) and so do not produce any toxic products as they are biocompatible and as a result have no toxic effects within organisms [80].

1.5. *Bacteria producing Poly-hydroxy-alkanoates*

PHA can be accumulated by a wide variety of bacterial species under unbalanced growth conditions [81]. An overview of PHA producing bacterial species including their carbon sources are outlined in Table 4.

Table 4: An overview of PHAs produced by various bacterial species and carbon sources.

Bacteria	Type of PHA produced	Carbon Source	Reference
Aeromonas hydrophila	PHA	Oleic and lauric acid	[82]
Alcaligenes Latus	PHB,PHBV, P3HB-co-3Hproprionate,P3HB-co-4HB	Sucrose	[64]
Azospirillum brasilence	PHA	Wheat lectin	[83]
Azotobacter vinelandii	PHBV	Fish peptone, glucose	[84]
Bacillius spp.	PHB,PHBV	Glucose, caprolactone, soy molasses	[85, 86]
Chromobacterium violaceum	P3HV homopolymer	Sodium valerate	[64]
Delftia acidovorans	PHBV	Nutrient broth	[87]
Escherichia coli (mutants)	PHB	Sucrose, glucose, ethanol, Palm Oil	[88]
Methylobacterium	P(3HB-co-4HB) co-polymers	Methanol +3-hydroxypropionate	[89, 90]
Pseudonomas spp.	aromatic polymers	Glucose, aromatic monomers	[91, 92]
Pseudonomas stutzeri	mcl-PHAs	Glucose, aclcohol, alkanoates, soybean oil	[42]
Pseudonomas guezennei	PHA	Nutrient broth	[93, 94]
Ralstonia eutropha (Cupriavidus nectar)	PHB, PHB co-polymers	Glucose,sucrose, caprolactone, rape seed oil, Olive oil, soybean oil,fructose,valerate,	[7, 95, 96]
Rhizobium spp.	PHB	Glucose, sucrose, lactose, pyruvate, whey, sugar beet, raffinose, xylose	[97]
Rhodobacter sphaeroids	PHA	Glutamate-acetate	[98]
Serratia sp.	PHB	Glycerol 2-phosphate, citrate	[28, 77]
Spirulina platensis (cyanobacterium)	PHB	Carbon dioxide	[99]
Sphaerotilus natans	P3HB-co-3HV	Glucose+sodium propionate	[64]
Staphylococcus epidermidis	PHB	Malt, soy waste, milk,sesame oil	[100]
Vibrio spp.	PHA	nutrient broth	[101]
Zoogloea sp.	PHA	nutrient broth	[26]

Table 4 shows how a large number of bacterial species are capable of accumulating PHAs by utilising a wide variety of substrates. Many species of bacteria are capable of producing a broad range of polymers including co-polymers and tercopolymers with varied functional groups. It has been reported that the *Pseudomonas* genus is the most versatile accumulator of PHAs [7, 32, 45, 64, 102].

PHA accumulating bacteria have been isolated from a wide range of environments including waste water, contaminated soil and activated sludge. A potential novel method of synthesising PHAs is through genetic engineering [28, 32, 103]. Slater *et al*. were able to clone the genes involved in the production of PHB from acetyl-CoA in *Ralstonia eutropha* [104, 105]. The genes were successfully introduced into wild type *E.coli* (unable to synthesise PHA), where the new recombinant strain of *E coli* was able to synthesise PHB in large quantities ~80 %w/w [40, 104]. Genetic engineering has been used to optimise bacterial production of PHAs [16].

1.5.1. *Ralstonia eutropha*

*R. eutropha (*also known as *Cupriavidus nectar* or *Alcaligene eutrophus)* is a gram negative soil bacterium belonging to the class of proteobacteria. *R. eutropha* is considered the most cost effective bacterium for the production of PHB and capable of accumulating PHB at ~90 %w/w [64]. In literature *R. eutropha* cultures with up to 6100 mg/1 PHB have been reported [25]. *R. eutropha* has been classed as the model organism for studying PHB synthesis and accumulation as they are also capable of utilizing a wide range of carbon sources such as plant and vegetable oils in order to accumulate PHB inclusions [27]. As the production of PHB by *R. eutropha* cells is highly dependent upon the carbon source and medium, a greater range of carbon sources can be utilised. In the late 1980s, the American company Imperial Chemical Industries (ICI plc) were the first to use *R. eutropha* to begin worldwide

commercialization of a PHB and PHV bi-polymer blend and was sold under the trade name of Biopol® [106]. The use of *R. eutropha* cells is commercially beneficial as they are capable of using a wide range of carbon sources as substrates in order to accumulate PHAs. They are also capable of using carbon dioxide and hydrogen as substrates [107, 108].

1.5.2. *Serratia* sp.

Serratia sp NCIMB 40259 belong to the Enterobacteriacease family. *Serratia* sp. are ubiquitous organisms and can be found within the intestine of mammals and other locations depending on the genus and species [109].

The most common species of the *Serratia* genus is the *Serratia marcescens,* which is highly pathogenic and known to cause nosocomial infections [110]. *Serratia* sp. strain NCIMB 40259 is an atypical, non-pathogenic strain isolated from polluted soil and metal contaminants and was originally misclassified as *Citrobacter* [109]. Further studies using more advanced molecular biology tests showed the organism to be *Serratia* sp. *Serratia* sp have the ability to produce three distinctive enzymes. These enzymes are deoxyribonuclease, a lipase, and a gelatinase [28]. Extracellular polymeric substances (EPS) are present covering the surface of the *Serratia* cells (Figure 5) [77]. EPS are high M_w compounds that are secreted by the cells. They consist mainly of polysaccharides and can also attach to the outer surface of the cell as well as being secreted into the environment. These compounds are important in biofilm formation and facilitate the cell's attachment to surfaces [77].

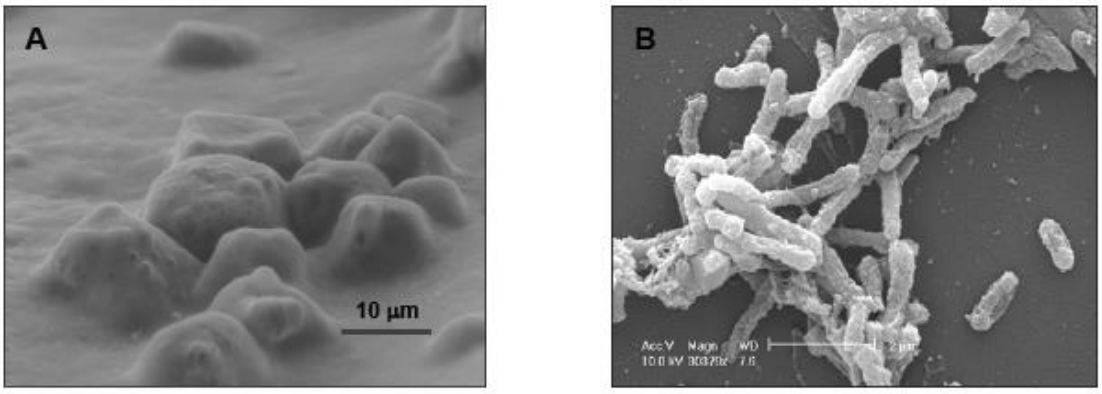

Figure 5: (A) Environmental scanning Electron Microscopy (ESEM) images of *Serratia* cells with EPS visible on the surface [77]. (**B)** *Serratia* cells viewed under scanning electron microscope (scale 2 µm)[3].

Phosphatase enzymes are known as phosphomonoesterases, which can be found in plants, microorganisms and animal tissue. Their primary role is the catalysis of a hydrolysis reaction involving the C-O-P linkage [111]. *Serratia* sp. produce two phosphatase enzymes, which are known as alkaline and acid phosphatases due to their optimal working pH range. In gram-negative bacteria acid and alkali phosphatases are located within the cell surface periplasmic space external to the cell membrane and are attached to other surface polymeric material. The phosphatase enzymes are comparatively resistant to inactivation and denaturation and have a greater rate of activity as they are located in the periplasmic space, which is subject to greater environmental variation compared to the interior of the cell. It has been reported, that *Serratia* sp. tends to over produce an acid phosphatase enzyme, while alkaline phosphatase is only produced during periods of phosphates starvation [112]. *Serratia* sp. produce an acid phosphatase enzyme both periplasmically and within the exopolymeric matrix, which is reported to be involved in liberating free phosphate ligands from a donor molecule [113]. The role of the phosphatase enzyme in the production of intracellular PHB is not fully understood.

Serratia sp. have been reported to bio-manufacture nanophase hydroxyapatite (HA) when fermented with specific substrates such as the phosphate donor glycerol 2-phosphate (G2P)

and Ca^{2+} [114, 115]. G2P is cleaved by the phosphatase enzyme resulting in the liberation of inorganic phosphate and providing a nucleation site for the growth of calcium phosphate crystals on the cell surface (Figure 6) [113, 116].

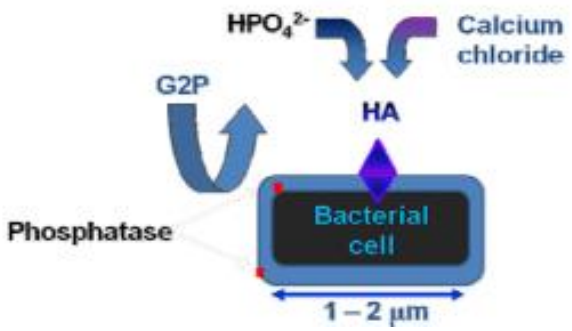

Figure 6: Metabolic pathways for PHA synthesis [7]

1.6. *Inclusion body formation*

PHAs produced in bacteria are water insoluble and consequently are accumulated in discrete spherical granules within the cell cytoplasm. During periods where cells are starved of essential nutrients the size and number of the spherical granules can vary, generally the size and number of PHA granules is in correlation with the length of starvation period [17]. The spherical granules within the cell have a diameter that typically ranges from 0.1 to 0.8 µm [117]. The membrane that the granules are enclosed in is around 2- 4 nm thick [118]. It is beneficial for bacteria to store nutrients in the form of insoluble polymers, this is as the granules do not interfere with physiological processes within the cell and therefore allow the bacterial cell to remain healthy [119]. The water present in the granules acts as plasticizer for the polymer and is a vital part of the granules [78]. Excess energy within the cell in the form of insoluble nutrients is converted and stored as insoluble PHAs, this is beneficial as it prevents changes within the osmotic environment of the cell [78]. These granules consist of around 98 % polymer and 2 % protein and phospholipids. At present two key models have been proposed for the formation of granules, the miccelle model involves the covalent

attachment of the PHB chains to synthase enzyme to form a micelle structure [120]. The second model involves the attachment of the synthase enzyme to the inner surface of the plasma membrane, which results in the budding of PHB and eventually forms granules with lipid monolayers [120]. The formation of PHB granules in *R. eutropha* is presented in Figure 7 and demonstrates the forms PHA after extraction process.

Bonthrone *et al*. used 13C-NMR studies to suggest that PHB is predominantly in a mobile state within the granules and so is not crystalline [121, 122]. However Dennis *et al*. discovered that PHAs are actually stored in a semi crystalline state within the cell. It was also shown by Okamura *et al*. using X-ray techniques, that a crystal structure was indeed present [18, 121]

1.7. *Bacterial synthesis pathway*

Bacterial synthesis was the first natural way of producing PHAs. The initial step in the biochemical synthesis involves the conversion of a carbon source into acetate [55] the steps can be observed in Figure 7. Coenzyme A (CoA) is a carrier of acyl groups; Acetyl-CoA is converted to PHA by the action of three enzymes [55]. Two molecules of acetyl-CoA combine together by a reversible condensation reaction to form the dimer acetoacetyl-CoA, this reaction involves the action of 3-Ketothiolase **(1)**. Subsequently the action of the NADPH-dependent enzyme acetoacetyl-CoA reductase **(2)** reduces acetoacetyl-CoA to form (R)-3-hydroxybutyryl-CoA. PHB can then be formed by the polymerisation of (R)-3-hydroxybutyryl-CoA by the enzyme PHA synthase **(3)** maintaining the asymmetric centre [81]. The process continues by the addition of a monomer to the free thiol group of the active site.

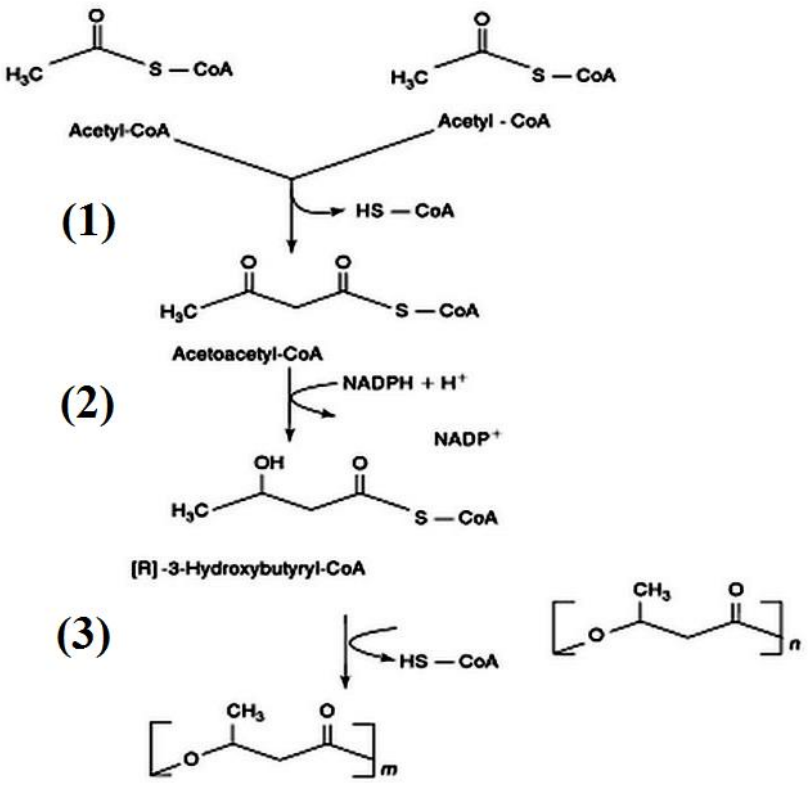

Figure 7: Bacterial synthesis of PHB [64]

Under conditions of balanced growth, the production of PHB within the cells is inhibited [119]. This is due to the high amounts of CoA that are present, which inhibit the action of 3-Ketothiolase . The acetyl-CoA is therefore converted to the krebs cycle [81]. During periods of essential nutrient limitation (excess carbon) the excess acetyl-CoA is converted into PHAs such as PHB [81, 123]. When bacterial cells are limited for essential nutrients and do not have an excess supply of carbon a build-up of NADH (electron carrier) is observed. The excess of NADH is a result of proteins unable to be synthesised. NADH acts to inhibit the synthesis of citrate, resulting in acetyl-CoA not being oxidised at a fast enough rate by the krebs cycle and consequently accumulates. At high concentrations of NADH and acetyl-CoA the equilibrium is shifted in favour of PHA biosynthesis[55, 64].

PHA is depolymerized by converting hydrocarboxylic acid to acetyl-CoA which is re used in metabolism by degradation enzyme systems [17]. All PHA synthesising microorganisms

contain a intracellular depolymerase system for the degradation of PHA [124]. The cyclic nature of PHB biosynthesis and degradation is presented in Figure 8.

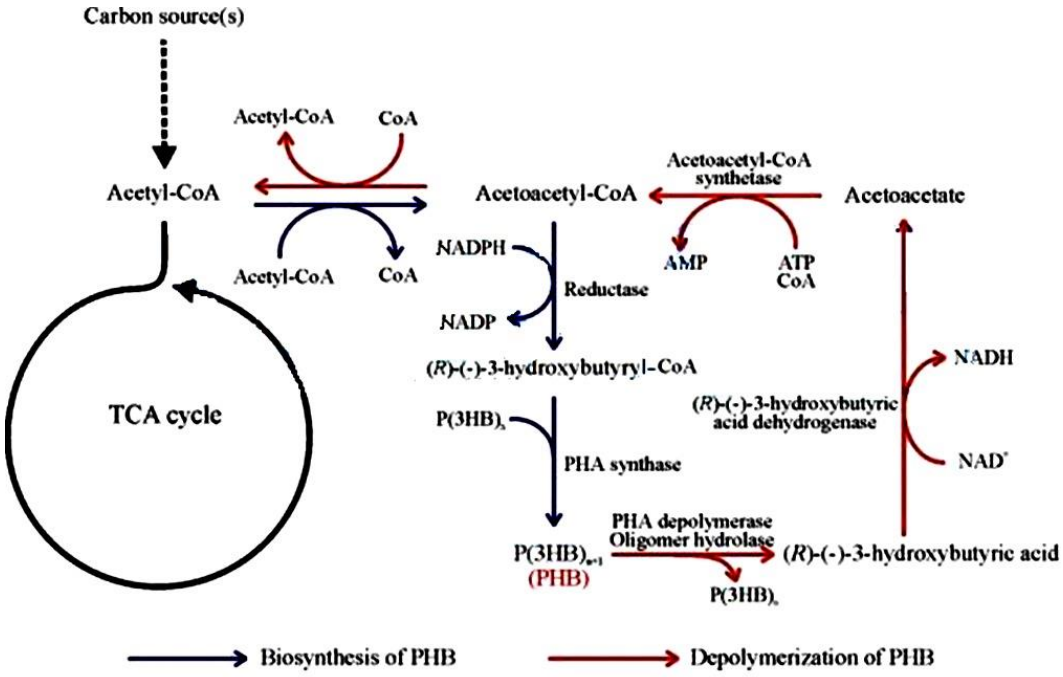

Figure 8: Cyclic biosynthesis and degradation of PHB [124]

The synthesis pathway presented in Figure 8 is for the processing of sugars such as glucose, yielding PHB homopolymers. Carbon substrates can be metabolised by many different pathways outlined in Figure 9. The use of fatty acid and sugars in pathways II and III can yield copolymers [123].

Fatty acids can be metabolised by its conversion to (R)-3-hydroxyacyl-CoA, which is subsequently converted into PHA by the action of PHA synthase. Fatty acids that are converted to acetyl-CoA by 3-ketoacyl-CoA can enter pathway I where PHB homopolymers can be produced [55].

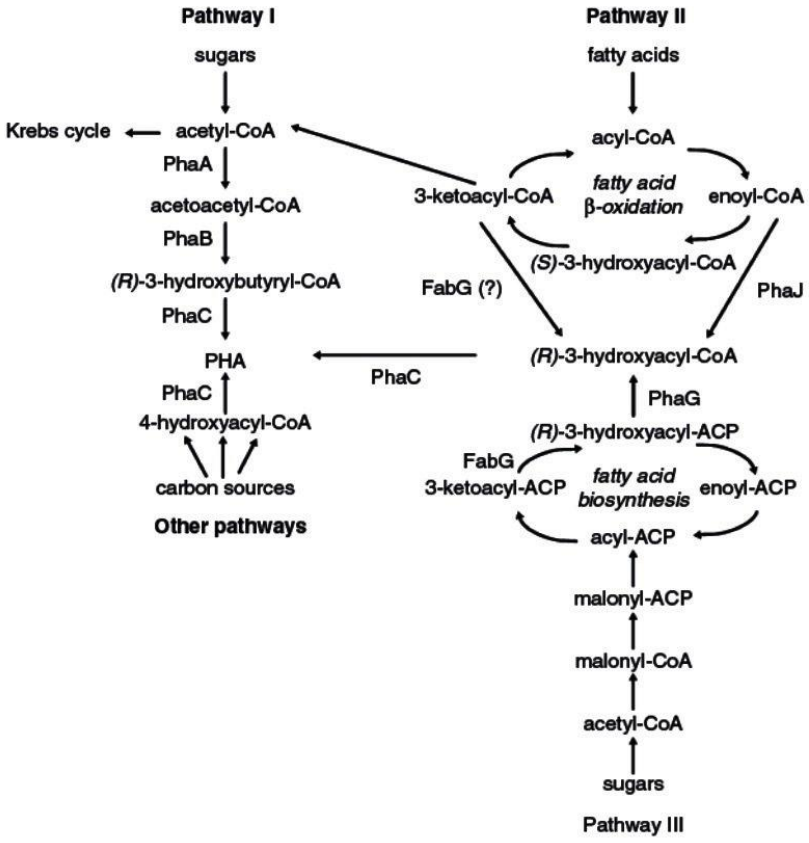

Figure 9: Mechanism of HA formation on the surface of *Serratia* sp

1.8. *Applications of Bioplastics*

1.8.1. *Advancements in the bioplastics market*

The use of bioplastics in packaging is currently very limited in comparison to plastics, according to the editorial director of Packaging Digest "Bioplastic's time has not yet come, but it can't be far off." Research conducted by the BBC has shown the growth of the Bioplastic's market rise from £541,000,000 in 2007 and was expected to reach £1,200,000,000 by 2012 [125].

The potential of bioplastics is largely dependent on the future cost of fossil fuels, as the low cost associated with the production of synthetic plastics make it a more viable option for many applications [119]. Bioplastics are a suitable replacement for synthetic plastics in most applications [13, 126]. However, in some cases the biodegradability of bioplastics can make it

unsuitable for certain applications. This is true for applications such as flower pots that can be placed in a greenhouse where the humid conditions accelerate the biodegradation process. Another property that makes bioplastics unsuitable for certain applications is the presence of a semi permeable membrane. This allows for air and moisture to penetrate the material, making it unsuitable for storing dry foods such as cereal. Biodegradable bags made from bioplastics are slowly making their way to the high streets around the world and are becoming the preferred choice. This is helping to reduce environmental pollution resulting from the use of synthetic plastics [10, 125, 127, 128]. Bioplastics are also being used for food packaging, mostly for fruits, vegetables and bread. The emergence of biodegradable stationary is also being seen. The U.S. Company Paper-mate has placed numerous adverts to encourage the sales of their biodegradable range of pens [129]. Figure 10 shows the biodegradable pen produced from the company Paper-mate.

Figure 10: Biodegradable ballpoint pen produced by PaperMate [130].

The trend towards using bioplastics is being adopted by many market leading companies. In 2009 the beverage retailer Coca-Cola announced plans for a new green initiative. The initiative involved the distribution of plastic bottles of cola and other beverages made with up to 30 % plant based material [131]. The move is a large step towards tackling the global waste problem with the Coca-Cola Company selling beverage products in more than 200 countries

[132]. Figure 11 below shows the new labelling on 500 ml Coca-Cola bottles indicating the biodegradability

Figure 11: Coca Cola plant bottle launched in 2009 [131].

Bioplastics are also used in many medical applications. Commercial bioplastics are available in many forms of pins, films, screws and other devices from various companies including TEPHA (U.S.A) and Metabolix (U.S.A) to name a few. The composition of bioplastics can be adjusted so that devices used for implantation can have a tailored degradation rate and maintain their mechanical strength for the desired duration [133].

There are various types of bioplastics that are currently being implemented as alternatives to synthetic plastics. Bioplastics made from starch and cellulose are becoming very popular with companies for use in packaging [134]. The production method is relatively simple as starch or cellulose is extracted from crop biomass. The Bioplastic polymer extracted requires chemical modification before it can be used as a functional material.

Production of PHB at a commercial capacity has always been limited by economic constraints. This is due to the high cost associated with the fermentation and extraction methods used and also the high cost of carbon substrates necessary for PHB production [135, 136]. In an attempt to make the process more economically viable, efforts are being made to use cheaper carbon sources such as vegetable oil and waste products [137]. It has been

suggested that commercial feasibility can only be achieved when 50 % of dry cell mass is produced as PHB [138].

1.8.2. *Applications of bacterially produced Poly-hydroxy-alkanoates*

Bacterially produced PHAs can be used for a range of applications including agricultural, medical and industrial applications. As previously mentioned, two of the primary properties of PHAs are there biodegradability and biocompatibility this makes it a suitable alternative material in many applications.

The medical applications of PHAs include implantable medical devices for skin surgery, orthopaedic, dental and cranio maxilla-facial. Medical devices that have been produced from PHB include: biodegradable screws and plates for the fixation of bone and cartridge, bioresorbable sutures, surgical meshes, nerve guides, tendon repair devices and wound covers [79, 139, 140].

A novel application for PHAs is for the production of sustained enzyme immobilisation. Fusion proteins are attached in vivo to the surface of PHA granules. As a result of PHAs low inflammatory tissue reaction at the site of implant makes them ideal for the design of prolonged local enzyme activation [141, 142].

As previously mentioned PHAs have been heavily researched as potential replacements for petrochemical polymers. The PHA family demonstrate a wide range of physical properties that can be tailored to applications such as packaging by producing blends and composites [143]. PHAs have a greater barrier to air and water while also demonstrating improved strength and flexibility making it ideal for packaging [144]. Composites of bioplastics have

recently been implemented in electronic products. In 2009 NEC developed flame retardant bioplastic capable of being used in electronic devices such as personal computers [145].

1.8.2.1. Tissue Engineering applications

Tissue engineering is used as a method to reconstitute and regenerate lost or damaged tissue [146]. A large amount of research is invested in the creation of scaffolds that have the ability to mimic both the function and structure of the extracellular matrix (ECM) [147].

A variety of polymers have been used to produce ECM scaffolds in tissue engineering. PHB has become a popular choice in producing scaffolds as it is a hydrophobic biomaterial, which exhibits a biodegradable surface necessary for a long half-life in vivo [148-150]. The ECM comprises of nanofibres, which provide structural support. Nanofibres are defined as fibres with diameters less than 100 nm, many processing techniques have been used to produce nanofibres such as template synthesis, drawing, phase separation, self-assembly and electrospinning [151, 152].

1.8.2.1.1. Electrospinning

The electrospinning process has been available since the beginning of the last century. It is only recently with the emergence of nanoscience and nanotechnology at the end of the 20th century that the potential of this technique has been realised [153]. As previously mentioned different approaches exist for the production of nanofibres. Electrospinning has become the favoured technique as other approaches do not provide the versatility, flexibility and ease of fibre production offered by electrospinning. Electrospinning allows for the fibre dimension to be controlled, in order to produce varied fibre assemblies, allowing for application specific modifications [151].

Electrospinning is a process where an electric field is applied to a drop of dissolved polymer solution injected from a needle tip of a syringe that acts as an electrode [154]. Most

electrospinning processes tend to use a polymer solution with a concentration of 5 % to 15 %, dependent upon the M_w of the polymer, as it can range from 50,000 to several millions. Molten polymer can also be used [155, 156]. Droplets of the polymer solution attach to the needle tip of the syringe as a result of the surface tension and viscoelastic stresses [157]. Electrical potential is applied between the drop and collector causing the charges within the fluid to reach a critical level [158]. At this point the force created by the repulsive charges at the surface of the fluid becomes greater than its surface tension. The drop then forms a taylor cone resulting in the release of a charged polymer jet from the tip [156]. The charged polymer jet leaves the tip of the syringe and takes a linear path parallel to its axis (Figure 18). The jet then accelerates as it is pulled towards the collector plate due to the coulomb forces that act against the opposing surface tension and viscoelastic forces [158, 159]. The linear segment of the jet eventually becomes unstable in response to the coulomb repulsion of the charges and elongates within the electric field between collector and syringe [159]. The polymer jet is capable of keeping its integrity as a result of the polymer molecules that become entangled [157].

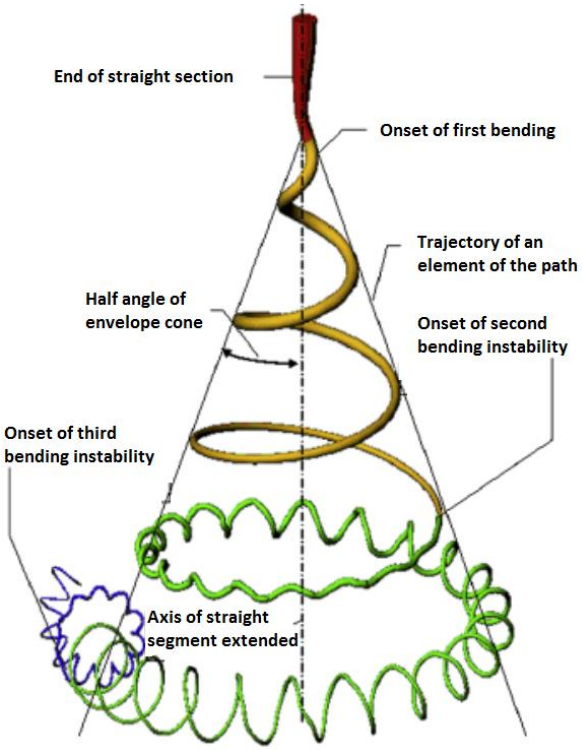

Figure 12: Thinning of a polymer jet in the electric field during a typical electrospinning experiment [160].

The path of the jet begins to coil due to the electrical charge while the trajectory for each segment of the coil becomes perpendicular to its own axis. The electrical bending instability results in the coiled jet forming a smaller coil after each turn, this process continues as the coils become even smaller until elongation stops [158, 161].

The jet is capable of elongating by a factor of 4 as a result of the coiled path [159]. The process of coiling elongates the jet by the electrical energy that is supplied, which results in a decrease in the jets diameter and thereby increases the surface area per unit mass ratio of fluid [160]. The bending instabilities of the polymer jet are critical to the electrospinning process as they cause stretching and bending of the jet [161]. As the charged jet leaves the tip of the syringe the solvent evaporates, leaving only a charged polymer fibre. The continuous fibre lands on the collector in the form of a nonwoven mesh commonly known as a scaffold [151,

160]. The low cost and high production rate associated with the electrospinning process has also contributed towards it becoming the most favoured technique [157].

1.8.2.1.2. Applications of Electrospun PHB

Electrospinning is a process where an electric field is applied from a high voltage power supply to a drop of dissolved polymer solution injected from a needle tip of a syringe, which acts as one of the electrodes [154]. Electrospun PHB nanofibres have promising applications in the repairing of human tissue such as blood vessels, nerves, cartilage and skin [162-165]. The structure and properties can be tailored to provide the necessary mechanical properties required to support the proliferation of cells [166].

Electrospun PHB nanofibres can be designed for the delivery of drugs to a specific site of action within the body. The encapsulation of drugs within a microsphere and microcapsule produced from PHB allows for the timed release of specific drugs at their intended site of action [164]. The drug release occurs by two separate processes of diffusion and degradation taking place simultaneously in vivo [71]. This mechanism of sustained drug delivery can be used for the delivery of antibiotics, anti-inflammatory and anti-tumour drugs [157]. The regulation of PHB M_w and crystallinity makes it possible to control the degradation rate of the polymer and hence the drug release [167]. The electrospun nanofibres have an inherent property whereby they mimic the ECM of tissue and organs. Studies have showed that cells are capable of adhering and proliferating when cultured on PHB electrospun nanofibres [168].

1.9. *Bacterially Produced Hydroxyapatite*

Lugg.*et al*. demonstrated how *Serratia* sp. are capable of mineralizing nanophase HA on their cell surface while simultaneously accumulating PHB inclusion bodies [28]. The mineral HA is capable of forming on the cell surface and has a crystallite size of ∼25 nm [115]. The biomineralisation of HA only occurs under certain growth conditions where *Serratia* sp. are

capable of producing a large amount of acid phosphatase [115, 169] using a phosphate donor such as G2P, which allows HA to be formed on the cell surface (Figure 13) [115].

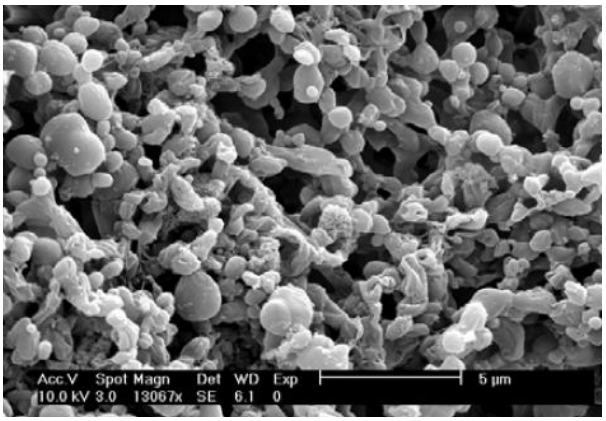

Figure 13: ESEM image of HA forming on surface of *Serratia* sp [77].

The co-production of a second high value material HA, that can be extracted and processed independently, will improve commercial feasibility for the production of PHB from *Serratia* sp.

1.9.1. *Properties of Hydroxyapatite*

HA is a naturally occurring form of calcium apatite with the formula $Ca_5(PO_4)_3(OH)$, however it is predominantly written as $Ca_{10}(PO_4)_6(OH)_2$ to signify that the crystal cell is made up of two molecules. HA has attracted much attention as a result of its similarities to the inorganic phases of bone and teeth [170]. HA exhibits good bioactivity, biocompatibility and osteoconductivity, however has poor mechanical properties [171, 172].

Nanophase HA exhibits greater biological efficacy compared to conventional HA and has the ability to promote osteoblast adhesion, proliferation, osteo-intergration and the deposition of calcium containing minerals on its surface [173]. It has been suggested that nanophase HA ceramics have the ability to improve sintering kinetics and subsequently enhance its

mechanical properties as a result of its greater surface area [174, 175]. A large amount of interest has been focused on the synthesis and potential applications of nanophase HA [176].

HA is a thermally unstable compound, decomposing at temperatures of approximately 800-1200°C depending on the purity of the mineral i.e. the ratios of other chemicals that are present (stoichiometry) [177]. HA that is made from powders and produced by chemical precipitation has poor mechanical properties and a low fracture toughness making it unsuitable for many applications that involve long-term load bearing [178]. On the Mohs hardness scale it scores 5 and has a specific gravity of 3.08 [144].

1.9.2. *Structural Characterisation of HA*

Synthetic HA is known to crystallize in a well ordered hexagonal crystal system. A single unit cell of HA consists of 44 atoms, which include ten calcium atoms, six PO_4 tetrahedra and two OH^- groups that are organized in a hexagonal system (Figure 14) [179].

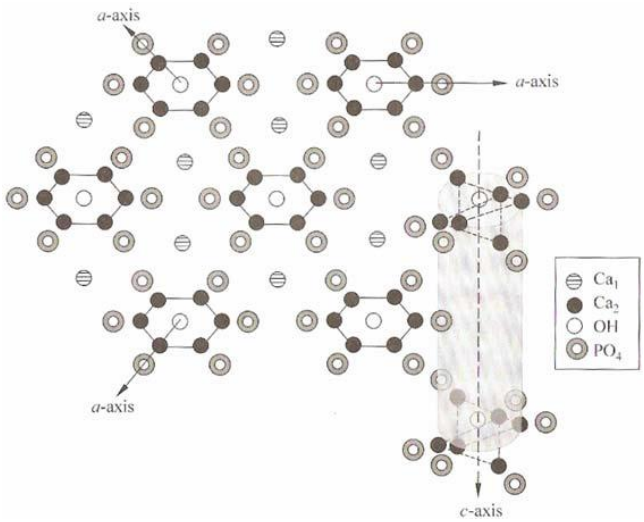

Figure 14: The schematic diagram for the hexagonal structure of HA crystals [180].

HA is capable of forming other structures. Ikoma *et al*. suggested an alternative monoclinic structure for HA [181]. The transition of HA between hexagonal and monoclinic has been extensively researched [182]. Suda *et al*. reported that the phase transition was highly

dependent on temperature [183]. At room temperature, the HA exhibited monoclinic structure, however the appearance of hexagonal structure was started at 473 K and at 483 K the hexagonal structure became the predominant phase (Figure 15) [183].

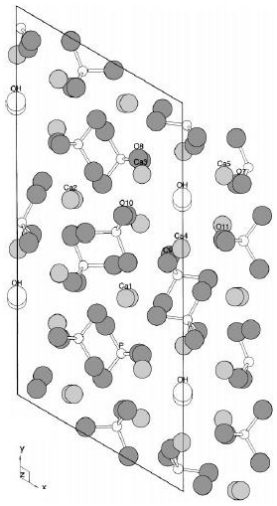

Figure 15: Projection of monoclinic HA on (001) plane. Small white balls phosphorus, grey balls= oxygen, white balls= hydroxyl oxygen, Light Grey= calcium [181].

This phase transition process is reversible as temperature was reduced. It was reported by Ikoma *et al*. that the greatest structural difference between the hexagonal and monoclinic HA was in the OH^- groups [181]. Monoclinic HA demonstrates an ordered structure with repeating O-H in one column and repeating H-O in another column. In the hexagonal HA phase the OH groups demonstrate an order of –H, H-O, O-H along the C-axis, which helps improve stability to the two fold disordered arrangement [184].

1.9.3. *Applications of HA*

The chemical composition of HA is very similar to that of bone and teeth and also HA's excellent biocompatibility and bioactivity properties as a result of this it can be applied to a wide range of applications including dentistry and orthopedics [170, 185]. HA is employed in different forms for the application of filling bone defects or voids, which are known to occur

when large sections of bone have to be removed (e.g. bone cancers) by surgical procedure or when bone augmentations have taken place such as. dental applications and maxillofacial reconstructions [186, 187]. HA can be employed in bone filling and reconstruction applications in the form of a powder, beads or porous blocks. The bone filling application of HA provides a scaffold structure and encourages the rapid filling of the empty void by naturally forming bone and acts as an alternative to the use of bone grafts. The application of bone filling has the ability to become part of the structure of bone and will also reduce the healing time compared to if no bone filler was used [187].

HA has become an important application in the coating of metallic implants [172]. These implants are mostly comprised of stainless steel. HA is used to coat the surface as a means of altering the surface properties of the implant material. As HA is biocompatible and bioactive, it is used as a coating material to biomedical surfaces in order to improve the surface-tissue interactions [187]. Plasma spraying is considered to be an efficient method of applying HA coating [172]. There is always a great risk of infection occurring when implanting any material within the body, plasma sprayed implants are susceptible to the formation of infections in the form of a bacterial plaque, which if occurs will be detrimental to the human body and immune system [187].

Synthetic HA produced from chemical precipitation are known to have poor mechanical strength and so can't be used in major load bearing applications [188]. As a result of large grain sizes that arise from densification of agglomerated particles during the process of manufacturing [115, 189]. The grain size of HA powders can be controlled during synthesis. Limiting the HA powders exposure time to high temperatures minimises the grain size and consequently improves the hardness and strength of the material [190].

HA has become the material of choice within orthopaedic and dental procedures, as a result of its chemical solidity and biocompatibility [191]. HA is commonly found within teeth and bones. Bone within the body consists of approximately 50 %w/w of HA (also known as Bone mineral).It is for this reason that HA is biocompatible within the body, .HA is commonly used as a filler to replace missing bone and also to coat the surface of bone in order to encourage bone growth within implants [192]. HA coatings are converted by osteoclasts activity as the HA is resorbed and actively partakes in the formation of new bone material. HA can also be coated onto the surface metallic implants by plasma spraying, this allows the implant to benefit from the biocompatible properties of HA whilst maintaining its mechanical strength [193]. Zhu *et al*. produced nano crystalline HA by a hydrothermal method. The nano crystalline HA showed biocompatibility in vitro and in vivo animal studies and did not exhibit any toxic effects. Zhu *et al*. suggested that the nano crystalline HA is a promising biomaterial to be employed as a gene carrier and vector [194].

HA has also been used in many environmental applications. Applications such as water purification [195-197] waste stabilization [198, 199], contaminated soil remediation [200, 201] and heavy metal absorption [174, 202, 203]. Handley-Sidhu *et al*. reported nanophase biomineral HA to be a promising material for the remediation of metal contaminated water and as a storage material [203]. Recent studies showed that the uptake of Sr^{2+} and Co^{2+} by nanophase biomineral HA was more efficient compared to commercial HA, this was as commercial HA had an uptake of 0.76 mg Sr^{2+}/g whereas biomineral HA resulted an uptake of 5.35 mg Sr^{2+}/g. Properties that increased metal uptake were smaller crystallite size (< 40 nm) and higher surface area (> 70 m^2 g^{-1}) [203]. Ozama *et al*. suggested that the porous HA derived from fish bone is a suitable material for the removal of chromium in water and fish waste management. The desirable properties of fish bone HA are suggested to be as a result of its porous structure and major crystalline phase [204].

1.10. *Aims and Objectives- Justification of work undertaken*

Production of PHB at a commercial capacity has always been limited by economic constraints. This is due to the high cost associated with the fermentation and extraction methods used and also the high cost of carbon substrates necessary for PHB production [135, 136].

The aim of this thesis is to bacterially synthesise PHB cost effectively and to demonstrate how the produced polymer can be processed for biomedical applications. PHB was chosen as a result of its wide range of potential applications as outlined in section 1.8.2 and its ability to be synthesised in great quantities by many bacterial species.

In order to synthesise PHB, bacterial strains of *Serratia* sp. and *R. eutropha* were used. The *Serratia* sp. was chosen due to its ability to accumulate PHB, while simultaneously mineralising HA on the surface. The simultaneous production of the second high value material makes the process of PHB production economically viable.

To maximise the yields of PHB and HA accumulated by *Serratia* sp. experimental conditions were replicated from Kashani 2007 [28, 77]. Kashani showed that *Serratia* sp. fermented for 216 h produced PHB yields as high as 26.6 %w/w compared to 96 h (2.96 %w/w) and 408 h (2.96 %w/w) fermentations [77]. However, Kashani conducted experiments using HPA *Serratia* sp. with no replicas. These experiments will be repeated with replicas in order to accurately determine the fermentation time that results in the maximum yields of PHB and HA. The role of the phosphatase enzyme in the production of intracellular PHB has not been previously reported. For this reason PHB and HA will be accumulated from both High Phosphatase Activity (HPA) and Low Phosphatase Activity (LPA) *Serratia* sp. The yields of PHB and HA from HPA and LPA *Serratia* sp. will be compared as a means of determining whether phosphatase activity has any effect on the yields of accumulated PHB and HA. The

extracted PHB will be characterised and compared to commercial PHB in order to determine whether any changes have occurred to the thermal and molecular properties. The extracted biomineral from *Serratia* sp. will be characterised in order to confirm the presence of HA and will be compared to a commercial sample of HA.

The *R. eutropha* bacterial strain has been chosen as it is considered the most cost effective bacterium for the production of PHB. The *R. eutropha* species of bacteria are capable of accumulating PHB at ~90 %w/w [64] *R. eutropha* is considered to be the model organism for studying PHB synthesis and accumulation as it is capable of utilizing a wide range of carbon sources [27]. In an attempt to make the process cost effective, two types of oil (rapeseed and olive oil) will be utilised as the carbon source. Oils have been chosen as carbon sources due to the bacterial mechanism involved in the conversion of fatty acids from oil to PHB. As fatty acids are metabolised they are converted into (R)-3-hydroxyacyl-CoA, which is subsequently converted into PHA by the action of PHA synthase. Since plant oils have a greater number of carbon atoms per gram compared to other substrates, they are potentially a better substrate for the production of PHB [205]. Rapeseed oil was chosen for these experiments as a result of its low cost (€ 985.24 per tonne) and high PHA production [27], which made it a viable option for large scale industrial use. In addition, cooking oils disposed of by many restaurants and fast food chains can be a low cost carbon source and can be readily available in large amounts [206]. Glucose was also used as a carbon source due to it being the most traditional and most researched carbon source for the production of PHB from bacterial cells. A substantial increase in PHB production has also been observed when using glucose as a carbon source in the *R. eutropha* strain of bacteria [27]. PHB production from sugars as outlined in Figure 9 follows a different synthesis pathway to fatty acids, as once converted to acetyl-CoA they do not undergo β-oxidation.

PHB synthesised from oil and glucose will be characterised and their thermal and molecular properties will be compared. It has been shown how various carbon sources can affect the properties of bacterial synthesised PHB, which in turn can affect the application of the polymer. It is therefore essential to study not only the effect of the carbon source on the percentage productivity but also its effect on the properties of the synthesised polymer. These properties affect the applicability of the polymer. In order to demonstrate that bacterially synthesised PHB can be successfully processed for biomedical applications, electrospinning will be carried out in order to produce nanofibres of PHB. The process of electrospinning has been chosen due to the low cost and high production rate associated with it and the versatility, flexibility and ease of fibre production offered. Electrospun nanofibres of PHB have a wide range of applications from filtration in the engineering industry to various medical applications such as wound dressing, tissue template, tissue engineering and medical prosthesis [207, 208]. The source and properties of the bacterial PHB, used for nanofibre production, is largely missing in literature. For this reason, the effects of carbon source on the properties of PHB and the consequent effects on the diameter size of electrospun nanofibes will be investigated in this study.

Lee *at al*. 2004 reported that controlling the fibre diameter size can result in a suitable pore size for fibre mats used as storage media for alternative energy sources [209]. Key factors known to impact the fibre diameter include the concentration of the polymer solution, the solvent used during electrospinning and the flow rate of the polymer solution out of the syringe [210]. Another property that can be affected by the electropsinning process is the degree of crystallinity in the electrospun fibres. Based on several accounts in literature, the degree of crystallinity can be affected during electrospinning and depending on the combination of electrospinning parameters used, it can be decreased [210] or increased [211].

Through the use of a constant set of electrospinning parameters it will be easier to study the effect of the carbon source on the crystallinity of the electrospun fibres.

The specific objectives of this research and how they have been achieved are listed below:

1. Utilise *Serratia* sp. to simultaneously produce PHB and HA.
2. Maximise the yields of PHB and HA accumulated from *Serratia* sp. by determining the optimum fermentation period for the accumulation of PHB from both HPA and LPA *Serratia* sp.
3. Examine the effect of phosphatase enzyme on the yields of mineralised HA and intracellular PHB. Experiments will be conducted with replicas as a means of validating the results and ensuring reproducibility.
4. Characterise the properties of PHB and HA obtained from HPA and LPA *Serratia* sp., as to determine whether changes in phosphatase activity and fermentation periods can alter their properties when compared to commercial samples.
5. Use the *R eutropha* genus of bacteria in order to produce PHB from olive oil, rapeseed oil and compare it to PHB produced from glucose. As glucose is a highly researched carbon source in the accumulation of PHB from bacteria.
6. To determine whether the use of oil as a carbon source can result in similar accumulated yields of PHB compared with conventional sugars such as glucose.
7. Examine whether the use of oils can be a viable replacement for sugars at industrial scale.
8. Electrospin PHB fibres from all three carbon sources in order to produce PHB nanofibres.
9. Study the effects of carbon source on the properties of PHB and the consequent effects on the diameter size and crystallinity of electrospun nanofibres. The source and properties of the bacterial PHB used for nanofibre production is largely missing in the literature.

Chapter 2 : Materials and Methods

2.1. *Preparation of Serratia cells for the production of PHB and HA*

2.1.1. *Growth of Serratia sp. NCIMB 40259*

The *Serratia* sp. NCIMB 40259 were grown under license from Isis Innovation (Oxford) in an air lift fermenter (2.5 L) under carbon limited conditions and lactose-based minimal medium in order to maximise phosphatase activity of the cells and consequently produce High phosphatase activity cells (HPA). The fermentation medium consisted of (12.0 g/L Tris; 0.62 g/l KCl; 0.96 g/L $(NH_4)_2HPO_4$; 0.063 g/L $MgSO_4 \bullet 7H_2O$; 0.32 mg/L $FeSO_4 \bullet 7H_2O$ and 0.6 g/L lactose) at 25-30 °C. The second category of growth fermentations were carried out under carbon limited conditions and phosphate-based minimal medium in order to minimize phosphatase activity of the cells and consequently grow Low phosphatase activity cells (LPA) (12.0 g/L Tris (buffer); 0.62 g/L KCl; 0.01 g/L $(NH_4)_2HPO_4$; 1.157 g/L $(NH_4)_2SO_4$; 0.063 g/L $MgSO_4 \bullet 7H_2O$; 0.32 mg/L $FeSO_4 \bullet 7H_2O$ and 3.0 g/L lactose) at 25-30 °C. The temperature of the fermentation was maintained by a heating mantle (Electrothermal HE08920) placed at the base of the fermenter. The pH of the fermentation was maintained at 8.6 by the addition of Tris buffer (12 g/L).

The cells were grown under the supervision of Prof Lynne Macaskie and her research group based at the department of Biosciences in Birmingham University. The *Serratia* cells were placed in an air lift fermenter for a period of 24 h in batch mode followed by 6 days in continuous mode (dilution rate = 0.113 h^{-1}). During the 6 day period of continuous culture the outflow was collected. The fermenter outflow consisted of *Serratia* cells to be harvested for experiments (Figure 16).

Figure 16: Air lift fermenter (2.5 L).

Serratia cells collected from the outflow were extracted by centrifugation. The fermenter outflow was centrifuged (SORVALL RC 3C Plus) for 20 min at a speed of 8,000 rpm to produce a pellet of cells allowing the resultant supernatant to be removed. Harvested cells were washed in isotonic saline (8.5 g/L NaCl).

2.1.2. *Assay of phosphatase activity*

The phosphatase activity of the cells was assayed by the release of p-nitrophenol (*p*NP) units from *p*-nitrophenyl phosphate (*p*NPP) [115]. One unit of *p*NP is defined as 1 nmol *p*NP released per min per mg of bacterial protein, with protein concentration measured using the $CuSO_4$/bicinchoninic acid method (Sigma protein test kit TPR0562) [138, 212, 213]. To estimate the enzyme activity, cell samples were washed with isotonic saline (8.5 g/L NaCl) and Vortex-mixed for 4 min in order to break apart the cell aggregates prior to the assay [212]. All experiments were conducted with HPA *Serratia* cells with a phosphatase activity of ~3800 nmol *p*NP and LPA cells with a phosphatase activity of ~500 nmol *p*NP

2.1.3. *Preparation of Serratia sp. for the accumulation of PHB and HA*

In order to prepare the *Serratia* cells for the accumulation of PHB and HA, the cells were initially re-suspended in TAPSO buffer (pH 9.2; 6.5 g/L), as to maintain the pH (9.2) and adjust the optical density (OD) of the cell solution to 1 at 600 nm (OD_{600}). OD has been widely used in microbiology as a means of providing the total cell dry weight of cells (DWC) in solution. OD involves the passing of light at a specific wavelength through bacterial culture in solution as the light is absorbed by the bacteria cells, light that is not absorbed or scattered is transmitted back. In optics, density is a unitless measure for the transmittance of an optical element for a given length and wavelength. OD is the logarithm for the amount of transmitted and incoming light.

$$OD = -log10\ \frac{I}{I_0} \qquad \textbf{Equation 1}$$

where **I**= Intensity of the transmitted light and $\mathbf{I_0}$= Intensity of the incident light.

The absorbance and scattering of light is increased by the bacteria in solution. Solutions with a higher cell concentration will have a greater optical density value. A linear relationship exists between the concentration of cells in solution and the OD.

2.1.4. *Dosing solutions and volumes for the production of PHB and HA*

Serratia sp. were fermented by the addition of daily doses of pre-prepared stock solutions in order to accumulate PHB and HA. As previously mentioned (section 1.9) G2P and $CaCl_2$ are required for the accumulation of HA. The carbon source necessary for PHB accumulation was obtained from sodium citrate ($Na_2C_6H_60_7$). The quantity and concentrations of the pre-prepared stock solutions are presented in Table 5.

Table 5: The quantity and concentrations of reagents required for the stock solutions**.**

Reagents	Concentration	Mw of Reagent (g/mol)	Reagent (g)	Volume (L)
G2P	1 M	216.04	108.2	0.5
$CaCl_2$	0.4 M	110.98	11.09	0.5
$Na_2C_6H_60_7$	0.2 M	294.1	58.82	0.5

The following equation was used in order to calculate the final dosing volume:

$$\frac{\text{Final concentration x Initial volume}}{\text{Initial concentration}} = \text{Final dosing volume} \qquad \textbf{Equation 2}$$

Final Concentration = concentration that is required for dosing, **Initial Volume =** volume of cells required to be dosed, **Initial Concentration =** concentration of the stock solution and **Final dosing volume =** volume of stock solution required for dosing. The volume and concentration of stock solutions used for each experiment are presented in Table 6.

Table 6: Concentration and volume of dosing solutions.

Reagents	Dosing concentration	Dosing volume (ml)
G2P	10 mM	1.86
$CaCl_2$	4 mM	1.86
$Na_2C_6H_60_7$	2 mM	1.86

2.2. *Fermentation experiments using HPA and LPA Serratia sp.*

The growth fermentations for HPA cells were repeated three times resulting in the production of three different batches of HPA *Serratia* cells (HPA (A), HPA (B) and HPA (C)). Each of

the three batches were utilised for the production PHB and HA under identical conditions. The fermentation experiments for each of the above batches were repeated 4 times. The yield of PHB and HA calculated for each batch represents the average value of the 4 experiments (HPA (A), HPA (B), HPA (C)).

Similarly, 3 different batches of LPA *Serratia* cells were fermented under the same conditions (LPA (A), LPA (B) and LPA (C)). The fermentation experiments for each of the above batches were repeated four times under the same conditions. Each one of the four experiments for each different batch consisted of 186 ml of cells placed in Erlenmeyer flasks and incubated at constant temperature (24 °C) in a water bath with rotary shaker. A water bath and rotary shaker were used to ensure the temperature remained constant throughout the experiments and the cells would be equally dispersed in solution. The 250 ml Erlenmeyer flasks containing cell solution were fermented by daily dosages of 1.86 ml with: ca 10 mM G2P, 4 mM $CaCl_2$ and 2 mM $Na_2C_6H_60_7$ in order to accumulate PHB and HA.

Fermentation experiments of 48, 120, 216 and 360 h durations were conducted with HPA and LPA cells in order to accumulate PHB and HA. The experiments conducted with HPA and LPA *Serratia* sp are presented in Table 7.

Table 7: Experiments conducted with HPA and LPA *Serratia* sp. at varying fermentation periods.

Fermentation period (h**)**	**Experiment**	**Phosphatase activity** (nmol *p*NP**)**	
48	HPA(A)	3851	
	HPA(B)	3730	
	HPA(C)	3823	
	LPA(A)		486
	LPA(B)		490
	LPA(C)		533
120	HPA(A)	3851	
	HPA(B)	3730	
	HPA(C)	3823	
	LPA(A)		486
	LPA(B)		490
	LPA(C)		533
216	HPA(A)	3851	
	HPA(B)	3730	
	HPA(C)	3823	
	LPA(A)		486
	LPA(B)		490
	LPA(C)		533
360	HPA(A)	3851	
	HPA(B)	3730	
	HPA(C)	3823	
	LPA(A)		486
	LPA(B)		490
	LPA(C)		533

2.2.1. *Serratia* sp. *fermented for 48 h*

The cells were fermented for 48 h as many species of PHB accumulating bacteria have been reported to require 48 h to accumulate optimum yields of PHB [7]. It may be possible for *Serratia* sp. to accumulate PHB after 48 h fermentation. For the 48 h fermentations the cells

were dosed with stock solutions at 24 h intervals. The experimental conditions for each of the fermentation experiments are outlined in Table 8 and 9.

Table 8: Experimental conditions for the production of PHB and HA from HPA *Serratia* sp. fermented for 48 h.

	48 h fermentation with HPA cells											
	HPA(A)				**HPA(B)**				**HPA(C)**			
Replicas	1	2	3	4	1	2	3	4	1	2	3	4
DWC (mg)	319	405	324	400	313	407	323	397	284	442	397	329

Table 9: Experimental conditions for the production of PHB and HA from LPA *Serratia* sp. fermented for 48 h.

	48 h fermentation with LPA cells											
	LPA(A)				**LPA(B)**				**LPA(C)**			
Replicas	1	2	3	4	1	2	3	4	1	2	3	4
DWC (mg)	357	445	436	366	386	418	379	441	384	421	429	377

2.2.2. *Serratia* sp. *fermented for 120 h*

The cells were fermented for 120 h and were dosed with 1.86 ml of stock solutions at 24 h intervals. The 120 h experiments were carried out with HPA and later with LPA cells. The experimental conditions for each of the experiments are outlined in Table 10 and 11.

Table 10: Experimental conditions for the production of PHB and HA from HPA *Serratia* sp. fermented for 120 h.

	120 h fermentation with HPA cells											
	HPA(A)				**HPA(B)**				**HPA(C)**			
Replicas	1	2	3	4	1	2	3	4	1	2	3	4
DWC (mg)	307	339	393	425	309	266	356	411	370	387	424	357

Table 11: Experimental conditions for the production of PHB and HA from LPA *Serratia* sp. fermented for 120 h.

	120 h fermentation with LPA cells											
	LPA(A)				**LPA(B)**				**LPA(C)**			
Replicas	1	2	3	4	1	2	3	4	1	2	3	4
DWC (mg)	307	339	393	425	309	266	356	411	370	387	424	357

2.2.3. *Serratia* sp. *fermented for 216 h*

The cells were fermented for 216 h and dosed with 1.86 ml of stock solutions at 24 h intervals. The 216 h fermentation experiments were carried out with HPA and later with LPA *Serratia* sp. It was suggested by Kashani 2007 that 216 h fermentation resulted in the greatest accumulation of PHB [77]. The experimental conditions for each of the experiments are outlined in Table 12 and 13.

Table 12: Experimental conditions for the production of PHB and HA from HPA *Serratia* sp. fermented for 216 h.

	216 h fermentation with HPA cells											
	HPA(A)				**HPA(B)**				**HPA(C)**			
Replicas	1	2	3	4	1	2	3	4	1	2	3	4
DWC (mg)	345	401	364	382	368	402	375	395	450	383	416	348

Table 13: Experimental conditions for the production of PHB and HA from LPA *Serratia* sp fermented for 216 h.

	216 h fermentation with HPA cells											
	LPA(A)				**LPA(B)**				**LPA(C)**			
Replicas	1	2	3	4	1	2	3	4	1	2	3	4
DWC (mg)	330	356	396	422	315	371	395	291	276	342	468	396

2.2.4. *Serratia* sp. *fermented for 360 h*

The cells were fermented for 360 h and dosed with 1.86 ml of stock solutions at 24 h intervals. The experimental conditions for each of the fermentation experiments with HPA and LPA cells are outlined in Table 14 and 15, respectively.

Table 14: Experimental conditions for the production of PHB and HA from HPA *Serratia* sp fermented for 360 h.

	360 h fermentation with HPA cells											
	HPA(A)				**HPA(B)**				**HPA(C)**			
Replicas	1	2	3	4	1	2	3	4	1	2	3	4
DWC (mg)	357	445	436	366	386	418	379	441	384	421	429	377

Table 15: Experimental conditions for the production of PHB and HA from LPA *Serratia* sp fermented for 360 h.

	360 h fermentation with LPA cells											
	LPA(A)				**LPA(B)**				**LPA(C)**			
Replica experiments	1	2	3	4	1	2	3	4	1	2	3	4
DWC (mg)	392	430	387	435	386	426	372	440	378	490	327	440

2.3. *Preparation of Ralstonia eutropha for the production of PHB*

2.3.1. *Chemicals*

K_2HPO_4 and KH_2PO_4 were purchased from Fischer scientific Ltd., Loughborough, UK while KNO_3, $(NH_4)2SO_4$, $MgSO_4.7H_2O$, NaCl, $CaCl_2$, $CuSO_4.5H2O$, $MnSO_4.5H_2O$, $ZnSO_4.5H_2O$, $FeSO_4$, $(NH_4)6M0_7O_{24}.4H_2O$ were purchased from BDH chemicals. Chloroform ($CHCL_3$)and Hexane (HPLC grade) were obtained from Sigma Aldrich, UK.

2.3.2. *R. eutropha H16* (NCIMB 10442, ATCC 17699)

R. eutropha cells were obtained from the National Collection of Industrial and Marine Bacteria, Aberdeen, UK. The stock culture was freeze dried and kept at -20 °C. In order to use the cells for fermentation experiments they were first revived and grown overnight at 30 °C, after which the organism was sub cultured on TSA media and incubated for 24 h at 30 °C.

2.3.3. *Media Preparation*

Tryptone soya agar (TSA) and tryptone soya broth, (TSB) supplied by Lab M Ltd., UK, and were prepared following instructions provided by manufacturer under aseptic conditions. Basal salt medium (BSM) supplied by Lab M Ltd., UK was used as described by Verlinden (unpulished work 2009) [27]. TSB and TSA were used for the shake flask fermentations and for growth analysis, respectively. TSB was prepared by dissolving 30 g of media in 1000 ml of distilled water using a magnetic stirrer (VELP Scientifica); 20 ml of the media was then transferred to 50 ml conical flask and autoclaved for 15 min at 121 ^oC. TSA was prepared by dissolving 37 g of media in 1000 ml of solution and autoclaved for 15 min at 121 ^oC before it was aseptically poured into Petri dishes and allowed to solidify. BSM was used for the fermentation experiments with oil and glucose. The composition of the BSM for cell growth medium is as follows: 1 g/l K_2HPO_4 (BDH Ltd,), 1 g/l KH_2PO_4 (Fishers Scientific Ltd), 1 g/l KNO_3 (Fishers Scientific Ltd), 1 g/l $(NH_4)_2SO_4$ (Fishers Scientific Ltd), 0.1 g/l $MgSO_4.7H_2O$

(BDH Ltd,), 0.1 g/l NaCl (Sigma Aldrich chemicals Ltd,) and 10 ml/l trace elements solution. The trace elements solution consisted of 2 mg/l $CaCl_2$ (Acros organics Ltd,), 2 mg/l $CuSO_4.5H_2O$ (BDH Ltd,), 2 mg/l $MnSO_4.5H_2O$ (Sigma Aldrich chemicals Ltd,), 2 mg/l $ZnSO_4.5H_2O$ (BDH Ltd,), 2 mg/l $FeSO_4$ (Sigma Aldrich chemicals Ltd,) and 2 mg/l $(NH4)6Mo_7O_{24}.4H_2O$ (BDH Ltd,). The final pH of the medium before autoclaving was 6.8. Volumes of 220 ml and 230 ml of the prepared media were transferred into 500 ml conical flasks and were autoclaved for 15 min at 121 ^oC. Ringer's solution (Lab M, UK) was made by the addition of distilled water and diluted to 1/4 strength. All media used was sterilised by means of autoclaving at 121 °C for a period of 15 min.

2.3.4. *Carbon Sources*

Three different carbon sources were utilised individually for the production of PHB. These carbon sources included rapeseed oil (purchased from ASDA supermarket), olive oil (purchased from Tesco stores, Wolverhampton) and glucose (Lab M Ltd, UK). The fat composition of the oil substrates are presented in Table 16.

Table 16: Types of fat contained in 100 ml of the different oils used as carbon sources for the production of PHB (data obtained from product information labels for the respective oil).

	Rapeseed oil (g)	**Olive oil (g)**
Saturated fat	7	13
Monounsaturated	54	66.36
Polyunsaturated	30	7.45

2.3.5. *Starter culture preparation*

Single colonies of *R. eutropha* were inoculated into 50 ml conical flasks containing 20 ml of TSB medium. All inoculated media were incubated aerobically for 24 h in a rotary incubator (New Brunswick Scientific, UK) at 30 ^oC and 150 rpm. They were then used as starter

cultures for fermentation experiments. The cultures were examined for purity by means of gram staining and microscopic observations at 1000x.

2.3.6. *Fermentations*

The fermentation media were each inoculated aseptically with 20 ml of the respective starter culture resulting in an inoculation ratio of 8 %v/v (%Volume/Volume). Fermentations for each carbon source were carried out in triplicates using 500 ml Erlenmeyer flasks. Each flask inoculated with oil consisted of 220 ml of BSM media, 20 ml of starter culture and 5 g/l (~10 ml) of the respective substrate. The oils were sterilised at 121 ^{o}C for 15 min. 5 g (approximately 10mls) of the respective oil was used to make an emulsion with BSM by sonication. The sonicator (Bandelin electronic, UW 2200) was set at 0.5 active and 0.5 passive intervals with a power of 60 % with the tapered tip for 7 min. This was as oil is immiscible in BSM and so had to be sonicated. This resulted in a final concentration of 20 g/l of the oil in each fermentation media. As the glucose substrate used was miscible in water it could be easily dissolved within the media. 5 g of glucose was dissolved with BSM giving a final concentration of 20 g /l. The medium was plated out by spread plating 100 µl of medium on TSA to test for the sterility of the media. The control flask however consisted of 230 ml of BSM, 20 ml of starter culture and no substrate. The flasks were placed in a rotary incubator at a speed of 150 rpm and a temperature of 30 ^{o}C for 48 h.

2.3.7. *Bacterial Growth*

The growth of bacteria was measured by conducting Miles and Misra technique. The samples were taken from aliquots at 0, 3, 6, 24 and 48 h of incubation and were collected aseptically into sterile Eppendorf tubes. A dilution of 10^{-1} was made up with 0.5 ml of sample transferred into a test tube containing 4.5 ml of sterile Ringer's solution. Serial dilutions were then made up to 10^{-8} for each test tube. Each flask was allocated two agar plates containing TSA that

were divided into four sections, one section per dilution. The agar plates were labelled 10^{-1} to 10^{-4} on one plate and 10^{-5} to 10^{-8} on the second plate. A Vortex mixer (Stuart, SA7) was used to adequately mix the contents of each tube. After mixing, 20 µl from each tube was inoculated aseptically onto the applicable section of each plate in triplicate by the use of a pipette. The plates were left until dried and then inverted and placed within an incubator (Laboratory Thermal Equipment Ltd, Greenfield) for 24 h at a temperature of 30 ^{o}C. After incubation, colony counts were taken, where the average count for each dilution was determined. All experiments were conducted three times and the results were expressed as $\log_{10}$ cfu/ml. The following formula was used to calculate the concentration of the undiluted sample:

$$\frac{cfu}{ml} = \text{ANC x } 50 \text{ x} \frac{1}{\text{df}} \qquad \textbf{Equation 3}$$

Where ***cfu/ml*** = colony forming unit per volume unit, **ANC**= average number of colonies and ***df*** = dilution factor.

The average concentration per sample was calculated and expressed as $\log_{10}$*cfu/ml* of undiluted sample. The average concentration of each sample was plotted against time to obtain a bacteria growth curve.

2.4. *Extraction*

2.4.1. *Extraction of PHB and HA from Serratia sp.*

After fermentation, the biomass and associated products (HA and PHB) were transferred to 50 ml centrifuge tubes and harvested by centrifugation (20 min at 8,000 rpm). The cells were washed with isotonic saline and air dried on a watch glass for 24 h in a fume cupboard (Figure 17).

Figure 17: Wet biomass left to dry on a pre-weighed watch glass.

The dried biomass was placed in a Soxhlet thimble (supplied by Ahlstrom, small cellulose thimble 25 x 80) for extraction. The Soxhlet extraction apparatus (200 ml of $CHCl_3$) was used in order to extract the polymer (At 80 °C for 7 h) and separate it from the dried biomass and HA (24 h).

After extraction, the resulting $CHCl_3$ was concentrated using a rotary vacuum evaporator. The polymer dissolved in $CHCL_3$ (~ 2 ml) was precipitated in a 500 ml beaker with equal volumes of n-hexane cooled to 4 °C to aid the polymer precipitation process. The precipitated polymer in solution was separated by centrifuged at 6,000 rpm for 5 min using a refrigerated centrifuge (Hermle Labortechnik, Z300K). After centrifugation a pellet of PHB was formed and the supernatant solution was disposed of. The PHB pellet was placed on a pre-weighed watch glass and air dried until a constant weight was reached. The HA and biomass contained within the Soxhlet thimble was placed in a fume cupboard and left to dry for >24 h. The %w/w of PHB produced from the bacteria was calculated using the following equation:

$$\%\, PHB \;= \frac{Weight\ of\ extracted\ polymer}{Cell\ dry\ weight}\ X\ 100 \qquad \textbf{Equation 4}$$

2.4.2. *Extraction of PHB from R. eutropha*

After the 48 h fermentation period, the samples were transferred from conical flasks into 50 ml centrifuge tubes and centrifuged (Hermle Labortechnik, Z300K) for 15 min at 6,000 rpm. The supernatant was discarded and the biomass was kept in the freezer overnight at ~20 ^{o}C. The biomass was then placed in a freeze drier (Edwards Freeze drier, Modulyo) for 72 h. The dried biomass was weighed out and then placed in a Soxhlet thimble for extraction with HPLC grade $CHCl_3$ (Acros organic). Soxhlet extraction was carried out in a fume cupboard and was left to run for 5 h.

After the extraction process the resulting $CHCl_3$ was precipitated with equal volumes of n-hexane (Sigma Aldrich) in a 500 ml beaker, a magnetic stirrer was used to aid the precipitation process. The precipitated polymer was extracted from solution using filter paper (Whatman No.1 paper) funnel and left to dry in air before being weighed.

2.5. *Electrospinning*

2.5.1. *Electrospinning apparatus*

The electrospinning apparatus used in this study was a custom built set up. The electrospinning set up was placed in a Perspex box in order to protect the operator from any risk associated with high voltages that the machine outputs. The apparatus was set up within a fume cupboard, this was necessary due to the use of $CHCl_3$ as a solvent when electrospinning PHB. The fume cupboard also provided an extra layer of protection against the risk of being injured by electric shock. The central part of the machine consisted of a standard 10 ml syringe (Cole Palmer Ltd, UK) in which the polymer solution was added. The polymer solution was driven out of the syringe using a NE-300 single syringe pump (Pump systems, Inc., UK) with a dispensing accuracy of +/- 1 %.

A metal 25 gauge syringe needle (Sigma Aldrich Ltd., UK) was attached to the syringe, which acted as the first electrode. The syringe needles were grinded down to produce a blunt needle tip allowing for greater tailor cone formation. The collector plate consisted of a steel sheet covered with aluminium foil. The collector plate was placed directly underneath the syringe to receive the fibre mesh, which acted as the second electrode. The electrodes were connected to the high voltage power supply system. The high voltage power supply used in this study (Genvolt Ltd., UK) (model 73030P) allowed for voltages as high as 30 kV with a direct current (DC) of 1 mA. In order to confirm the accuracy of the voltage provided by the power supply system, a multimeter (Rapid Ltd., UK) was also used.

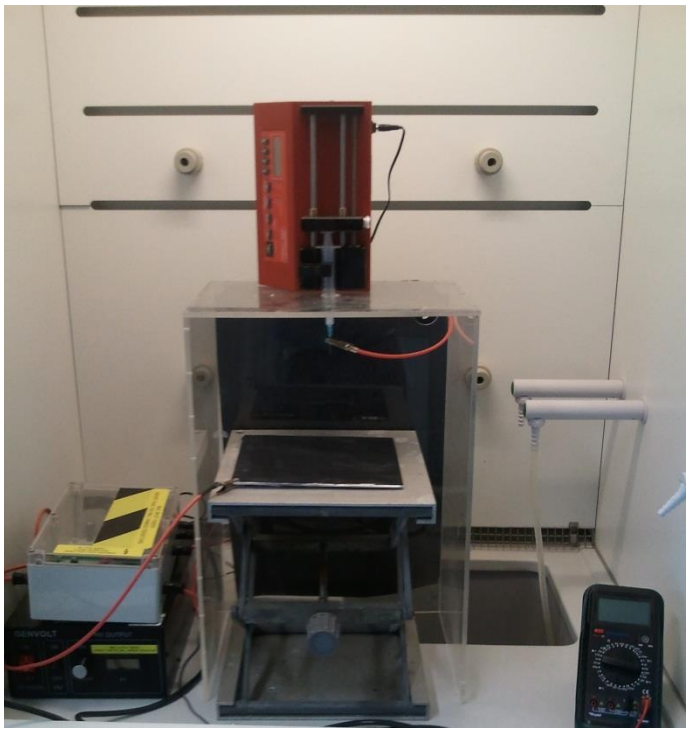

Figure 18: Electrospinning apparatus set up within a fume cupboard.

2.5.2. *Processing parameters*

Many processing parameters are capable of influencing the properties of the electrospun fibres. The applied voltage is an important variable. The voltage was set at 7 kV for all experiments this was as previous attempts to produce electrospun PHB at other voltages were unsuccessful. The voltages that were used in literature for electrospinning PHB were also reported to be ~8 kV [214]. The flow rate of the polymer solution out of the syringe is another important variable. The flow rate could be easily adjusted on the single syringe pump (NE-300). The flow rate was adjusted to a rate at where the fluid forced into the drop equals the average rate at which the fluid was carried away by the jet to create a stable system. In this study a flow rate of 1 ml/h was used. The distance between the needle tip and the collecting plate was another important parameter to consider [151]. In all experiments the distance was maintained at 12.5 cm. This was decided based on previous preliminary experiments. The distance between the needle tip and the collecting plate was adjusted using a manually controlled rising platform. The fume cupboards ventilation system was switched off for the periods in which electrospinning was taking place. This is as the airflow influences the electrospinning process by affecting the evaporation rate and path of the jet [151, 157].

2.5.3. *Experimental protocol*

In this section the steps followed during each electrospinning experiment are outlined. Initially the polymer solution was drawn into a syringe (around 5 ml) and excess air was removed. The electrodes were then connected to a high voltage power supply while ensuring the collecting plate was covered with a sheet of aluminium foil and placed upon the rising platform below the needle tip. The flow rate of the single syringe pump was set to 1 ml/h and the high voltage power supply and single syringe pump were then turned on.

2.5.4. *Preparation of PHB solutions*

PHB from various carbon sources was obtained from the fermentations of *R. eutropha* as previously described in section 2.3.6. Three individual samples of PHB were produced and used in order to produce nanofibres of G-PHB (PHB produced from glucose), O-PHB (PHB produced from olive oil) and R-PHB (PHB produced from rapeseed oil). For each PHB sample three separate solutions were made up at 1.5, 2 and 2.5 %w/v (% weight/Volume). To ensure reproducibility, experiments for each concentration were carried out in triplicate using two different preps. The appropriate mass of PHB was dissolved in 5 ml of $CHCl_3$. The polymer solution was then placed on a magnetic stirrer overnight as to ensure all PHB was fully dissolved in $CHCl_3$.

2.6. *Characterisation techniques*

2.6.1. *Fourier transform infrared spectroscopy (FTIR)*

Fourier transform infrared spectroscopy (FTIR) is an analytical technique that collects spectra based on the temporal coherence measurements from an infrared source. It is primarily used for identifying unknown substances by producing an infrared absorption spectrum that can identify chemical bonds present in the molecule. Samples of PHB and HA were identified using a Nicolet FTIR spectrometer (MGNA-IR 860) with a golden gate single reflection diamond Attenuated total reflectance (ATR) attachment.

The spectra for PHB and HA extracted from *Serratia* sp. were characterised and compared against the spectra of commercial PHB (24862200, Sigma-Aldrich Ltd., UK) and HA (Part number: 289396, Sigma-Aldrich Ltd., UK) reference samples. The commercial sample of PHB and HA were treated with chloroform and hexane for a period of 24 h. This was to ensure both samples were accurately compared.

FTIR spectra were obtained for PHB extracted from *R. eutropha* cells and were compared to electrospun samples, this was in order to observe whether the chemistry of the polymer was

modified by the elctrospinning process. It is possible that the chemical composition of the electrospun fibres may be altered under high voltage during the electrospinning process [215].

2.6.2. *Differential scanning calorimetry (DSC)*

Differential scanning calorimetry (DSC) is a thermo-analytical technique that is used to assess the energy difference that is required to raise the temperature of a given sample. DSC can be used to observe phase transitions that occur during the heating and cooling process. The phases that are observed include the T_g, melting temperature (T_m), and crystallisation temperature (T_c). DSC experiments were carried out using a Perkin-Elmer DSC7 instrument. For each sample ~5 mg of the extracted polymer was placed in a covered aluminium pan, a covered empty pan was used as a reference. The DSC traces were performed from 30 ^{o}C to 200 ^{o}C at a heating rate of 10 °C/min and was initially held at 30 °C for 5 min to stabilise the equipment. The sample was then held at 200 °C for 1 min and then cooled from 200 °C to 30 °C at a rate of 10 °C/min.

DSC analysis was carried out on PHB extracted from HPA and LPA *Serratia* sp. after fermentations of 24, 120, 216 and 360 h. The extracted polymers were compared to the DSC trace obtained for commercial PHB. The reference sample was treated the same as the extracted PHB by being dissolved in $CHCl_3$ and consequently precipitated in n-hexane.

DSC analysis was carried out on electrospun nanofibres of G-PHB, O-PHB and R-PHB at concentrations of 1.5, 2 and 2.5 %w/v. The DSC traces were compared to those obtained for non-electrospun samples of G-PHB, O-PHB and R-PHB extracted from *R. eutropha* cells. The DSC analysis will provide information regarding the arrangement of polymer chains and also any changes in crystallinity of the fibres after electrospinning.

The degrees of crystallinity (%) of the PHB samples were calculated using the following equation:

$$C(\%) = \frac{H_f^m}{H_f^{100\%}} \times 100 \qquad \textbf{Equation 5}$$

Where **C** is the % crystallinity, $\boldsymbol{H_f^m}$ is the measured heat of fusion (J/g), and $\boldsymbol{H_f^{100\%}}$ = enthalpy of fusion (for fully crystalline PHB = 146 J/g [216]) and assuming that no cold crystallisation on heating was observed.

2.6.3. *Gel permeation chromatography (GPC)*

Gel permeation chromatography (GPC) is a chromatographic technique that separates particles based on their molecular size in solution. It is used to measure the M_w distribution of organic-soluble polymers and involves the use of an organic solvent as a mobile phase.

A single solution of the sample was separated by adding 10 ml of $CHCl_3$ to 20 mg of sample. The solution was left overnight to dissolve before being filtered through a 0.2 µm polyamide membrane. The sample was analysed at a flow-rate of 1.0 ml/min using PLgel guard plus 2 mixed bed-B columns with a 1.0 ml/min (nominal) flow rate at 30 °C was used. The chromatography was carried out in duplicate Cirrus GPC (Version 3.2) software by polymer laboratories and was used to produce the GPC calibration curve from where the weight average M_w and the number average M_n were obtained. The PD of the polymers was calculated using the formula $\mathbf{PD = M_w/M_n}$ [217]. GPC was used to compare the M_w of PHB extracted from *Serratia* sp. after fermentations of 24, 120, 216 and 360 h and were compared to a commercial reference sample of PHB. GPC was also carried out on electrospun nanofibres of G-PHB, O-PHB and R-PHB at concentrations of 1.5, 2 and 2.5 %w/v. Those were compared with non-electrospun samples of G-PHB, O-PHB and R-PHB extracted from *R. eutropha*.

2.6.4. *Scanning electron microscopy (SEM)*

The Philips XL 30 ESEM FEG was used in order to observe high resolution images of HA formation on the surface of *Serratia* sp. and also high resolution images of electrospun PHB nanofibres.

The *Serratia* cells were dehydrated with increasing concentrations of alcohol. The dehydrated cells were then coated with platinum using a Polaron SC 7640 Sputter coater at a current of 25 mA for 3 min and mounted onto an aluminium stub with the aid of adhesive carbon film. SEM was also carried out on electrospun PHB fibre meshes. Small sections of fibres were cut out from the centre of the electrospun PHB fibre mesh for each sample. Samples were placed on an aluminium stub with the aid of adhesive carbon film. The samples were then coated with platinum using a Polaron SC 7640 Sputter coater at a current of 25 mA for 3 min. For each electrospun sample three different areas were selected in order to measure the fibre diameters. Average fibre diameter values were obtained from measuring 120 random fibre diameters from each sample using Image J software (National institute of Health, USA).

2.6.5. *Transmission electron microscopy (TEM)*

Transmission electron microscopy (TEM) is a microscopy technique whereby a beam of electrons is transmitted through an ultra-thin specimen, interacting with the specimen as it passes through. TEM was carried out using the JEOL TEM-1200x using HPA and LPA *Serratia* sp. During fermentation experiments of 48, 120, 126 and 360 h periods ~1 ml of *Serratia* cells was extracted from the cell solution. This was in order to observe inclusion bodies of PHB during various fermentations.

Sample preparation:

Aliquots of *Serratia* cells in solution were taken during periods of PHB accumulation at various fermentation periods and placed in individual Eppendorf tubes. The Eppendorf tubes

containing *Serratia* cells in solution were centrifuged for 5 min at 3,000 rpm, the supernatant was discarded leaving a pellet (biomass). The cells were then fixed with glutaraldehyde fixative and left for 1 h. After, which the Eppendorf tubes were centrifuged once again and the supernatant (Glutaraldehyde) discarded leaving a pellet. Osmium tetroxide fixative was then added to the Eppendorf tubes and left for 1 h as to allow it to be absorbed by the cells. The Eppendorf tubes were centrifuged in order to remove the osmium tetroxide. Increasing concentrations of alcohol were then added to the Eppendorf tubes as to dehydrate the cells. Increasing concentrations of alcohol 70 %, 90 %, 100 % and dried 100 % were added to the Eppendorf tubes and left for 15 min at a time, starting with 70 % alcohol. After the cells were fully dehydrated propylene oxide was added and left for 1 h. The propylene oxide was removed from the Eppendorf tubes by centrifugation. A mixture of propylene oxide resin at a 1:1 ratio was added to the Eppendorf tubes and left for 45 min. The polypropylene oxide/resin solution was removed from the Eppendorf tubes by centrifugation leaving a pellet of biomass. The Pellet was placed under the surface of pure resin in embedding moulds. The Eppendorf tubes containing the resin were placed in a vacuum embedding oven and left under vacuum for 20 min. The cells were later embedded in resin at the tip of the Eppendorf tubes and left under vacuum overnight.

The resin block was then removed from the Eppendorf tubes casing and trimmed to the shape of a trapezium (Figure 19). The resin block was placed in the Reichert ultra-cut microtome in order for ultra-thin sections to be taken.

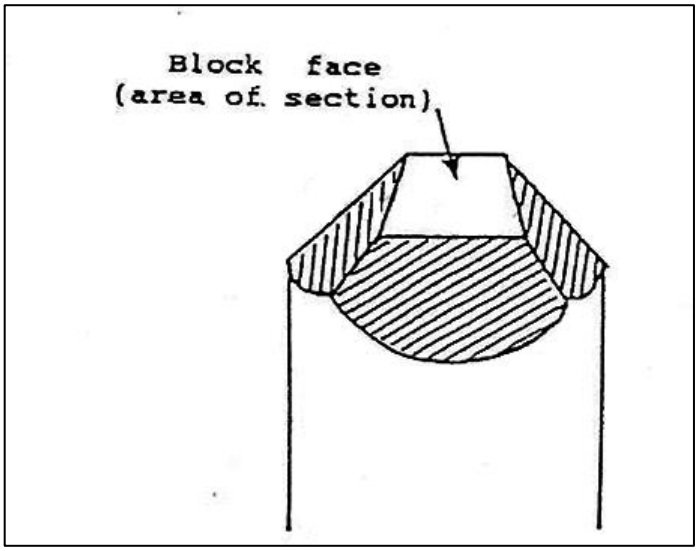

Figure 19: Resin Block with face trimmed to a trapezium.

A glass knife was placed in the microtome and secured before cutting the resin face in order to obtain ultra-thin sections. The glass knife assembly was pushed close to the block face with the aid of the binocular microscope attached to the microtome. The knife edge was adjusted so that it was parallel to the bottom edge of the block face (Figure 20). The automatic cutter allowed for the thickness of the sections to be adjusted to between 50 nm and 80 nm. The cut sections were expanded on filter paper and placed carefully on the dull side of aluminium grids.

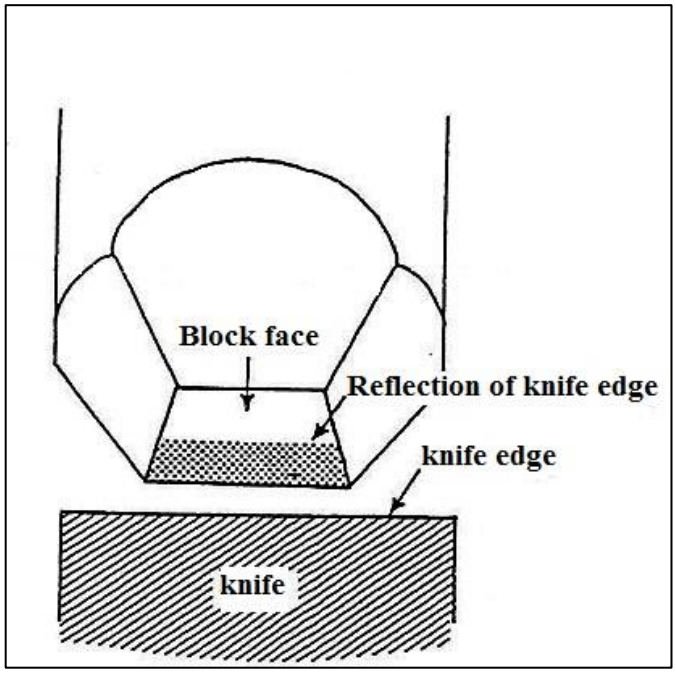

Figure 20: The edge of the glass knife was placed parallel to the bottom edge of the block face in order to obtain ultra-thin sections.

The grids containing the cut sections were required to be stained. This was carried out by leaving the aluminium grids in 30 % uranyl acetate for 7 min. The grids were then washed with sonicated ultra-pure water before being placed in 7 ml of lead citrate for 7 min. The grids were then washed with sonicated ultra-pure water. The excess water was removed using a filter paper and were ready for TEM analysis.

2.7. *Statistical analysis*

Graphpad Prism 5 was used for the statistical analysis. Two way ANOVA with Bonferroni multiple comparison test was used to analyse the difference in cell count of *R. eutropha* in various substrates at specific growth times with a P-value of < 0.05. It was also used to analyse the difference in the crystallinity of electrospun and non-electrospun polymers from all carbon substrates and the differences in the overall average yields of PHB and HA from various fermentation periods using LPA and HPA cells. Two way ANOVA with Bonferroni

multiple comparison test was also used to calculate the difference in fibre diameter of PHB from different carbon sources at different concentrations with a P-value of < 0.05.

Chapter 3 : Results and Discussion

The Production of PHB and HA from *Serratia* sp.

3.1. *Introduction*

To maximise the yields of PHB and HA accumulated by Serratia sp. experimental conditions were replicated from Kashani 2007 [28, 77]. Kashani showed that Serratia sp. fermented for 216 h produced PHB yields as high as 26.6 %w/w compared to 96 h (2.96 %w/w) and 408 h (2.96 %w/w) fermentations [77]. However, Kashani conducted experiments using HPA Serratia sp. with no replicas. These experiments will be repeated with replicas in order to accurately determine the fermentation time that results in the maximum yields of PHB and HA. The role of the phosphatase enzyme in the production of intracellular PHB has not been previously reported. For this reason PHB and HA will be accumulated from both HPA and LPA Serratia sp. The yields of PHB and HA from HPA and LPA Serratia sp. will be compared as a means of determining whether phosphatase activity has any effect on the yields of accumulated PHB and HA. The extracted PHB will be characterised and compared to commercial PHB in order to determine whether any changes have occurred to the thermal and molecular properties. The extracted biomineral from Serratia sp. will be characterised in order to confirm the presence of HA and will be compared to a commercial sample of HA.

3.2. *Experiments with HPA and LPA Serratia* sp

Fermentation experiments were conducted with HPA and LPA *Serratia* cells for 48, 120, 216 and 360 h time periods in order to accumulate yields of PHB and HA.

3.2.1. *Recovered yields of PHB and HA after 48 h fermentation*

The 48 h experiments with HPA and LPA *Serratia* sp. were dosed with stock solutions at 24 h intervals. The HPA(A), (B) and (C) consisted of four replicas each (1,2,3,4). The average yields of PHB and HA from HPA(A), (B) and (C) are presented in Table 17 along with their relevant standard error values.

Table 17: Average yields of PHB and HA from HPA cells recovered after 48 h fermentation.

	HPA(A)	HPA(B)	HPA(C)
HA recovered (mg)	598 ± (45.4)	595 ± (9.9)	594 ± (11.9)
PHB recovered (mg)	4 ± (0.8)	4 ± (1.6)	5 ± (0.8)

The average yields of PHB and HA produced from HPA(C), HPA(A) and HPA(B) were all within the same region.

After 48 h of fermentation HPA(C) on average produced 5 mg ± 0.8 of PHB representing ~2 % weight by weight (w/w) compared to the dry cell weight. (dry weight of extracted PHB/dry weight of cells x 100).The average yields of PHB from HPA(A) and (B) were identical at 4 mg and represented 1 and 2 %w/w, respectivley.

The average yields of HA from HPA (A), (B) and (C) were similar, at 598 mg ± 45.4 representing ~ 165 %w/w, 595 mg ± 9.9 representing ~ 164 %w/w and 594 mg ± 11.9 representing ~ 164 %w/w, respectively. The standard error value for HPA(A) was considerably greater compared to HPA(B) and (C) after 48 h of fermentation.

LPA(A), (B) and (C) experiments each consisted of four replicas (1,2,3,4). The average yields of HA and PHB were calculated from the replicas of LPA(A), (B) and (C) and are presented in Table 18 along with their standard error values. The recovered average yields of PHB from LPA(C) were considerably higher than those from LPA(A) and (B).

Table 18: Average yields of PHB and HA from LPA cells recovered after 48 h of fermentation

	LPA(A)	LPA(B)	LPA(C)
HA recovered (mg)	40 ± (11)	60 ± (19.9)	100 ± (21.2)
PHB recovered (mg)	10 ± (3.4)	5 ± (1.6)	25 ± (4.8)

The yield of HA recovered from LPA(A) at 40 mg ± 11 representing ~ 11 %w/w and was considerably less compared with LPA(C) at 100 mg ± 21.2 representing ~ 27 %w/w. This shows that there can be variations in HA production even when experimental conditions are kept identical.

The average yield of PHB recovered from LPA(C) was found to be 25 mg ± 4.8 which accounts for 7 %w/w. LPA(C) resulted in the greatest average yield of PHB compared to LPA(A) and (B) at 10 mg ± 3.4 representing ~ 3 %w/w and 5mg ± 1.6 representing ~1 %w/w, respectively.

3.2.2. *Recovered yields of PHB and HA after 120 h fermentation*

In the 120 h fermentations HPA and LPA *Serratia* sp. were dosed at 24 h intervals for 120 h with stock solutions.

The average yield of PHB and HA produced from HPA(A), (B) and (C) after 120 h of fermentation were calculated along with their standard error values and presented in Table 19.

Table 19: Yields of PHB and HA from HPA cells recovered after 120 h fermentation.

	HPA(A)	HPA(B)	HPA(C)
HA recovered (mg)	775 ± (64.8)	735 ± (31.8)	795 ± (53.7)
PHB recovered (mg)	5 ± (0.8)	5 ± (1.6)	2 ± (1.2)

The average yields of HA from HPA(A), (B) and (C) were found to be similar at 775 mg ± 64.8 representing 214 %w/w, 735 mg ± 31.8 representing 203 %w/w and 795 mg ± 53.7 representing 220 %w/w, respectively. HPA(A) and HPA(B) yielded identical values of recovered PHB at 5 mg ± 0.8 and 5 mg ± 1.6 respectivley and represent ~ 1 %w/w.

The average yields of HA and PHB were calculated from the replicas of LPA(A), (B) and (C) and are presented in Table 20 along with their standard error values.

Table 20: Yields of PHB and HA from LPA cells recovered after 120 h fermentation.

	LPA(A)	LPA(B)	LPA(C)
HA recovered (mg)	70 ± (9.1)	44 ± (6.6)	47 ± (13.6)
PHB recovered (mg)	20 ± (5.0)	70 ± (16.5)	50 ± (8.2)

The average yield of HA recovered from LPA(A) was greater than that from LPA(B) and LPA(C). LPA(A) produced 70 mg ± 9.1 of HA representing ~19 %w/w. The average yield of HA recovered from LPA(B) and LPA(C) were comparable at 44 mg ± 6.6 representing ~ 12 %w/w and 47 mg ± 13.6 representing ~13 %w/w, respectively. LPA(B) resulted in the greatest average yield of PHB at 70 mg ± 16.5 representing 18 %w/w. The lowest average yield of PHB was obtained from LPA(A) at 20 mg ± 16.5 ~5 %w/w while LPA (C) showed an average PHB yield of 50 mg ± 8.2 ~14 %w/w.

3.2.3. *Recovered yields of PHB and HA after 216 h fermentation*

In the 216 h fermentation experiments HPA and LPA *Serratia* cells were dosed nine consecutive times with stock solutions at 24 h intervals. The yields of HA and PHB recovered from the replicas of HPA(A), (B), (C) and LPA(A), (B), (C).

The average yields of HA and PHB after 216 h of fermentation were calculated from the replicas of HPA(A), (B) and (C) and are presented in Table 21 along with their standard error values.

Table 21: Average yields of PHB and HA from HPA cells recovered after 216 h of fermentation.

	HPA(A)	**HPA(B)**	**HPA(C)**
HA recovered (g)	2.36 ± (0.27)	2.20 ± (0.15)	3.42 ± (0.30)
PHB recovered (mg)	10 ± (1.6)	10 ± (0)	15 ± (2.4)

The average yield of HA recovered from HPA(C) was greater than those from HPA(A) and (B). HPA(C) on average produced 3.42 g ± 0.30 of HA representing ~944 %w/w. The average yield of HA recovered from HPA(A) and HPA(B) were almost identical with values of 2.36 g ± 0.27 representing ~651 %w/w and 2.20 g ±0.15 representing ~607 %w/w, respectively. The average yields of PHB from HPA(C) yielded the greatest recovered yields of PHB at 15 mg ± 2.4 representing ~4 %w/w. The lowest average yield of PHB was observed from HPA(B) and (C) at 10 mg ~3 %w/w.

The average yields of HA and PHB after 216 h of fermentation were calculated from the replicas of LPA(A), (B) and (C) and are presented in Table 22 along with their standard error values.

Table 22: Average yields of PHB and HA from LPA cells recovered after 216 h fermentation.

	LPA(A)	LPA(B)	LPA(C)
HA recovered (g)	1.89 ± (0.15)	3.08 ± (0.36)	1.40 ± (0.09)
PHB recovered (mg)	50 ± (9.1)	60 ± (15)	50 ± (6.6)

LPA(A) and (C) produced an average PHB yield of 50 mg ± 9.1 and 50 mg ± 6.6, respectively and represents 10 %w/w and 13 %w/w. LPA(B) presented a greater average yield of PHB at 60 mg ± 15 representing 16 %w/w. The average recovered yields of HA were greater in LPA(B) at 3.08 ± 0.36 representing 751 %w/w compared to LPA(A) and LPA(C). The average yield of HA recovered from LPA(C) was lowest at 1.40 g ± 0.09 representing ~ 341%w/w.

3.2.4. *Recovered yields of PHB and HA after 360 h fermentation*

In the 360 h of fermentations, HPA and LPA *Serratia* cells were dosed for 15 days with stock solutions at 24 h intervals. The yields of HA and PHB recovered from replicas of HPA(A), (B), (C) and LPA(A), (B), (C). The average yields of HA and PHB after 360 h of fermentation were calculated from the replicas of HPA(A), (B) and (C) and are presented in Table 23 along with their standard error values.

Table 23: Average yields of PHB and HA recovered from HPA cells after 360 h of fermentation.

	HPA(A)	HPA(B)	HPA(C)
HA recovered (g)	2.29 ± (0.27)	2.31 ± (0.47)	3.29 ± (0.14)
PHB recovered (mg)	8 ± (0)	9 ± (0.8)	5.5 ± (1.7)

The average yields of HA from HPA(A) and (B) were almost identical with values of 2.29 g ± 0.27 representing ~632 %w/w and 2.31 g ± 0.47 representing ~639 %w/w, respectively. The

greatest average yield of HA was obtained from HPA(C) with a value of 3.29 g ± 0.14 representing 908 %w/w. The average yield of PHB recovered was greatest in HPA(B) at 9 mg $\pm$ 0.8 representing ~2 %w/w, which was almost identical to 8 mg $\pm$ 0 recovered from HPA(A) representing ~2 %w/w. HPA(C) showed the lowest average recovered PHB at 5.5 mg ± 1.7 representing ~1 %w/w.

The average yields of HA and PHB after 360 h of fermentation were calculated from the replicas of LPA(A), (B) and (C).

The average yields of HA and PHB after 360 h of fermentation were calculated from the replicas of LPA(A), (B) and (C) and are presented in Table 24 along with their standard error values.

Table 24: Average yields of PHB and HA recovered from LPA cells after 360 h of fermentation.

	LPA(A)	**LPA(B)**	**LPA(C)**
HA recovered (g)	2.28 ± (0.10)	2.84 ± (0.08)	3.08 ± (0.09)
PHB recovered (mg)	10 ± (1.6)	10 ± (2.4)	5 ± (2.4)

The average yield of HA recovered from LPA(C) was 3.08 g ± 0.09 representing ~816 %w/w. The average recovered yield of HA from LPA(C) was 2.84 ± 0.08 representing ~784 %w/w. LPA(A) demonstrated the lowest recovered average yield of HA with a value of 2.28 ± 0.10 representing ~556 %w/w. LPA(A) and (B) resulted an average PHB yield of 10 mg ± 1.6 representing ~3 %w/w and 10 mg ± 2.4 also representing ~3 %w/w, respectively. The LPA(C) resulted in the lowest yield of PHB at 5 mg ± 2.4, representing only 1 %w/w.

3.3. *Comparison and discussion of the overall average yields of HA from LPA and HPA Serratia* sp.

The overall average yields of HA accumulated from HPA cells are compared with those from LPA cells for the given fermentations (i.e. 48, 120, 216 and 360 h) and are presented within a bar chart in Figure 21.

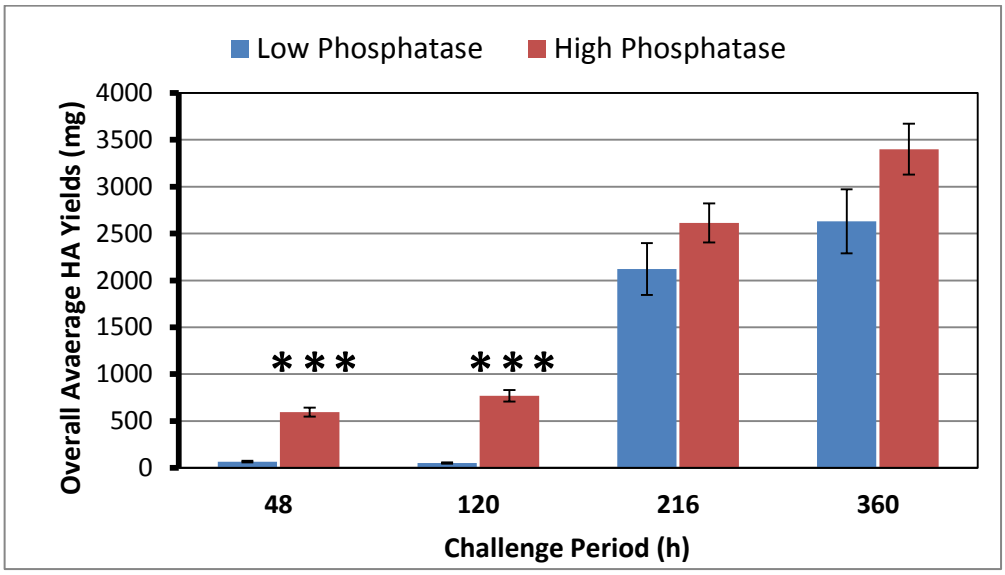

Figure 21: Bar chart accompanied with standard error values for the overall average yields of HA recovered from HPA and LPA cells after 48, 120, 216 and 360 h fermentations. Level of significance: one star (*) for 0.05, two (**) for 0.01, and three (***) for 0.001 or 0.005.

A notable difference was observed in the yields of HA from HPA and LPA *Serratia* sp. The overall average yield of HA from LPA cells after 48 h of fermentation was found to be 596 ± 2.1 mg (163 %w/w) compared with 67 ± 6.5 mg (18%w/w) from HPA cells. Statistical analysis (T test; $p < 0.05$) confirmed that there is a significant difference ($p = 0.000007$) between HA yields produced from HPA and LPA *Serratia* sp. The HPA cells fermented for 120 h resulted an overall average yield of 768 ± 30.6 mg (210 %w/w) whereas LPA cells yielded 54.0 ± 4.2 mg (14.8 %w/w). Statistical analysis confirmed that there is a significant difference ($p = 0.000003$) between HA yields produced from HPA and LPA *Serratia* sp.

A greater overall average yield of HA from HPA cells were observed after 216 h of fermentation. HPA cells yielded 2.61 ± 0.30 g (715 %w/w) whereas LPA cells yielded 2.12 ± 0.27 g (580 %w/w). Statistical analysis confirmed that there is no significant difference ($p = 0.485316$) between HA yields produced from HPA and LPA *Serratia* sp. after being fermented for 216 h. A fermentation period of 360 h showed a greater overall average yield of HA from HPA cells, which yielded 3.40 ± 0.41 g (931 %w/w) compared to LPA cells 2.63 ± 0.36 g (720 %w/w). Statistical analysis confirmed that there was no significant difference ($p =0.128746$) between HA yields recovered from HPA and LPA *Serratia* sp. after 360 h fermentation period.

The overall average yields of recovered HA from HPA and LPA cells were compared on the basis of their fermentation period. Statistical analysis (T test; $p < 0.05$) showed a significant difference between the recovered yields of HA from HPA and LPA cells after 48 h and 120 h fermentation. No statistical significant difference was observed between yields of recovered HA from HPA and LPA cells after 216 h and 360 h fermentation. As expected the greatest overall average yield of HA from LPA and HPA cells was observed after 360 h fermentation. The overall average yield of HA recovered from HPA cells was observed to be 3.40 ± 0.41 g (931 %w/w) compared to 2.63 ± 0.36 g (720 %w/w) for the LPA cells. The increase in phosphatase activity is observed to increase the production of HA, however after 216 h of fermentation the LPA cells produced a similar yield of HA to that obtained from HPA cells.

Kashani conducted similar experiments using HPA cells and reported similar recovered average yields of HA [77]. After 360 h of fermentation a maximum yield of 2.137 g of recovered HA was reported compared to the 3.41 g obtained from this study using HPA cells (LPA cells yielded 2.63 g). Kashani also reported an increase in the recovered HA over time. This trend was also observed in this study when using LPA and HPA cells. These results

suggest that the phosphatase activity of *Serratia* cells does have a significant effect on the initial production of HA. However, after longer fermentation periods the LPA cells begin to accumulate almost identical yields of HA compared to the HPA cells.

Serratia sp. are known to over produce an acid phosphatase enzyme located in the periplasmic space attached to fimbriae or other surface materials [169]. The phosphatase enzyme cleaves G2P, which liberates inorganic phosphate and provides the nucleation site for the growth of calcium phosphate crystals on the bacterial cell surface, biomineralization is controlled within spatial localisation of the biological space on and around cells [114]. It has been previously reported, that the yield of HA produced is heavily dependent upon the solution chemistry (G2P, $CaCl_2$) [203]. In this study a greater initial accumulation of HA was observed with HPA *Serratia* sp. compared to LPA cells. This was expected as the higher concentrations of phosphatase enzymes would cleave the G2P and liberate the inorganic phosphate which combine with calcium present within the cell solution to produce calcium phosphate crystals in the form of HA [28, 213]. *Serratia* sp. fermented for longer periods demonstrated a gradual increase in HA accumulation. This was expected as the daily additions of stock solutions (G2P and $CaCl_2$) over time would provide a constant supply of phosphate ions that would precipitate as extracellular HA on the cell surface.[115] However, after longer fermentation periods the LPA *Serratia* sp. showed similar accumulated yields of HA compared with HPA cells. The increased accumulation of HA after longer fermentation periods was not expected as the decreased in cell phosphatase activity meant that phosphate ions would not be liberated at the same rate as observed in HPA cells and hence would result in a lower accumulation of extracellular HA [213]. This increase in HA accumulation may be attributed to previously unreported enzymatic pathways involved in the liberation of phosphate ions from G2P, that would increase the concentration of free phosphate ions. Previous work by Macaskie *et al.* showed how *Serratia* cells with a phosphatase activity of ~4500 and ~2250 units produced

similar yields of HA. However, the differences in the specific phosphatase activities were considered to be compensated by an increase in phosphate ions concentration in the fermentation media [218].

3.4. *Comparison of overall mean yields of PHB from LPA and HPA cells*

The average recovered PHB from HPA(A),(B) and (C) and LPA(A),(B) and (C) were compared on the basis of their fermentation time. The overall average yields of recovered PHB from HPA cells are compared with those from LPA cells for given fermentations (i.e. 48, 120, 216 and 360 h) are presented within a bar chart in Figure 22.

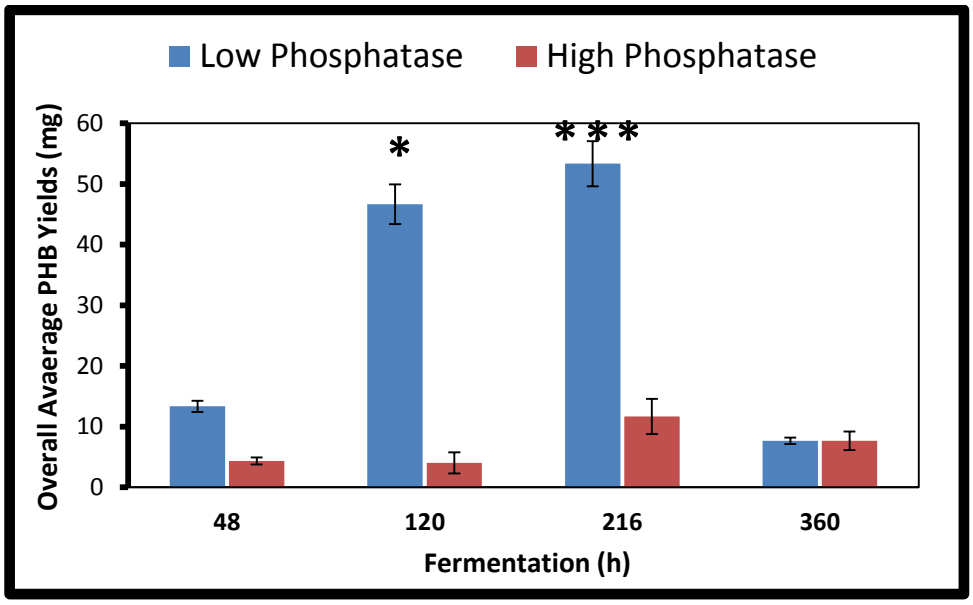

Figure 22: Bar chart accompanied with standard error values for the overall average yields of PHB recovered from HPA and LPA cells after 48, 120, 216 and 360 h fermentations. Level of significance: one star (*) for 0.05, two (**) for 0.01, and three (***) for 0.001 or 0.005.

The difference in overall average yields of PHB from HPA and LPA after 48 h fermentation was 13 ± 1.4 mg representing 6 %w/w compared to 4 ± 0.57 mg from HPA representing 1 %w/w. Statistical analysis (T test; $p < 0.05$) confirmed that there was no significant difference ($p = 0.208000$) between PHB yields produced from HPA and LPA *Serratia* sp. The

production of PHB has been researched in numerous bacterial species. The Institute of Microbiology affiliated to the Chinese Academy of Science produced PHB using *R. eutropha*, the cells were fermented for 48 h in glucose mineral medium. At the end of the fermentation, the cells yielded 80 %w/w PHB [219]. *Alcaligenes latus* grown in molasses medium has been found to accumulate PHB up to 90 %w/w and after 48 h fermentation, the cells were found to produce 72 %w/w [220]. These studies demonstrate that many strains of bacteria are capable of accumulating high yields of PHB after 48 h fermentation. A fermentation of 48 h is an ideal period for PHB accumulation at an industrial scale in order to maximise profitability. The LPA and HPA *Serratia* sp. clearly require longer fermentation in order to accumulate greater yields of PHB. After 48 h the *Serratia* sp. produced a maximal PHB yield of 6 %w/w. The fermentation conditions in this work were optimised for maximum production of HA rather than PHB which was a side product of the fermentation, the result of which, as expected, was lower yields of accumulated PHB in comparison to other studies [7, 64, 219]. In order to make the process viable for large scale production of PHB, the effect of additional carbon sources that could be used together with G2P, such as glucose should be examined in order to determine the optimum carbon source for PHB accumulation by *Serratia* sp. and what effect this addition would have on the mineralisation of HA.

Serratia sp. fermented for 120 h exhibited an overall average recovered yield of 47 ± 4.5 mg (13 %w/w) from LPA cells compared to 4 ± 0.4 mg (1 %w/w) from HPA. Statistical analysis confirmed a significant difference ($p = 0.042814$) between the PHB yields recovered from HPA and LPA *Serratia* sp.

A greater overall average yield of PHB from HPA and LPA cells was observed after 216 h of fermentation. The LPA cells yielded 53 ± 5.8 mg (15 %w/w) compared to 12 ± 1.9 mg (3 %w/w) from HPA cells. Statistical analysis resulted in a significant difference ($p = 0.000362$)

between the recovered PHB from HPA and LPA *Serratia* cells after 216 h of fermentation. Previous work carried out by Kashani, with identical fermentation conditions to this study, showed that 216 h fermentation also produced the greatest yield of PHB [77]. In these experiments HPA cells were utilised and yielded 90 mg of PHB equivalent to 26.6 %w/w. Those results support the findings of this study as 216 h of fermentation produced the greatest yield of PHB from LPA *Serratia* cells with a maximal yield of 16 %w/w (LPA(B)) [77]. However, the yields of PHB obtained from HPA cells in this study were found to be lower than reported by Kashani after 216 h fermentation producing a maximal yield of 3 % PHB w/w (HPA (C)) [77]. As the findings of Kashani were not repeated, they cannot be accurately compared to the results of this study consisting of replicas in order to validate the findings.

HPA and LPA *Serratia* cells fermented for 360 h resulted equal overall mean yields of PHB at 8 mg ± 1.1 (2 %w/w) and 8 mg ± 1.5 (2 %w/w) for LPA and HPA cells, respectively. Statistical analysis showed that there was no significant difference ($p = 0.741211$) between the yield of PHB obtained from HPA and LPA *Serratia* cells. After 360 h in both cases of LPA and HPA cells, the PHB production yield was significantly decreased. It was expected, that longer exposure of cells to a carbon source would result in greater accumulation of PHB. Many species of bacteria have been reported to have optimal concentrations of a carbon source, which will accumulate an optimum yield of PHB. Kim *et al*. reported that high concentrations of glucose as a carbon source can inhibit the growth and PHB accumulation in *R. eutropha* [27, 221].

Due to the lack of literature present, it is not yet clear as to what role the phosphatase enzymes play in the production of PHB in *Serratia* sp. The relative phosphatase activity of the cells should not directly affect the accumulation of PHB within the cell cytoplasm. The increase in PHB accumulation observed in LPA *Serratia* sp. may be attributed to the up regulated activity

of specific enzymes involved in PHB synthesis pathway as a consequence of the decreased phosphatase enzyme activity of the cells.

As outlined in the introduction, the PHB metabolic pathway (Figure 10) involves a series of enzyme-catalysed chemical reactions. Acetyl-CoA is generated by sugars and is involved in the first step of PHB production [55]. It is possible that the lack of phosphatase enzyme activity has a role in up regulating the activity of specific enzymes e.g pyruvate dehydrogenase that is involved in the conversion of pyruvate to acetyl-CoA. If this is the case it would result in *Serratia* sp. with LPA producing a greater quantity of acetyl-CoA. It has been shown that mutations that increase the level of acetyl-CoA act to increase the accumulation of PHB [7, 222, 223]. The presence of a mutation may help explain the decrease in PHB accumulation at 360 h, however greater research is necessary to confirm or deny this theory.

The Primary focus of this study was to produce high yields of PHB in order to characterise the thermal and molecular differences between the PHB from HPA and LPA cells after various fermentation periods. Further research is required in order to investigate the up regulation of specific enzymes within the PHA synthesis pathway in LPA cells compared with HPA cells.

3.5. *Characterisation of PHB extracted from Serratia* sp.

3.5.1. *Gel Permeation Chromatography*

GPC was carried out to determine the M_w, M_n and PD of the extracted PHB and commercial PHB. The GPC results for PHB extracted from LPA cells are summarised in Table 25 and those for HPA in Table 26.

In Table 25, it can be observed that the M_w of PHB after 48 h and 120 h of fermentation were identical at 1 x 10^6 g/mol. The M_w of PHB showed a decrease after 120 h. PHB from 216 h and 360 h fermentation were also identical at 5 x 10^5 g/mol.

The PD of PHB increased with increasing the fermentation time, whereas the M_w and M_n decreased with increasing fermentation time. PHB from HPA cells after 48 h of fermentation resulted in a PD of 4.5, which is closest to the value obtained for the commercial PHB.

Table 25: M_w**,** M_n and PD results for PHB from LPA *Serratia* sp. after various fermentations, the results for commercial PHB were obtained from Sigma-Aldrich.

	PHB from LPA cells				
	Commercial PHB	**48 h**	**120 h**	**216 h**	**360 h**
Mw (g/mol)	6 x 10^5	1 x 10^6	1 x 10^6	5 x 10^5	5 x 10^5
Mn (g/mol)	1 x 10^5	4 x 10^5	5 x 10^5	1 x 10^5	9 x 10^4
Polydispersity(PD)	3.2	4.5	4.6	5.0	5.1

The M_w obtained for commercial PHB was found to be 6 x 10^5 g/mol. The PHB extracted after 216 h from LPA and HPA *Serratia* sp. resulted in the closest M_w compared with the commercial sample. The M_w values were within the expected range of 5x10^5 g/mol. The PD for commercial PHB was lower than the PHB obtained from *Serratia* sp. This suggests a greater distribution of polymer chain length for PHB obtained from *Serratia* sp.

From Table 26, it can be observed that the M_w of PHB after 360 h of fermentation was lowest at 4 x 10^5 g/mol. The PD of PHB increased with increasing the fermentation time, whereas the M_w and M_n decreased with increasing fermentation time. PHB from HPA cells after 48 h of fermentation resulted in a PD of 4.5, which was identical to the value obtained for LPA fermented for 48 h and was the closest value to that obtained for the commercial PHB.

Table 26: M_w**,** M_n and PD results for PHB from HPA *Serratia* sp. after various fermentations, the results for commercial PHB were obtained from Sigma-Aldrich.

	PHB from HPA cells				
	Commercial PHB	**48 h**	**120 h**	**216 h**	**360 h**
Mw (g/mol)	6×10^5	1×10^6	1×10^6	5×10^5	4×10^5
Mn (g/mol)	1×10^5	2×10^5	3×10^5	1×10^5	8×10^4
Polydispersity(PD)	3.2	4.5	4.7	4.9	5

The M_w values of PHB from experiments with HPA and LPA *Serratia* sp. were compared. A correlation can be observed between the fermentation periods and M_w. The PHB from HPA and LPA *Serratia* sp. resulted in similar M_w values which were greatest at 1×10^6 g/mol for 48 h and 120 h fermentations and increased at 216 h fermentation. After 216 h fermentation the M_w decreased to 5×10^5 g/mol, which were closest to the values obtained from commercial PHB. The M_w showed a further reduction after 360 h fermentation 4×10^5 g/mol for PHB from HPA and LPA cells.

PHB accumulation observed after 48 h and 120 h fermentation showed the highest M_w of 1×10^6 g/mol. It has been reported that increase in the M_w of PHB could be facilitated by the addition of intermediate substrates in the bacterial culture, such as citric acid, malic acid, succinic acid and malonic acid [224]. The presence of intermediate substrates, promote transport systems and enzymes within the TCA cycle (see in section 1.6) resulting in accumulation of PHB with increased M_w. However, no intermediate substrates were used in the present work and the increase in the M_w was explained by the expected accumulation of PHB by the bacteria through the normal TCA cycle.

The M_W for PHB from the various fermentations were within the expected range for *Serratia* sp. Kashani 2007 reported identical M_w of 1 x 10^6 g/mol for PHB extracted from Serratia sp. after 96 h of fermentation with almost identical experimental conditions [77]. The decrease in M_w and the increase of the PD at 216 h and 360 h fermentations can be due to the depletion of the available carbon source in the culture solution over long fermentation times [7]. The depletion of carbon source results in the bacteria utilising PHB inclusions as energy reserves [16]. All PHB synthesising microorganisms contain intracellular depolymerase systems for the degradation of PHB [225]. This degradation process occurs along the polymer chain in a random manner and can result in greater variation of polymer chain lengths [226]. In this study *Serratia* cells were continuously dosed (24 h intervals) with stock solutions which included the carbon sources of citrate (2 mM every 24 h) and glycerol (10mM every 24 h). *Serratia* sp. demonstrated an increased rate of PHB accumulation at 216 h of fermentation. The yield of PHB after 360 h fermentation appeared to decrease, which was not expected considering *Serratia* cells were dosed daily with specific carbon sources. It was thought that the rate of accumulation of PHB prior to 216 h fermentation was much greater. The high rate of PHB accumulation resulted in the utilisation of the available carbon sources, the remaining carbon sources in solution was not enough to sustain the PHB accumulation and therefore *Serratia* sp. might have begun to utilise the PHB inclusions as energy reserves [227]. The subsequent depolymerisation of the PHB chains would give rise to a variety of polymer chain lengths [228], resulting in the increase in PD and decrease in M_w that was observed at 216 h and 360 h of fermentation.

Another possible cause for the decrease in PD at 216 h fermentations is the occurrence of spontaneous chain termination (SCT). SCT is based on a set range of Mw values and thus when a polymer chain reaches a certain Mw (cut off M_w) value it will spontaneously terminate the chain elongation [226]. A lower PD indicates a narrow range of cut of M_w

values [226].The results of this study demonstrate an increase in PD at 216 h fermentation in PHB from both LPA and HPA cells. This suggests that at 216 h fermentation with LPA and HPA cells, the PHB chain length becomes too long and consequently can no longer be tightly held by the synthase active site. PHB synthase enzyme is accountable for the production of an individual polymer chain. This will result in the occurrence of chain termination, causing a variation in chain length that will increase the PD [229]. The SCT theory goes some way in explaining why a sudden increase in PD between PHB from 120 h and 216 h fermentations was observed.

The reduction in the M_w of PHB at 216 h and 360 h of fermentation may be due to changes in the pH of the culture solution. *Serratia* cells were dosed daily with citrate, which may have acted to reduce the pH of the solution. Xin *et al*. reported that the M_w of PHB accumulated from *Methylosinus trichosporium* IMV 3011 was not significantly affected by the pH of the fermentation solution controlled by the addition of citric acid, α-ketoglutaric acid, sodium formate, malic acid and succinic acid [230]. DSC

DSC was conducted on samples of bacterially derived PHB from HPA and LPA *Serratia* sp. in order to observe the T_m, T_c and % crystallinity. The DSC traces are shown in Figures 24, 28, 30 and 33. The DSC scans were compared to that obtained for commercial PHB shown in Figure 23.

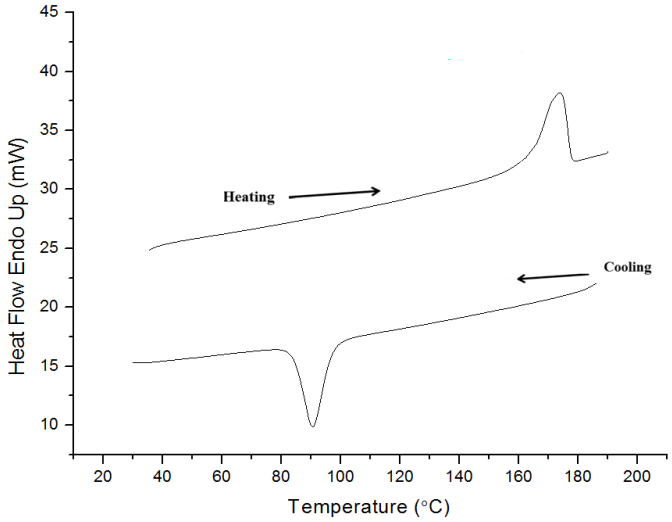

Figure 23: DSC scan demonstrating the heating and cooling trace for a powder sample of commercial PHB (Sigma-Aldrich Ltd., UK).

The T_m for commercial PHB was found to be 173.7 °C with an onset melting temperature of 152.6 °C and an end melting temperature of 179.3 °C. The T_c on cooling was found to be 90.6 °C with an onset crystallisation temperature of 105.5 °C and end crystallisation temperature of 74.4 °C. The % crystallinity for the commercial PHB was calculated using Equation 5 (Section 2.6.2) and was found to be 59 %.

3.5.1.1. DSC scans of PHB from HPA Serratia sp *cells*

The DSC traces A, B, C and D shown in Figure 24 demonstrate the T_m of PHB from HPA *Serratia* sp. after fermentations of 48, 120, 216 and 360 h time periods, respectively. The T_m values obtained for PHB from the various fermentations were within the expected region for PHB as shown in Figure 24.

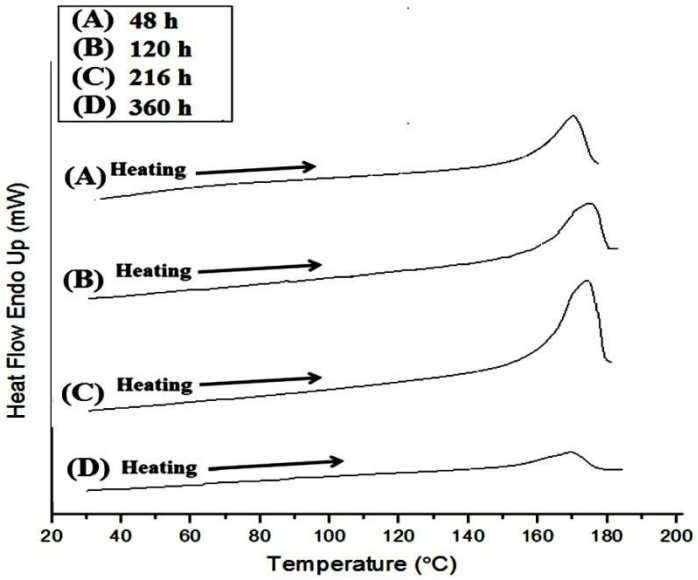

Figure 24: DSC traces for the heating of PHB samples from HPA *Serratia* sp. after fermentations of (A) 48 h, (B) 120 h (C) 216 h and (D) 360 h time periods.

Thermal characterisation of commercial PHB compared to PHB from HPA *Serratia* sp. is presented in Table 27.

Table 27: Thermal characterisation of commercial PHB compared to PHB from HPA *Serratia* sp. fermented for 48, 120, 216 and 360 h time periods.

	PHB from HPA cells				
	Commercial PHB	**48 h**	**120 h**	**216 h**	**360 h**
T_m (°C)	173.7	172.6	174.7	175	168.3
T_c (°C)	90.6	107.6	104.9	92.13	95.6
Crystallinity (%)	59	45.4	46.2	56	43.3

The onset of melting temperatures for each DSC trace against their respective M_w and PD values are presented in Figure 25 and 26 below.

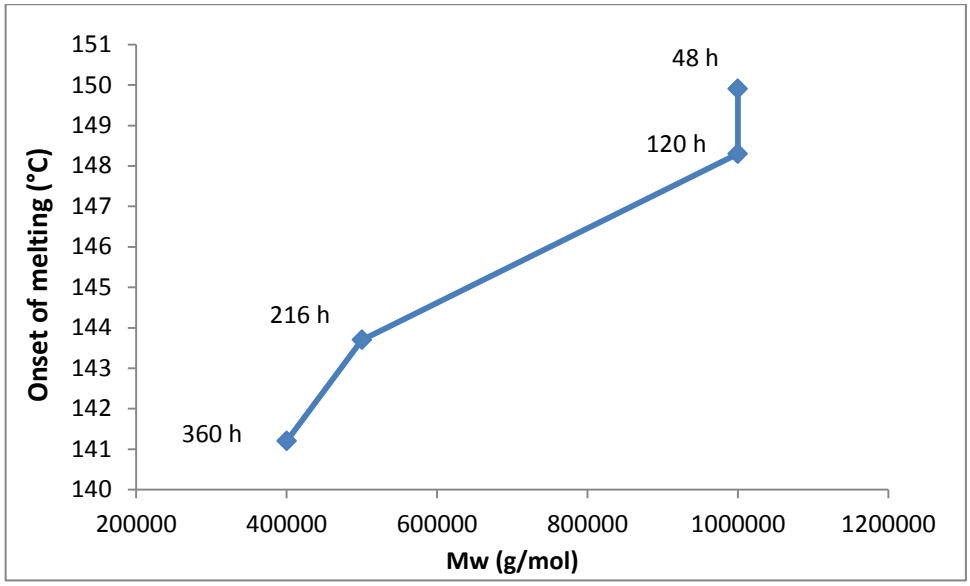

Figure 25: Line chart representing the onset of melting against M_w for PHB from HPA *Serratia* sp. fermented for 48, 120, 216 and 360 h.

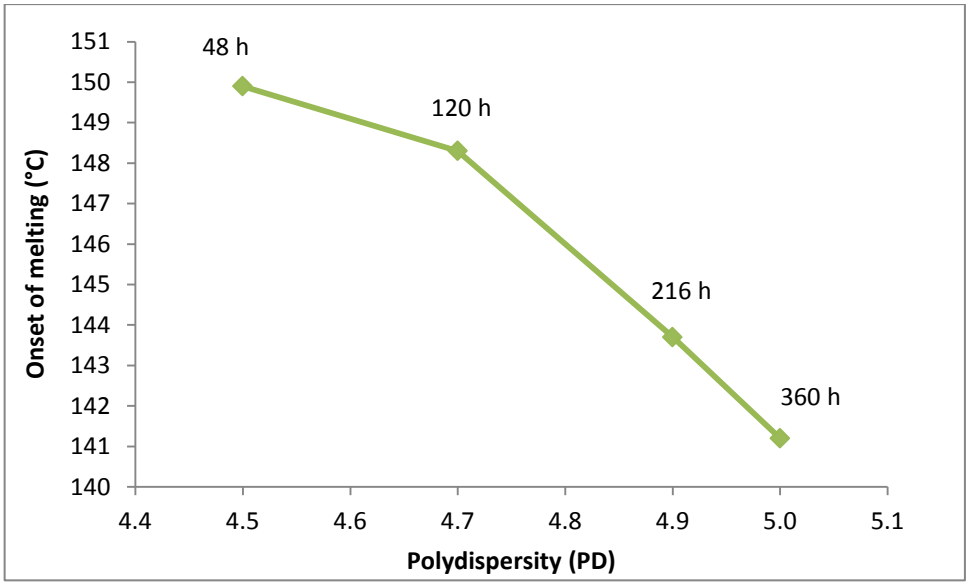

Figure 26: Line chart representing the onset of melting against PD for PHB from HPA *Serratia* sp. fermented for 48, 120, 216 and 360 h.

The onset of melting was within the expected regions for PHB samples from various fermentation periods. A clear correlation between the onset melting temperatures, M_w and PD

for samples of PHB was observed. As previously discussed (Section 3.4) longer fermentation periods result in the production of lower M_w PHB with an increased PD, the decrease in M_w and subsequent increase in PD of the PHB samples gave rise to early onset melting temperatures. PHB fermented for 48 h presented the highest onset melting temperature along with the highest M_w and the lowest PD. PHB fermented for 360 h showed the lowest onset melting temperature along with the greatest PD and the lowest M_w compared with PHB from 48, 120 and 216 h fermentations.

A comparison of the breadth of the endothermic melting peaks and PD for PHB from various fermentations is presented in Figure 27.

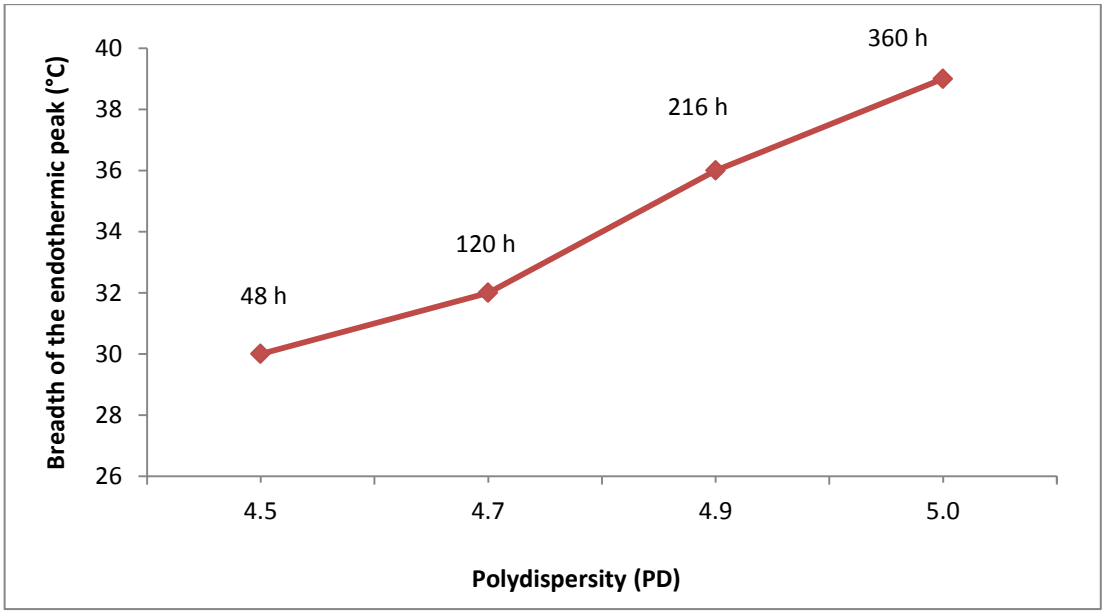

Figure 27: Line chart representing the breadth of the melting endothermic peaks against the PD for PHB from HPA *Serratia* sp. fermented for 48, 120, 216 and 360 h.

The observed increases in the breadth of the melting peak with increasing fermentation period can be attributed to the greater PD [228]. PHB fermented for 48 h showed the lowest PD and smallest melting peak breadth. PHB from 360 h fermentation demonstrated the largest melting peak breadth along with the highest PD. The breadth of the melting peaks was

observed to increase with increasing PD. As explained previously a polymer's PD can affect the breadth of the endothermic melting peak, as a narrow PD will mean a lower distribution of polymer chains exists and therefore will reach complete melt at approximately similar temperatures [224]. A high PD indicates that the polymer has chain lengths that vary over a wide range of M_w values and will reach complete melt at different temperatures, resulting in a larger melting peak breadth [230].

A comparison of the peak intensities against the % crystallinity for PHB from various fermentations is presented in Figure 28.

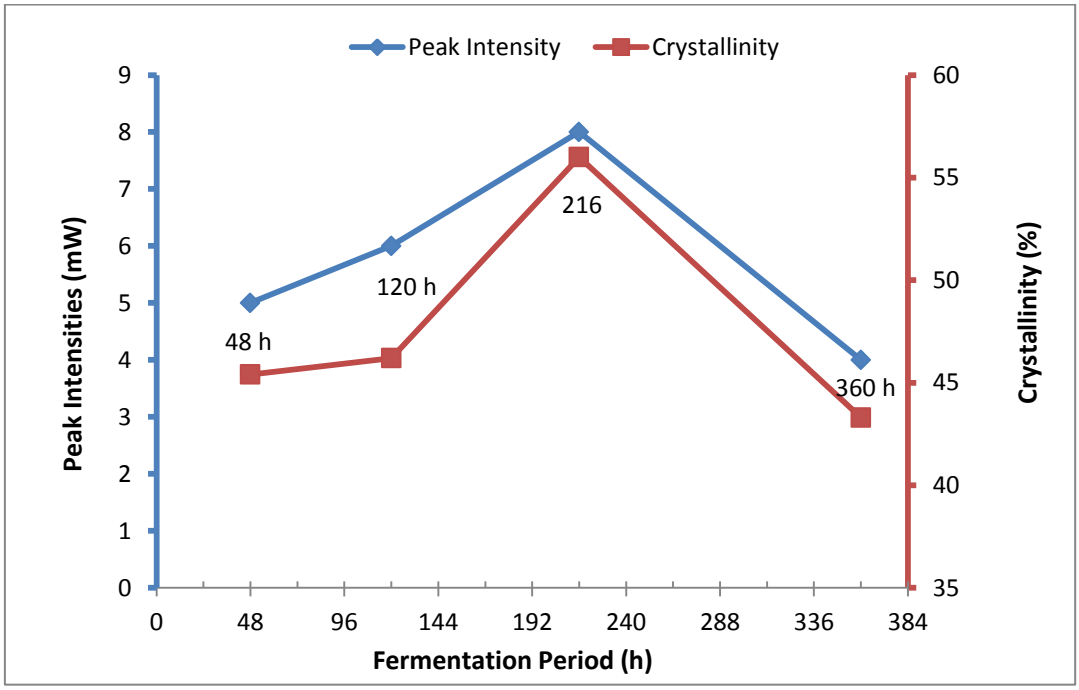

Figure 28: Line chart representing the peak intensities against the % crystallinity for PHB from HPA *Serratia* sp. fermented for 48, 120, 216 and 360 h. The peak intensities (mW) is used as a measure of polymer crystallinity.

PHB from 360 h fermentation resulted in the smallest peak intensity, this may be attributed to the lower degree of crystallinity as the peak intensity is related to the size and degree of perfection of the polymer crystals [231]. The sharpness of the endothermic peak is related to

the degree of crystallinity of the polymer. The presence of a single sharp endothermic peak is indicative of a distribution of mostly larger lamella thicknesses with stable crystallite structures [232]. Results obtained from GPC analysis of PHB from 216 h fermentation showed the highest % crystallinity of 56 %. The % crystallinity for commercial PHB was found to be 45.4 %. The % cystallinity for the extracted PHB appeared to be dependent upon the fermentation time. The % crystallinity increased from 45.4% (48 h) to 46.2% (120 h) and then increased to 56 % (216 h) before decreasing to 43.3 % for 360 h of fermentation. The increase in crystallinity with increasing fermentation time clearly correlates with the peak intensities of the endothermic peaks, as the peak intensities are greater with increasing crystallinity.

The increase in the % crystallinity after 126 h fermentation may be as a result of initial degradation of the PHB inclusions [77]. Spyros *et al*. reported that the initial degradation of PHB occurs primarily in the amorphous regions of the polymer. This is as the amorphous regions are much more susceptible to the action of depolymerase enzymes. It is suggested that an increase in PHB degradation will initially result in PHB with a greater % crystallinity and a decrease in the polymer M_w [72]. As previously discussed (Section 3.4) it is believed that the degradation of intracellular PHB by *Serratia* sp. may begin prior to the 216 h fermentation period, resulting in a decrease in M_w and an increase in PD. The initial degradation of PHB inclusions around 216 h would explain the increase in % crystallinity observed, as the initial degradation is occurring within the amorphous regions of the polymer.

It was expected that the % crystallinity of PHB from 360 h fermentation would be greater compared to that from 216 h fermentation as a result of the increased depolymerisation of the PHB inclusions and also the decrease in M_w that was observed. This decrease in crystallinity has been attributed to the increase in pH that may have occurred as a result of the increased

dosing of the stock solution citrate over a longer fermentation period. The effect of pH on crystallinity has been discussed in greater detail in section 3.4.2.3.

The T_c obtained on cooling was within the expected range for PHB. The onset crystallisation temperatures from each DSC scan were (A) 123.4 °C, (B) 125.1 °C, (C) 127.4 °C, (D)120.3 °C and the end crystallisation temperatures were (A) 91.2 °C, (B) 92.1 °C, (C) 92.2 °C, (D) 93.7 °C. The DSC traces in Figure 29 were obtained during the cooling stage and show the T_c of PHB from HPA *Serratia* sp. after fermentations of 48, 120, 216 and 360 h time periods.

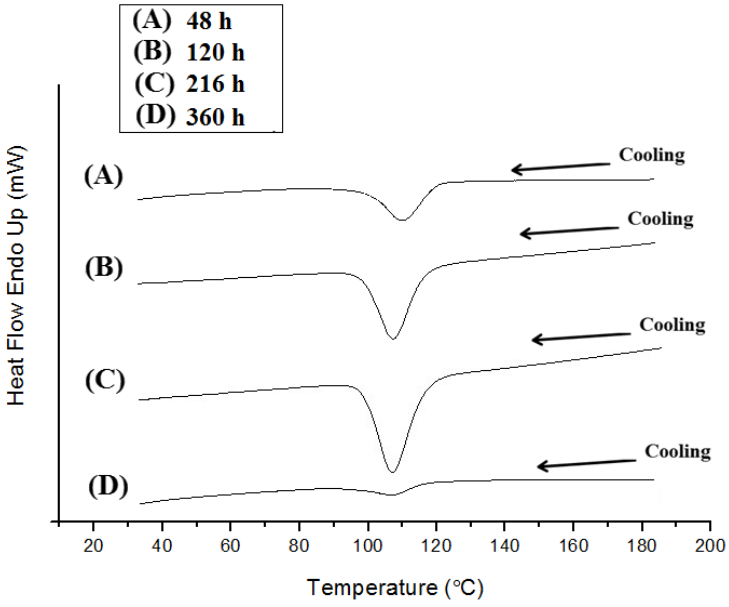

Figure 29: DSC traces for the cooling of PHB samples from HPA *Serratia* sp. after fermented for various time periods (A) 48 h, (B) 120 h (C) 216 h and (D) 360 h.

No major differences in T_c peak positioning were observed for PHB fermented for 48, 120 and 216 h.

The T_m and T_c obtained from the DSC traces of PHB were plotted against M_w and are presented in Figure 30.

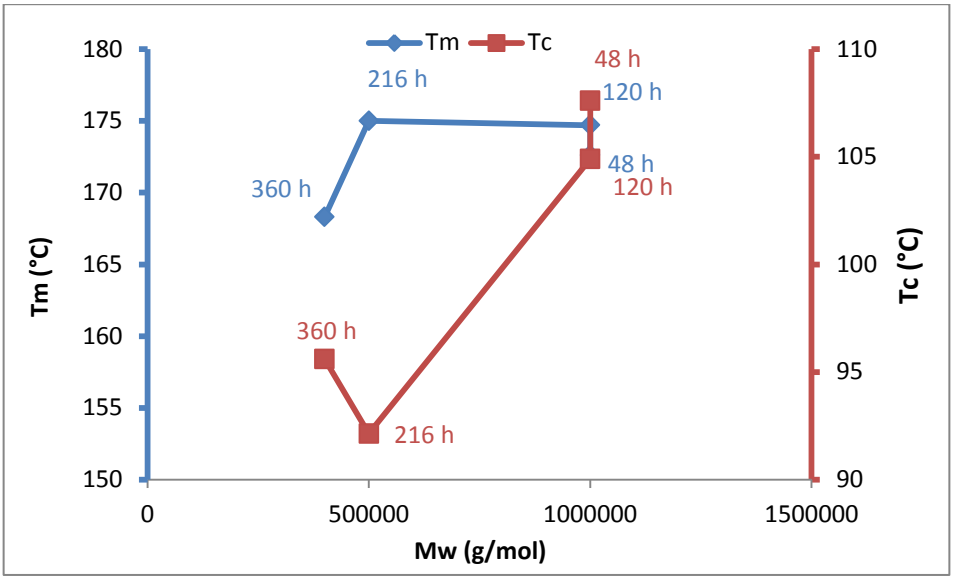

Figure 30: Line graph representing the T_m and T_c against the M_w for PHB from HPA *Serratia* sp. fermented for 48, 120, 216 and 360 h.

The T_m and T_c for PHB from the various fermentation periods demonstrated a clear correlation. A lower T_m for PHB resulted in higher T_c. This suggests that PHB samples which reached complete melt at higher temperatures will reach crystallisation at lower temperatures. No major differences were observed in the T_m after 48, 120 and 216 h fermentations. It was observed that a higher M_w will result in a lower T_m. The exception however, was PHB from 360 h that showed the lowest T_m along with the lowest M_w. This may be attributed to the larger proportion of small polymer chains that begin to melt at lower temperatures and so reach complete melt at a lower temperature [230].

3.5.1.2. DSC scans of PHB from LPA Serratia sp.

The DSC traces A, B, C and D in Figure 31 were obtained during the heating stage and demonstrate the T_m of PHB from LPA *Serratia* sp. after fermentations of 48, 120, 216 and 360 h, respectively. The T_m obtained for PHB from the various fermentations was within the expected region for PHB as shown in Figure 31.

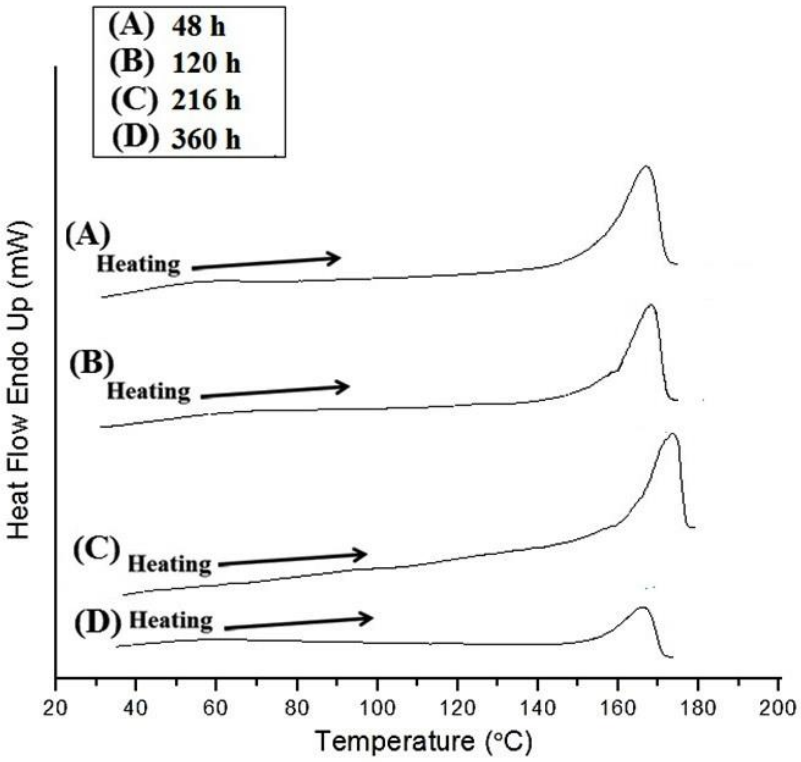

Figure 31: DSC traces for heating of PHB samples from LPA *Serratia* sp. after fermentations of (A) 48 h, (B) 120 h (C) 216 h and (D) 360 h time periods.

The thermal characterisation of PHB from LPA *Serratia* sp. is summarised in Table 28.

Table 28: Thermal characterisation of commercial PHB compared with recovered PHB from LPA *Serratia* sp. fermented for: 48, 120, 216 and 360 h time periods.

		PHB from LPA cells			
	Commercial PHB	**48 h**	**120 h**	**216 h**	**360 h**
T_m (°C)	173.7	168.8	170.1	175.7	166.2
T_c (°C)	90.6	93.4	92.2	91.5	94.1
Crystallinity (%)	59	48.2	53.3	54.55	47.1

The onset of melting temperatures for each DSC trace against their respective M_w and PD values are presented in Figure 32 and 33 below.

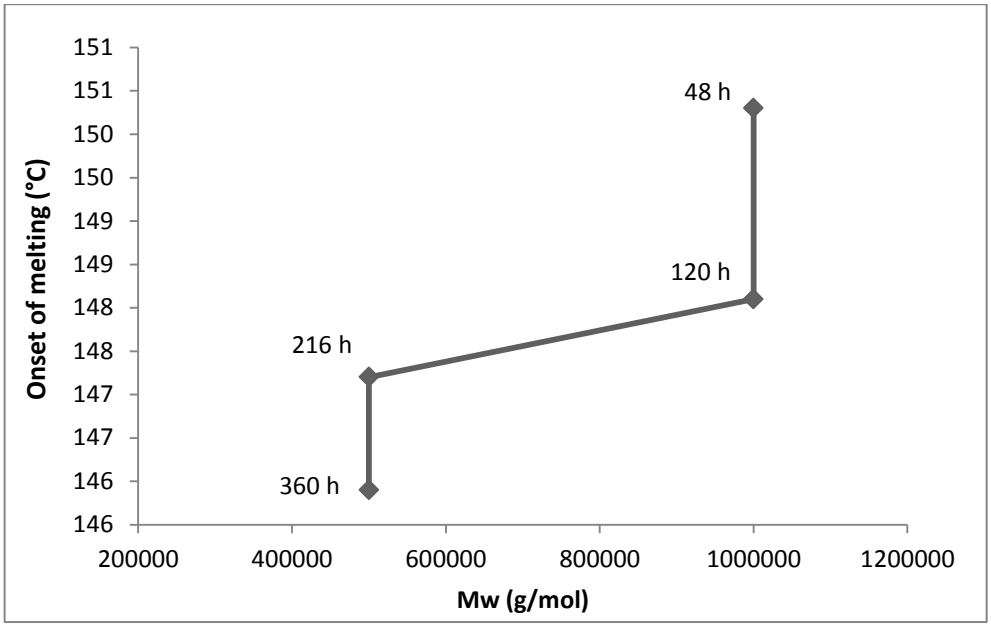

Figure 32: Line chart representing the onset of melting against M_w for PHB from LPA *Serratia* sp. fermented for 48, 120, 216 and 360 h.

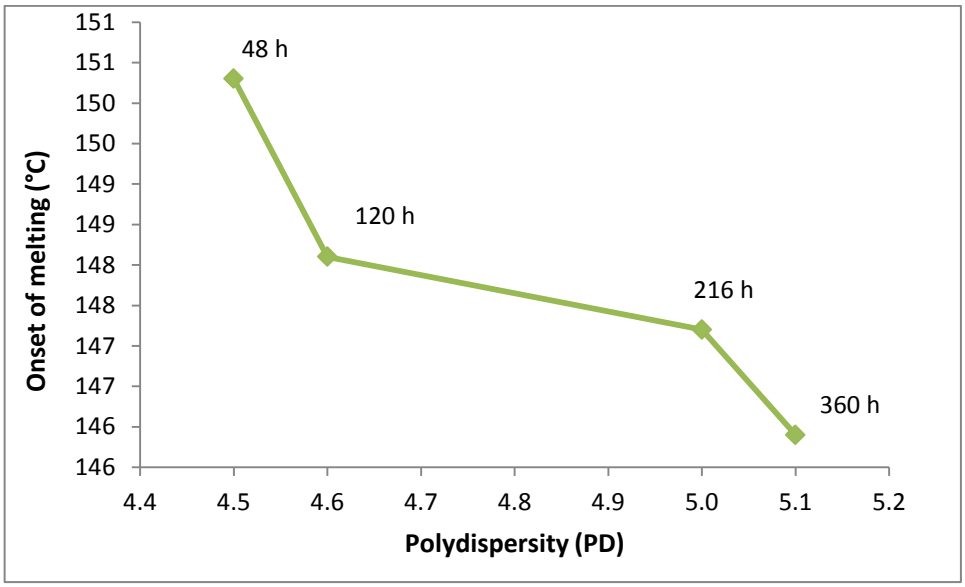

Figure 33: Line chart representing the onset of melting against PD for PHB from LPA *Serratia* sp. fermented for 48, 120, 216 and 360 h.

The onset melting temperatures were within the same region for PHB fermented for 48, 120 and 216 h time periods. A correlation between the onset melting temperatures, M_w and PD for

samples of PHB were observed. This correlation was similar to that obtained for PHB from HPA as previously outlined (Section 3.4.1.1). The value for the onset of melting was reduced for PHB from 360 h fermentation and can be attributed to the presence of lower M_w polymer chains that will begin to melt at lower temperatures. In contrast the value for the onset of melting was much higher (150.3 °C) for PHB from 48 h fermentation and can be attributed to the decreased PD resulting in the presence of higher M_w polymer chains that will begin to melt at higher temperatures, resulting in a late onset of melting. A comparison of the breadth of the endothermic melting peaks and PD for PHB from various fermentations is presented in Figure 34.

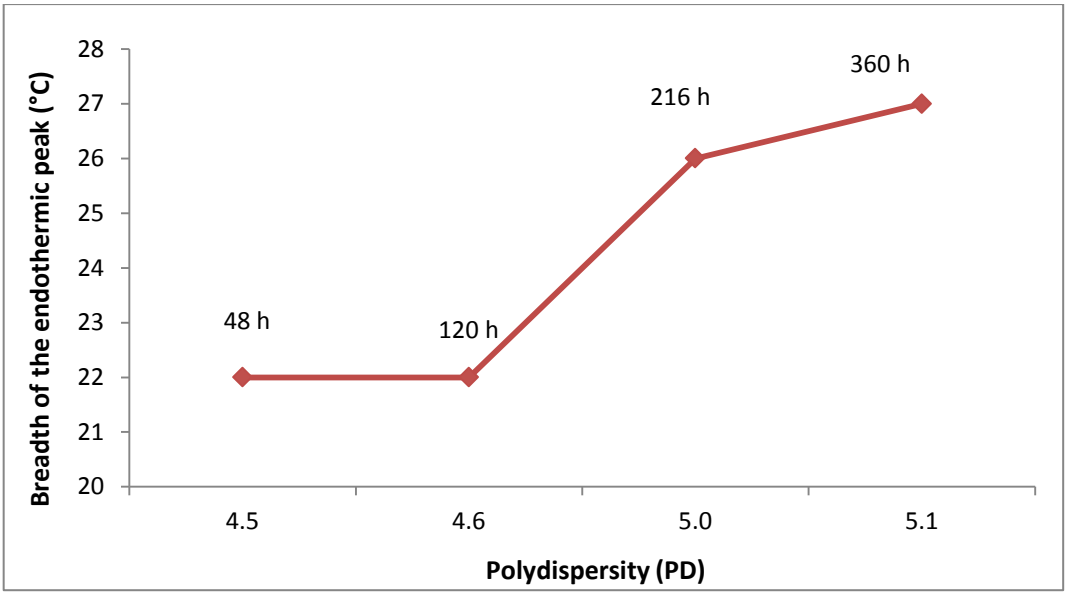

Figure 34: Line chart representing the breadth of the endothermic melting peaks against PD values for PHB from LPA *Serratia* sp. fermented for 48, 120, 216 and 360 h.

The observed increase in the breadth of the melting peak with increasing fermentation period was similar to that obtained for PHB from HPA cells and can be attributed to the higher PD [228].

The breadth of the endothermic melting peak was greatest for the DSC trace of PHB fermented for 360 h. This was also observed in the DSC scans for HPA cells after 360 h fermentation and as previously discussed (Section 3.4.1.1) is as a result of a greater PD of the polymer chains.

The GPC analysis demonstrated how PD values are higher with increasing fermentation period and supports the finding of the DSC traces for PHB from LPA cells. A comparison of the peak intensities (mW) relating to the degree of crystallinity is plotted against the % crystallinity for PHB from various fermentations is presented in Figure 35.

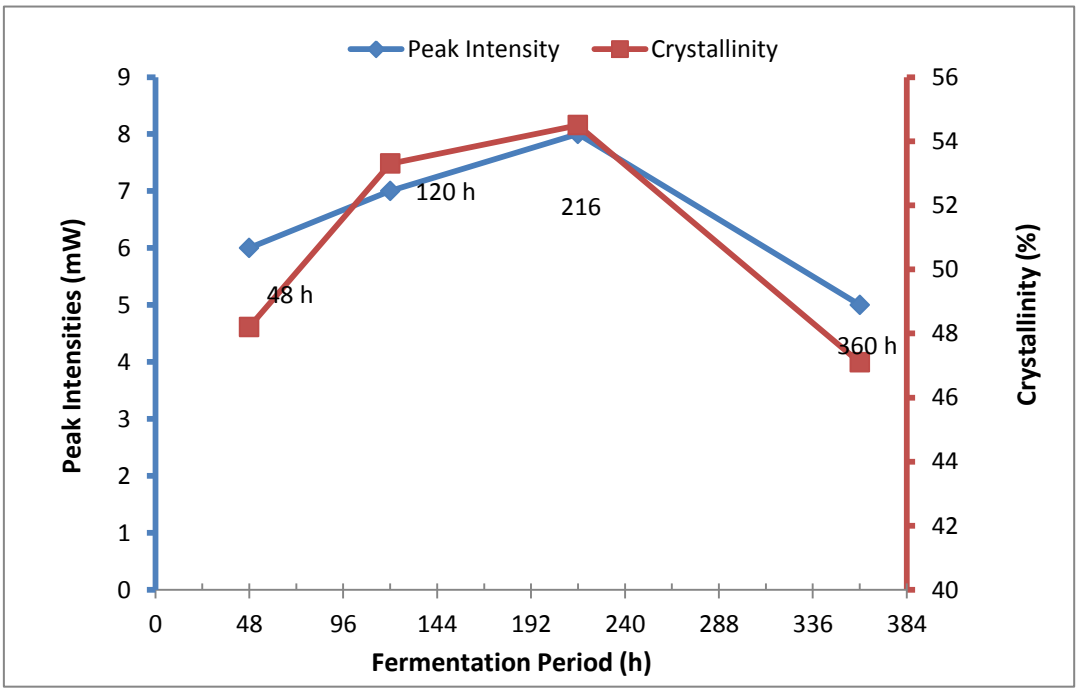

Figure 35: Line chart representing the peak intensities and % crystallinity for PHB from LPA *Serratia* sp. against fermentation time. The peak intensities (mW) is used as a measure of polymer crystallinity.

A correlation between the % crystallinity and peak intensity values was observed. As smaller peak intensity attributed to greater % crystallinity. The smallest peak intensity was observed

for PHB from 360 h fermentation, which also demonstrated the lowest % crystallinity. The peak intensity was greatest for PHB from 216 h fermentation and also demonstrated the highest % crystallinity.

The % crystallinity increased from 48.2 % (48 h) to 54.5 % (216 h) and decreased to 47.1 % (360 h). The % crystallinity appeared to be dependent upon the fermentation time as was also observed in the DSC traces for HPA cells. The increase in crystallinity with increasing fermentation time clearly correlates with the peak intensities of the endothermic peaks, as the peak intensities are greater with increasing crystallinity.

The DSC traces in Figure 36 were obtained during the cooling stage and demonstrate the T_c of PHB from LPA *Serratia* sp. after fermentations of 48, 120, 216 and 360 h. The onset crystallisation temperatures from each DSC scan was (A) 111.6 °C, (B) 110.13 °C, (C) 111.1 °C, (D)108.4 °C and the end crystallisation temperatures (A) 83.6 °C, (B) 82.2 °C, (C) 82.2 °C, (D)82.6 °C. No major differences in peak positioning were observed for PHB fermented for 48, 120, 216 h and 360 h.

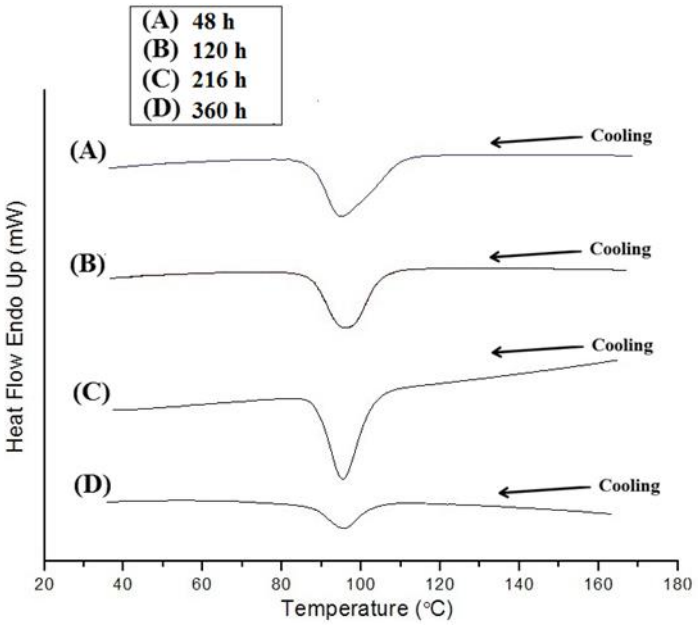

Figure 36: DSC traces for the cooling of PHB from LPA *Serratia* sp. after fermentations of (A) 48 h, (B) 120 h (C) 216 h and (D) 360 h.

The T_c obtained on cooling were in the expected region for PHB and within the same region as the T_c for commercial PHB. The T_m and T_c values obtained from the DSC traces of PHB were plotted against M_w and are presented in Figure 37.

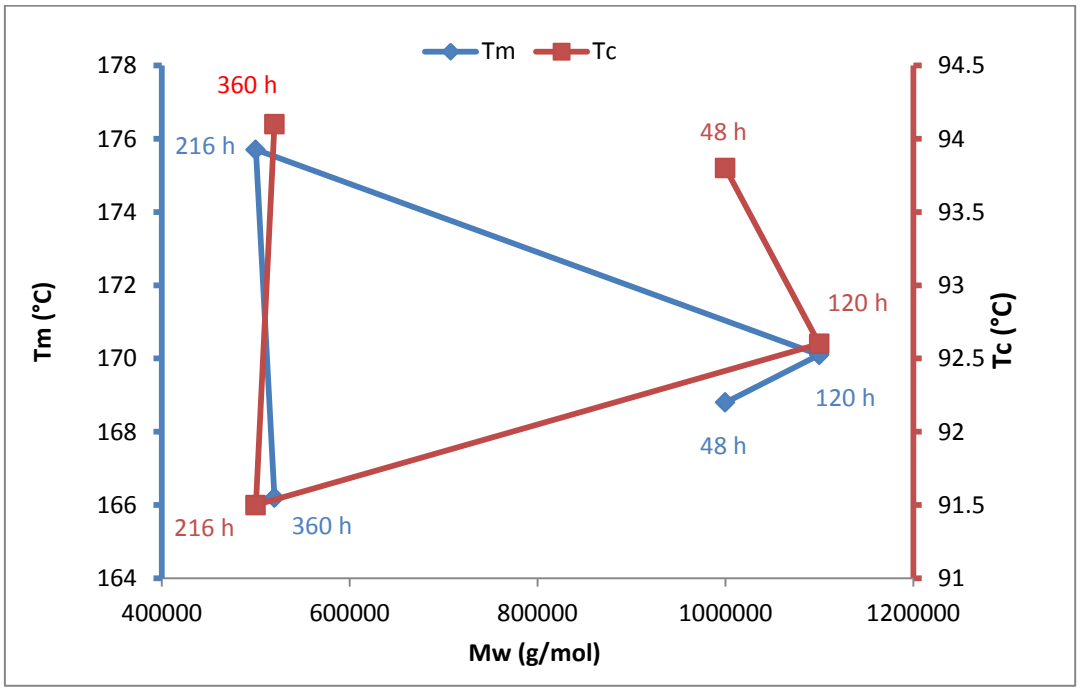

Figure 37: Line chart representing the T_m and T_c against the M_w for PHB from LPA *Serratia* sp. fermented for 48, 120, 216 and 360 h.

The T_m and T_c values for PHB from the various fermentation periods demonstrated a clear correlation. Lower T_m temperatures for PHB resulted in higher T_c temperatures. This suggests that PHB samples that reached complete melt at higher temperatures would reach crystallisation earlier. The same correlation was observed with PHB from HPA cells.

3.5.1.3. Comparison of DSC traces for PHB from LPA and HPA

Comparing the DSC traces from LPA and HPA PHB presented no major differences in peak positioning after 48, 120, 216 and 360 h fermentations. The breadth of the melting peaks also

presented the same pattern of broadening at 360 h fermentation periods and as previously discussed is as a result of the increase in polymer chain lengths that melt at varying temperatures [230]. The onset melting temperatures for PHB from both LPA and HPA cells presented an identical pattern. Lower fermentation times resulted in a greater onset melting temperature that decreased with longer fermentation times, which was attributed to the increase in PD and the presence of lower M_w polymer chains that will begin to melt at lower temperatures. PHB from 360 h fermentations demonstrated the lowest onset melting temperatures at 141.2 °C (HPA) 145.9 °C (LPA) and as previously discussed is as a result of the lower PD.

The intensity of the endothermic peaks presented an identical pattern for the PHB samples from HPA and LPA cells. The increase in the peak intensity was correlated to the % crystallinity. PHB from 216 h fermentation presented the sharpest endothermic melting peak and was attributed to the greater % crystallinity at 56 %(HPA) and 54.5 % (LPA) [119].

The thermodynamic properties of PHB from LPA and HPA cells after the various fermentation times were almost identical and demonstrated identical patterns for endothermic peak intensities, peak breadth and onset of melting. This suggests that the endothermic differences observed between PHB from various time periods were as a result of the fermentation conditions and not as a result of the differences in phosphatase activity.

The process of crystallisation is primarily dependent upon the thermodynamic change from an amorphous melt to an crystalline phase, the nucleation process and also the environmental factors such as pH and fermentation temperature [119, 232-235]. Once PHB is heated above its melting temperature it transforms to an amorphous structure [232, 236]. As PHB cools from the melt, macromolecules crystallise and form anti parallel helical chains linked by hydrogen bonds between the carbonyl and methyl groups of the polymer backbone [237].

Generally, crystallisation in polymers takes place as groups of amorphous molecules combine into tiny clusters forming nuclei [238]. Once the nuclei have formed, sheet like structures known as lamellae will grow radically out from the nuclei in the form of spherulites [216, 236, 238]. Porter *et al*. conducted a study focused on the crystallisation of PHB within granules under various environmental conditions. It was reported that the crystallinity of PHB granules within *R. eutropha* were affected by pH during fermentation [236]. The pH of cells in solution was raised from 2 to 12 in ambient conditions, the results showed an increase in granule crystallinity with increasing pH. The increase in pH may result in dissolving of the lipid and protein membrane of the granule, which would induce a partial crystallisation at the surface. A % crystallinity of 40.59 % at pH 12 was reported. PHB inclusions exposed to a low pH (~2 °C) in solution resulted in PHB with a maximum crystallinity of ~35 %. The citrate present in the stock solutions may have gradually reduced the pH of the cell solution over time. This reduction in pH may be an contributing factor responsible for the observed decrease in crystallinity after 360 h fermentation [235, 236] In both cases the % crystallinity for PHB from 360 h resulted in a slight decrease compared to PHB from 216 h fermentations. The effect of high temperature on PHB crystallinity was also reported by Porter *et al.* [236]. It was reported that heating of *R. eutropha* cells at 80°C - 140°C for 0-4 h resulted in an increase in crystallinity 20 to 30 %. It was suggested that heating the cell solution may have induced crystallinity, as intra granule water as proteins and lipids would be removed from the granule membrane [236]. In this study the temperature was kept constant throughout the fermentation period by the implementation of a water bath. The water bath kept the cell solution at ambient temperature, which was measured manually and recorded three times a day.

3.5.2. *FTIR*

The FTIR spectra for PHB samples extracted from LPA and HPA *Serratia* sp. after 216 h fermentations were compared with the spectrum obtained from commercial PHB in Figure 38. The FTIR spectra obtained for extracted PHB presented almost identical peak positioning when compared to the spectrum obtained from commercial PHB.

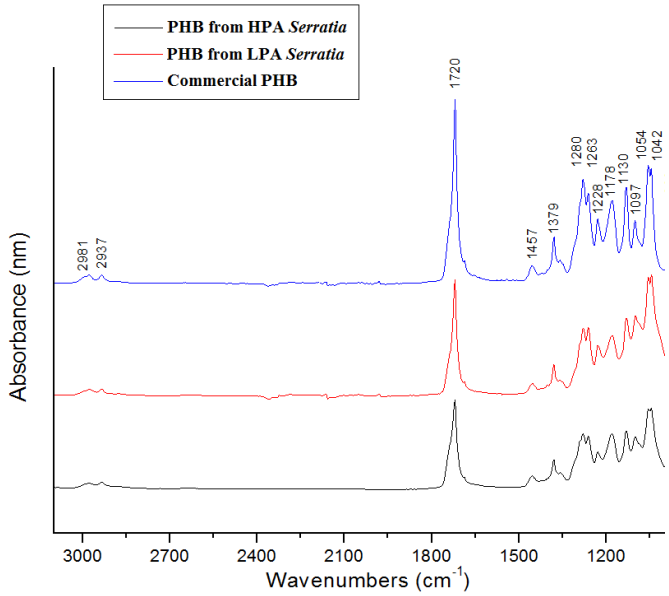

Figure 38: FTIR spectra of PHB extracted from HPA and LPA *Serratia* sp. after 216 h of fermentation compared to the spectrum of commercial PHB.

The characteristic FTIR peaks for PHB are summarised in Table 29. The most prominent marker band for the identification of PHB is the ester carbonyl band at 1720-1740 cm^{-1}. The bands present at 1178 cm^{-1}, 1228 cm^{-1} and 1263 cm^{-1} are bands sensitive to crystallinity and are characteristic of C-O-C. There were no major differences observed amongst the FTIR spectrum for extracted PHB from 216 h fermentation and commercial PHB. However, peak intensities observed for commercial PHB were greater than those for extracted PHB from 216 h fermentation.

Table 29: Description of the main FTIR peaks in the spectra of PHB from HPA and LPA *Serratia* sp. compared to that of commercial PHB.

Characteristic peaks cm^{-1}			
PHB (LPA)	**PHB (HPA)**	**Commercial PHB**	**Description**
~2900	~2900	~2900	C-H Vibration
1720	1720	1720	C=O Stretching
1457	1457	1457	CH_3 Asymmetric deformation
1380	1380	1379	CH Symmetric deformation
1279	1279	1280	C-O-C stretching
1261	1261	1263	C-O-C stretching + CH deformation
1228	1228	1228	C-O-C stretching
1178	1179	1178	C-O-C stretching
1128	1132	1130	CH_3 rocking
1096	1099	1097	C-O-C stretching
1054	1054	1054	C-O stretching
1042	1042	1042	C-CH_3 stretching

The FTIR spectra for extracted PHB from HPA and LPA were compared with the spectrum obtained from commercial PHB. The spectra were found to be identical, which confirms the extracted polymer as PHB. It is worth noting that the spectra for the extracted PHB resulted in a subtle difference in absorbance intensity. A greater absorbance correlates to a higher degree of crystallinity; this observation could lead to the inclusion that the PHB extracted from *Serratia* sp have lower degree of crystallinity compared to that of the commercial PHB. [231, 239]. The % crystallinity values that were calculated from DSC analysis, as previously

discussed, resulted in slightly higher % crystallinity for commercial PHB compared with PHB extracted from HPA and LPA *Serratia* sp. after 216 h fermentation period. DSC results support the theory that the presence of greater peak intensities for the FTIR spectrum of commercial PHB is a result of a higher degree of crystallinity.

Randriamahefa *et al*. reported that FTIR can also be used to evaluate the crystallinity Index (CI) of PHB quantitatively. A relative measure of the degree of crystallinity can be obtained by calculating the CI and can be used to compare the relative crystallinity obtained from the various FTIR spectra. In the literature, the CI is defined as the absorbance ratio of the reference band at 1724 cm^{-1} which is insensitive to the degree of crystallinity to the crystallinity sensitive band at 1228 cm^{-1} [236, 239]. The equation for calculating the CI is demonstrated in Equation 6 below.

$$CI = \frac{A_{1228}}{A_{1724}} \qquad \textbf{Equation 6}$$

The CI obtained for commercial PHB was 0.6, which was greater compared to the values obtained for PHB extracted from HPA and LPA cells (after 216 h fermentation) with values of 0.34 and 0.42, respectively. Greater CI correlates to a higher % crystallinity. This CI is not to be confused with an absolute degree of crystallinity but is useful for comparison. The results obtained in this study complement the findings from the DSC scans of the PHB samples. Commercial PHB showed higher % crystallinity compared to extracted PHB from HPA and LPA *Serratia* sp. The correlation between the % crystallinity obtained from DSC and the CI obtained from the FTIR spectra of PHB from HPA and LPA fermented for 216 h and commercial PHB is presented in Figure 39.

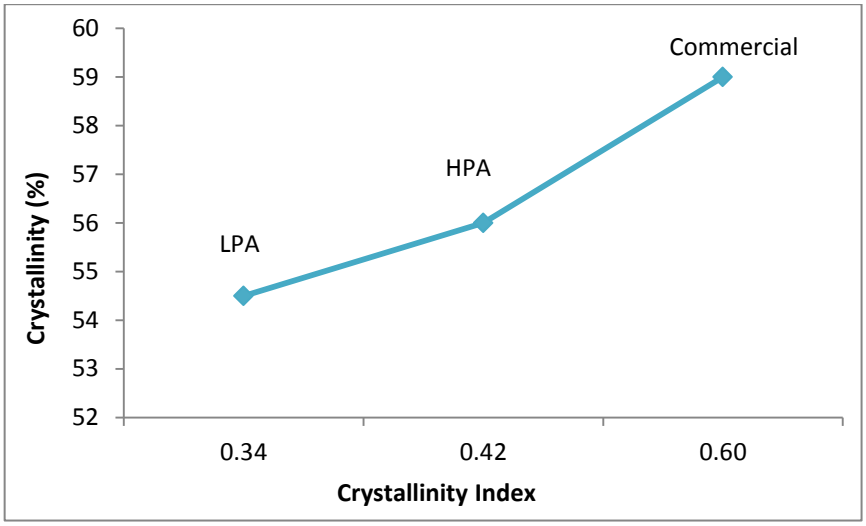

Figure 39: Line chart demonstrating the correlation between the % crystallinity obtained from DSC traces and the CI obtained from the FTIR spectra.

A clear correlation can be observed between the CI and the actual % crystallinity for commercial PHB and PHB from LPA and HPA *Serratia* sp. fermented for 216 h time period. The line chart supports the findings of the CI, as they are in agreement with the % crystallinity obtained from the DSC traces.

3.6. *Characterisation of HA extracted from Serratia* sp.

3.6.1. *FTIR*

The FTIR spectra of *Serratia* HA from HPA and LPA cells were found to be identical. The spectrum of *Serratia* HA (Figure 40) obtained from HPA cells was compared to the spectra for commercial and *Serratia* HA reported by other research groups [169, 212]. In comparison, the spectra were almost identical.

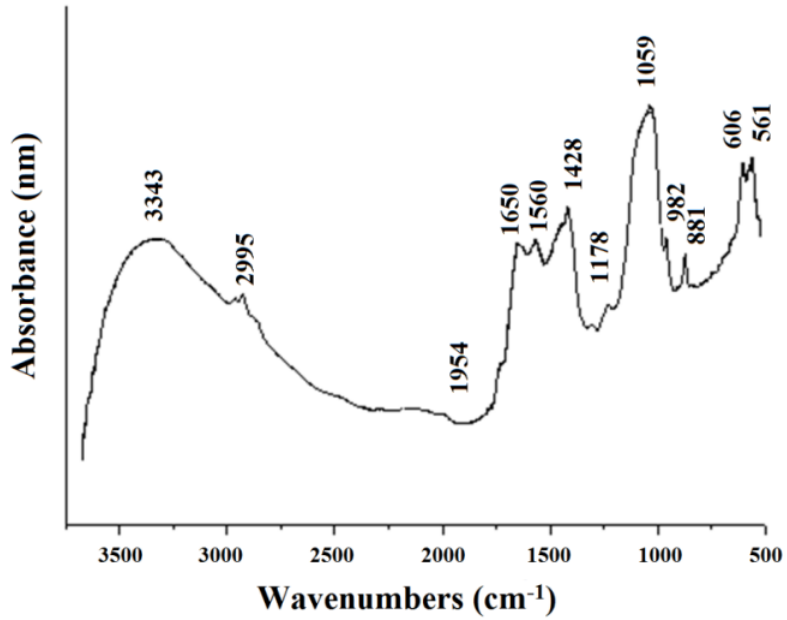

Figure 40: FTIR spectra of HA from HPA *Serratia* sp. fermented for 216 h time period.

The characteristic FTIR peaks for biological HA compared to commercial HA are summarised in Table 30.

Table 30: Description of the main FTIR peaks in the FTIR spectra of *Serratia* HA from HPA compared to that of commercial HA [190].

Characteristic peaks cm^{-1}		Assignment
Serratia HA	**Commercial HA**	
470	470	O-P-O bending mode v2
568-601	561-601	O-P-O bending mode v4
634	634	OH- vibration mode
871	878	B-type CO_3^{2-} vibration v2 / HPO_4^{2-}
963	963	P-O stretching vibration v1
826, 831, 878,	830	Residual Nitrate
1029, ~ 1095	1029, ~ 1096	P-O stretching vibration
1411-1450	~ 1443	B-type CO_3^{2-} vibration
1562, 1582	-	A-type CO_3^{2-} vibration
1654, 3424	1634, 3010	Absorbed water
2851	-	CH_2 stretching vibration
-	3751	OH- stretching mode

The position of the absorption peaks at wavelengths 1095, 1029 and 963 cm^{-1}, indicating the presence of P-O-H bonds, were identical to those found in commercial HA as reported by Sammons *et al*. and Yong *et al.* [115, 169]. The band at 963 cm^{-1} is characteristic of the symmetric stretching vibrations of $-PO_4^{3-}$ in HA [113]. A similar FTIR spectrum of *Serratia* HA was reported by Sammons *et al.* who also observed the lack of the OH- stretching and vibration mode [169]. The broad asymmetric bands in the range of 3512 to 2937 cm^{-1} together

with an absorption band centred at approximately 1599 cm^{-1} can be assigned to the presence of O-H bonding in water and were observed in both spectra [240]. The addition peak at 2995 cm^{-1} can be attributed to the presence of residual chloroform from the extraction process of HA and represents C-H stretching [241]. The FTIR band for *Serratia* HA at around 878 cm^{-1} confirms the presence of HPO_4^{3-} suggesting that it is in fact calcium deficient. Furthermore, the presence of HPO_4^{3-} in *Serratia* HA was confirmed by *Sammons et al*. who reported the presence of an FTIR peak at 870 cm^{-1} [169].

3.6.2. *X-ray Diffraction*

X-ray diffraction powder patterns for the *Serratia* HA and commercial HA (Figure 41) were matched against calcium hydrogen phosphate hydroxide (JCPDS database; Pattern number 00-046-0905), confirming a hydroxyapatite material. Similar observations were reported by Prakash *et al.* [242] and Macaskie *et al.,* 2000 [243].

The crystallite size was calculated from the characteristic peak 2θ = 26° ,corresponding to 002 plane, using the Scherrer equation (Equation 7) [244], where **D** = crystallite size (Å), **k** = shape factor (0.95), λ = X-ray wavelength (1.5406 Å), θ = diffraction angle (12.95) and β = diffraction peak width at half height (corrected for instrument broadening using NIST AL_2O_3 reference spectra) [203]

$$D\,(\text{Å}) = \frac{k\lambda}{\beta cos\theta} \qquad \textbf{Equation 7}$$

The crystallite size for *Serratia* HA (HPA) was found to be 31 nm compared to 85 nm for commercial HA.[174, 212].

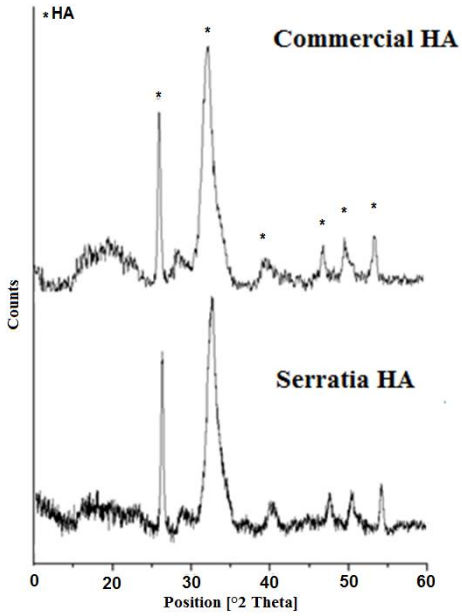

Figure 41: XRD pattern for commercial HA and *Serratia* HA from HPA cells.

The XRD pattern for *Serratia* HA showed significant peak broadening with a decrease in peak intensity, which is associated with a lower HA crystallite size (31 nm) [245]. Posner *et al*. reported that an increase in peak broadening and a decrease in peak intensities is associated with a decrease in the HA crystallite size [245]. Harper and Posner reported greater peak intensities in synthetic HA when compared to natural bone mineral HA [245, 246]. It was suggested that the decrease in peak intensities can be attributed to a larger degree of disordered phase, referred to as a phase of smaller degree of crystallinity [190, 246].

The commercial HA spectrum demonstrates higher intensity peaks as a result of its larger crystallite size (85 nm). Handley-Sidhu *et al.* reported a crystallite size of 26 nm for HA obtained from LPA *Serratia* sp. with a phosphatase activity of ~500 units [203].

Li 2009 conducted XRD analysis on samples of *Serratia* HA (HPA) and reported broader peaks with lower intensities compared with other samples of synthetic HA. Li 2009 compared the crystallite size of three samples of HA synthesised by hydrothermal method, precipitation method and bacterial biosynthesis from *Serratia* sp. It was reported that *Serratia* HA showed

the smallest crystallite size of 8 nm compared with 39 nm for hydrothermal and 16 nm for chemically precipitated HA. The decrease in crystallite size has been reported to be in part a result of the processing temperature, with a lower processing temperatures resulting in a smaller crystallite size [190].

Fathi *et al.* and Webster *et al.* reported how a smaller crystallite size of HA will result in a greater contact reaction and stability at the interface between implanted HA and the natural bone [173, 247]. They also reported higher levels of early bone growth promotion from HA with a smaller crystallite size[190].

3.7. *Optical analysis of Serratia sp. during fermentation*

3.7.1. *SEM*

Representative images of HA formation on the surface of LPA and HPA *Serratia* cells fermented for 48, 120, 216 and 360 h are shown below. From each fermentation experiment three SEM images were obtained and compared. The SEM images that are presented for the various fermentation periods are those that represent the average HA accumulation best.

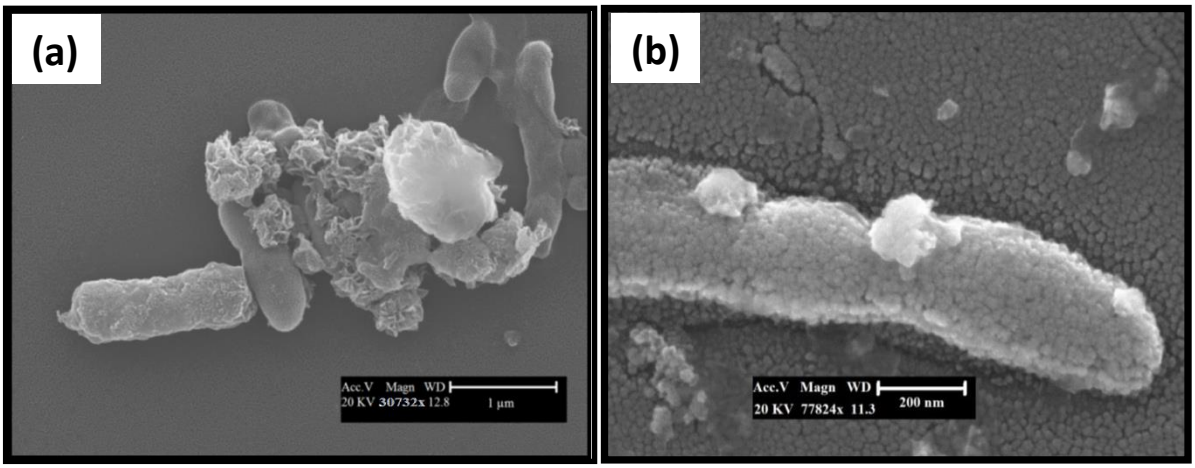

Figure 42: SEM images of *Serratia* cells with HA mineralisation on the cell surface after 48 h fermentation (a) HPA *Serratia* cells (b) HA formation on LPA cell.

Figure 42(a) demonstrates an area of the *Serratia* cells where HA mineralisation has occurred. Small amounts of HA can be seen on the surface of the cells after fermented for 48 h. The small amounts of HA observed in Figure 42(a) reflected the low yields that were extracted from the cells after 48 h. The overall average yield of HA extracted after 48 h fermentation with HPA cells was 67 mg.

Figure 42(b) is focused with greater magnification on an area of the cell where HA mineralisation had taken place. The overall average yield of HA from HPA cells was 596 mg. In both SEM images the amount of HA mineralisation observed on the cells was greater in HPA compared to LPA. Most of the LPA cells showed little to no HA mineralisation. This suggests that HA mineralisation does occur after 48 h fermentation, however a limited quantity of HA is produced. Statistical analysis (T test; $p < 0.05$) confirmed that there is a significant difference ($p = 0.000007$) between HA yields produced from HPA and LPA *Serratia* sp.

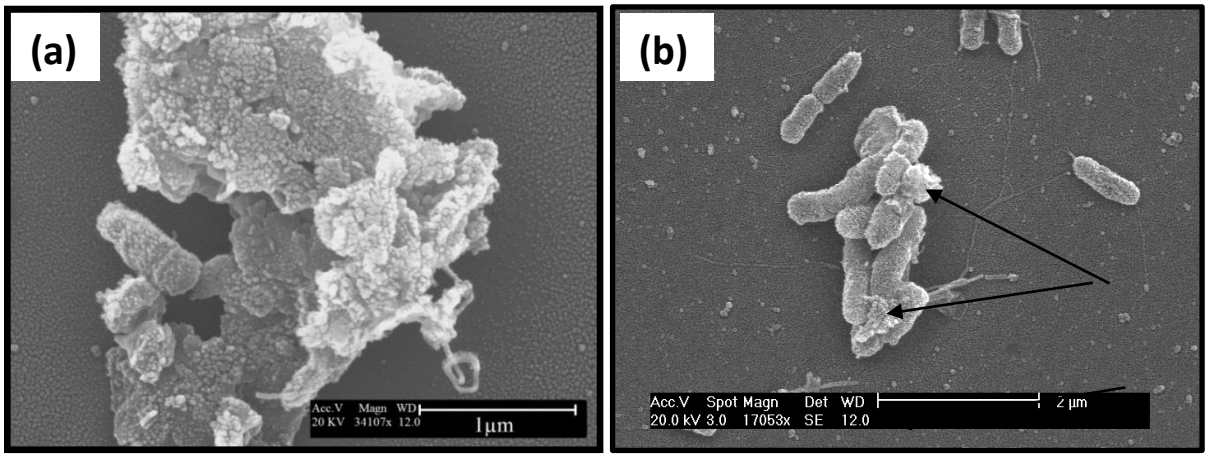

Figure 43: SEM images of *Serratia* cells with HA mineralisation on the cell surface after 120 h fermentation (a) HPA *Serratia* sp. (b) LPA *Serratia* sp, black arrows indicate areas of HA mineralisation.

Figure 43(a) shows HPA *Serratia* cells after a 120 h fermentation where a large amount of HA mineralisation has taken place making the cell morphology barely visible. The majority of HPA *Serratia* cells presented high amounts of HA mineralisation on the surface. The HPA cells fermented for 120 h showed an overall average yield of 768 mg.

Figure 43(b) shows an area of the sample where LPA *Serratia* cells have mineralised HA in small amounts on the surface. *Serratia* cells with HA mineralisation are identified with black arrows. LPA *Serratia* cells demonstrated an overall average yield of 54 mg. Statistical analysis confirmed that there is a significant difference ($p = 0.000003$) between HA yields produced from HPA and LPA *Serratia* sp.

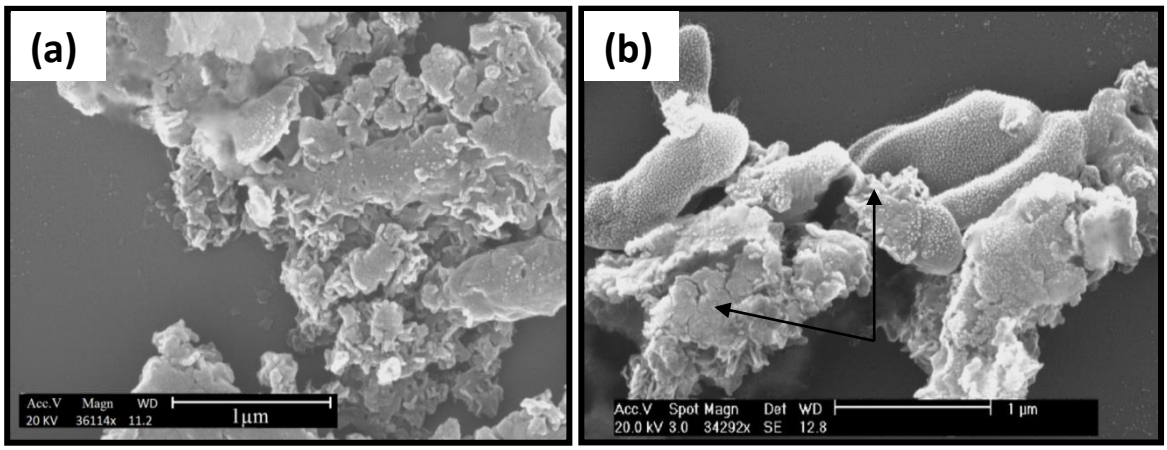

Figure 44: SEM images of *Serratia* cells with HA mineralisation on the cell surface after 216 h fermentation (a) HPA *Serratia* cells (b) LPA *Serratia* cells, black arrows indicate areas of high HA mineralisation.

Figure 44(a) shows HPA *Serratia* cells after a 216 h fermentation where a large amount of HA mineralisation had taken place to the extent where the cells were no longer visible. Large accumulation of HA in the HPA cells fermented for 216 h was consistently observed. A greater overall average yield of HA from HPA cells were observed after 216 h of fermentation. HPA cells yielded 2.61 g whereas LPA cells yielded 2.12 g.

Figure 44(b) demonstrated SEM images of accumulated HA in large amounts on the surface of LPA cells. In both SEM images (a) and (b) the amount of HA mineralisation observed on the cells was similar, all the observed cells presented significant HA mineralisation. Statistical analysis showed that there is no significant difference ($p = 0.485316$) between HA yields produced from HPA and LPA *Serratia* sp. after being fermented for 216 h. It has been previously reported that the yield of mineralised HA is heavily dependent upon the concentration of substrates (G2P, $CaCl_2$) that the cells are dosed with and that longer fermentations will result in greater HA mineralisation by the cells. [115].

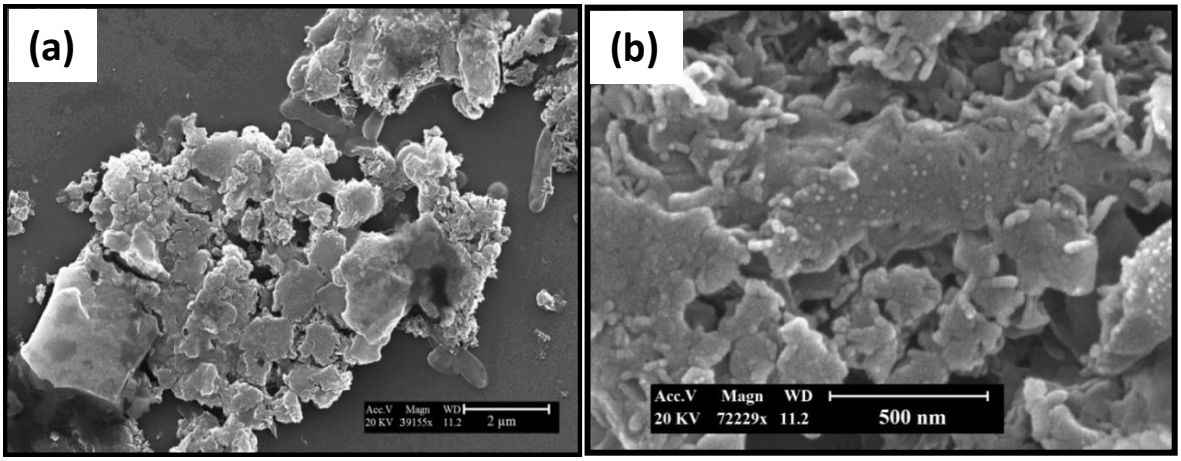

Figure 45: SEM images of *Serratia* sp. with HA mineralisation occurring on the cell surface after 360 h fermentation (a) HPA *Serratia* sp. (b) LPA *Serratia* cells.

HPA *Serratia* sp. were observed under SEM after 360 h fermentation in order to observe the yield of accumulated HA. The majority of cells in Figure 45(a) appeared to be coagulated as a result of HA mineralisation on the cell surface. All the cells appeared to have large quantities of HA mineralisation. Figure 45(b) demonstrates LPA *Serratia* sp. after 360 h fermentation. The high magnification SEM image shows the surface of the mineralised HA in greater detail with strands of HA protruding away from the HA mass on the surface of the cells. A greater overall average yield of HA from HPA cells were observed after 360 h of fermentation. HPA cells yielded 3.40 g whereas LPA cells yielded 2.63 g.

A highly magnified image of HPA cells fermented for 360 h is presented in Figure 46 and shows a large degree of porosity within the surface structure of HA

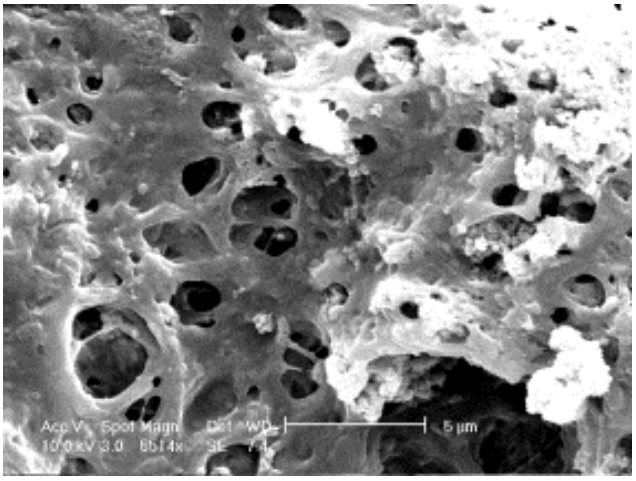

Figure 46: SEM images of HPA *Serratia* sp. with HA mineralisation occurring on the cell surface after 360 h fermentation.

Figure 46 shows a highly magnified image of HPA cells fermented for 360 h, showing a large degree of porosity within the surface structure of HA. The pores present on the surface significantly vary in diameter and appear to be present throughout the HA sample. The SEM images obtained in this study were compared to images from other research groups. Sammons *et al*. cultured *Serratia* sp. as a biofilm in solution containing an organic phosphate and calcium. The SEM image revealed a highly porous surface, which was similar to the SEM images obtained in this study. The porosity of HA presented by *Sammons et al.* was more distinct as the cells were purposely grown on biofilm in order to produce a large porous microstructure, which has potential advantages for cell and biomolecule attachment [169].

The SEM images obtained for HA mineralisation on the surface of *Serratia* sp. from the various fermentation periods correlate with the results obtained for the overall mean yields of HA. The SEM images obtained after 48 h and 120 h of fermentation with LPA cells showed a limited quantity of HA mineralisation, however HPA cells demonstrated visibly superior HA accumulations after 48 h and 120 h fermentations. HPA cells fermented for 48 h and 120 h produced an average mean yield of 596 mg and 768 mg respectively. Kashani 2007 presented

a yield of 297 mg of HA when using HPA cells cultured for 48 h under the same experimental conditions. [77].

The process of HA mineralization as previously described involves G2P becoming cleaved by the phosphatase enzyme resulting in the liberation of inorganic phosphate and providing a nucleation site for the growth of calcium phosphate crystals on the cell surface [113, 116]. Taking this into consideration it was expected that the LPA *Serratia* sp. would mineralise lower yields of HA, which was observed after 48 h and 120 h fermentations. However, the LPA *Serratia* sp. produced similar yields of HA compared to HPA cells after 216 h and 360 h fermentations. This sudden increase in HA mineralisation for LPA cells at 216 h and 360 h fermentations may be as a result of up regulation of another enzymatic pathway responsible for the liberation of inorganic phosphate. Further research is required into the various enzymatic pathways responsible for the liberation of phosphate on the surface of *Serratia* sp.

3.7.2. *Transmission electron microscopy*

TEM images of PHB were obtained from LPA and HPA *Serratia* sp. fermented for 48, 120, 216 and 360 h. The majority of the cytoplasmic space was taken up by densely packed inclusion bodies of PHB varying between 0.2 – 0.5 μm in diameter. The majority of PHB inclusions within the cytoplasm appeared to be densely packed in the centre of the cells, which would suggest is where PHB production and storage is initially taking place. Even though many of the inclusions are densely packed free space is available within the cytoplasm which suggests that the maximum storage potential of the cells has not been reached. Previous work by Lugg *et al.* showed similar TEM images of *Serratia* sp cells with varying number of PHB inclusions shown to be dependent on the fermentation [28].

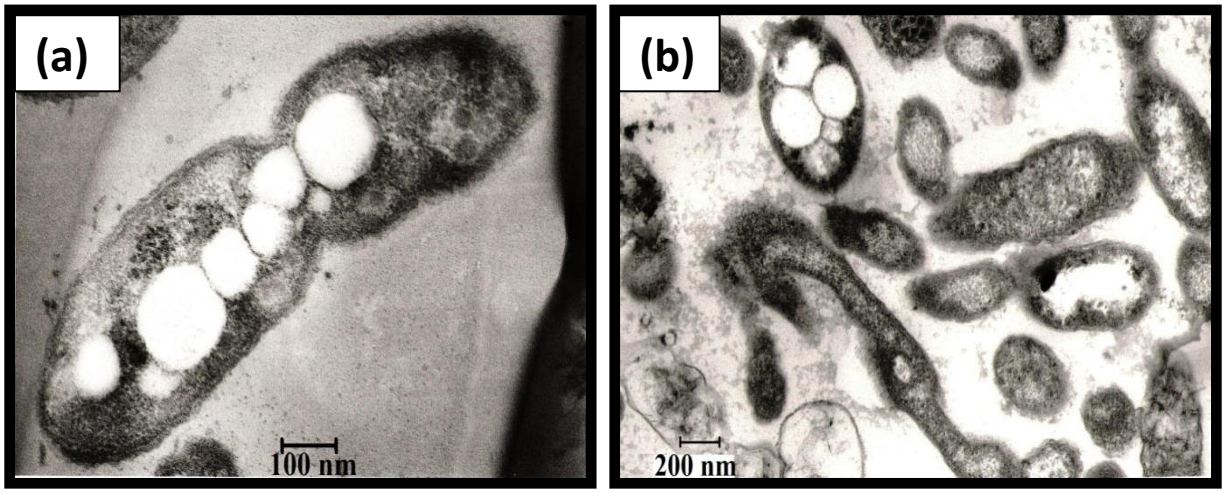

Figure 47: TEM images of inclusion bodies accumulated within the cells after 48 h fermentation. (a) LPA *Serratia* sp. (b) HPA *Serratia* sp.

Figure 47(a) focuses on an individual LPA *Serratia* cell fermented for 48 h and shows the presence of eight inclusion bodies of PHB within the cytoplasm. Free space can be observed within the cytoplasm indicating that a greater number of inclusion bodies can be packed within the cell. The majority of cells did not show any inclusion body formation within the cytoplasm. Figure 47(b) shows a group of HPA *Serratia* cells. A single *Serratia* cell can be observed with five PHB inclusions, however the majority of cells observed did not contain any inclusion bodies within their cytoplasm. The inclusion body formations in Figure 47(a) and (b) appeared to be similar with a high number of cells not containing any PHB inclusions.

The results of the TEM images after 48 h of fermentation were consistent with the yields of PHB that were extracted from both types of cell. Statistical analysis of the overall average yields of PHB after 48 h fermentation (T test; $p < 0.05$) confirmed that there was no significant difference ($p = 0.208000$) between PHB yields produced from HPA and LPA *Serratia* cells. The overall average yield of PHB from LPA cells was 6.2 %w/w compared with only 1.1 %w/w for HPA cells. The TEM images observed for LPA cells on average appeared to have greater numbers of PHB inclusions per cells compared with those of HPA

cells. The TEM images support that fact the cells do begin to form PHB inclusions after 48 h fermentations in both LPA and HPA *Serratia* cells.

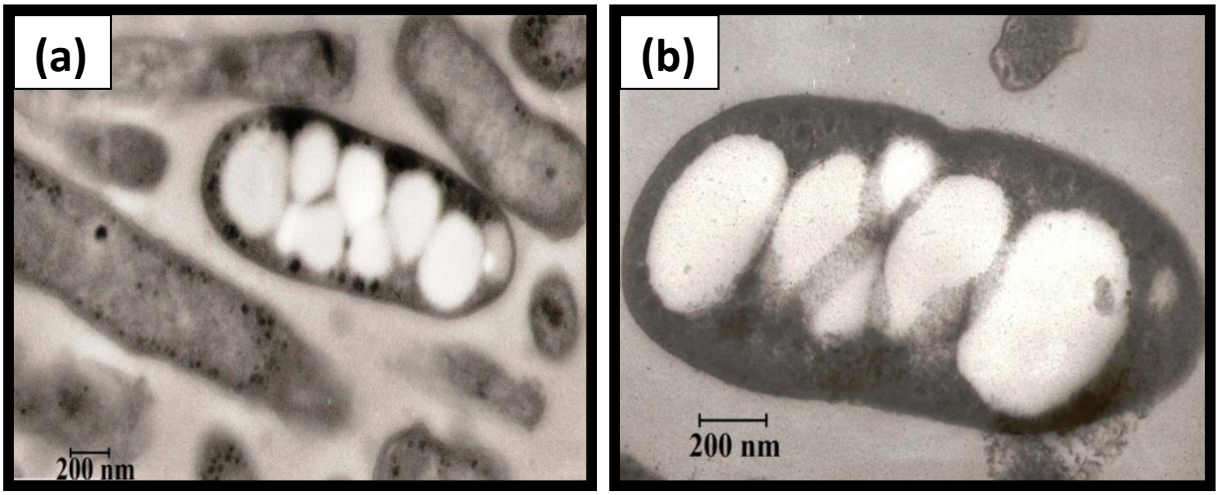

Figure 48: TEM images of inclusion bodies developed within the cells after 120 h fermentation. (a) LPA *Serratia* cells (b) HPA *Serratia* cell.

Figure 48(a) shows PHB inclusion body formation from LPA cells fermented for 120 h, where a single *Serratia* cell consisting of eight tightly packed PHB inclusion bodies can be observed. The surrounding cells do not show any inclusion body formation. The observed *Serratia* cells with PHB inclusions do not appear to have much free cytoplasmic space available. This suggests that the cells with PHB inclusions had reached their maximum capacity for the storage of PHB. A large population of the LPA *Serratia* cells still did not include any inclusions. *Serratia* cells with minimal PHB formation were also observed, suggesting that many of the cells were at the initial stages of PHB inclusion accumulation.

Figure 48(b) shows a single HPA *Serratia* cell after 120 h fermentation. The cell consists of six individual PHB inclusions within its cytoplasm. TEM images of HPA cells on average appeared to have greater number of inclusions compared to the HPA cells fermented for 48 h. The LPA *serratia* cells on average demonstrated greater number of PHB inclusions per cell compared to those of HPA. Observations made from the TEM images were in agreement with

the extracted yields of PHB. LPA *Serratia* cells produced an overall average yield of 13 %w/w compared to only 1.1 % from the HPA cells. Statistical analysis confirmed a significant difference ($p = 0.042814$) between the PHB yields recovered from HPA and LPA *Serratia* sp after 120 h fermentation.

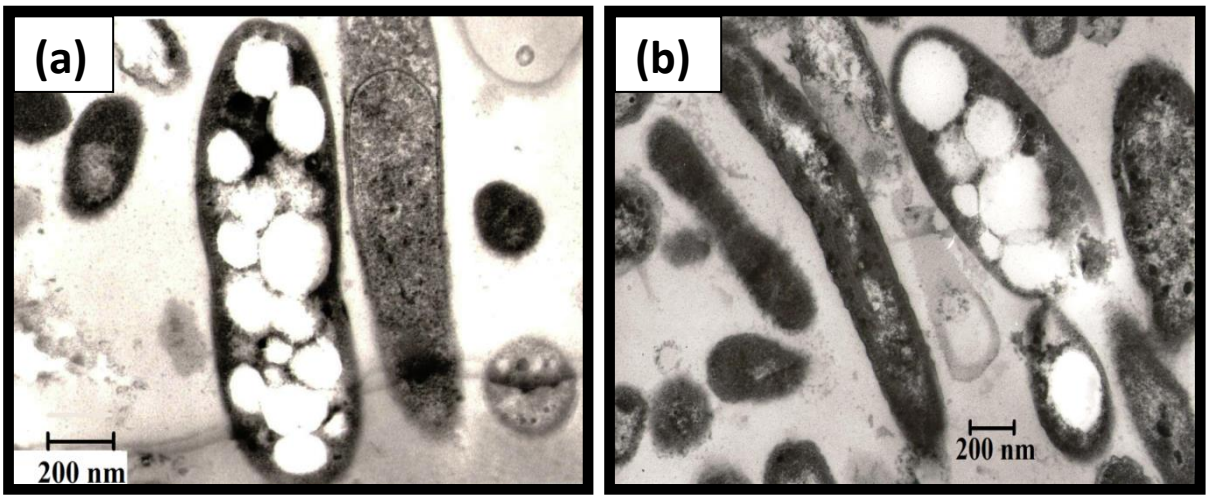

Figure 49: TEM images of inclusion bodies developed within the cells after 216 h fermentation. (a) LPA *Serratia* cells showing PHB inclusion bodies (b) HPA *Serratia* cells showing PHB inclusions.

Figure 49(a) represents LPA cells fermented for 216 h and shows the formation of a large amount of PHB inclusions by a single cell. Fifteen PHB inclusions in total were accumulated by the cell that ranged in diameter from 0.1 to 0.3 µm. The cell appears to be limited for cytoplasmic space as a result of the large number of inclusions. A large proportion of the cells observed by TEM resulted in large numbers of PHB inclusions with little space available for any further inclusion body formation. However, many cells still demonstrated minor PHB inclusion formation, on average five inclusions per cell was observed.

Figure 49(b) shows HPA *Serratia* cells after 216 h fermentation. Two PHB accumulating cells can be observed. The larger cell contains seven PHB inclusions with diameters ranging

from 0.1 to 0.4 µm, the smaller cell consists of only one large PHB inclusion with a diameter of 0.2 µm. The majority of cells observed did not appear to be saturated by PHB inclusions and could potentially store many more PHB inclusions within their cytoplasm. LPA *Serratia* sp. fermented for 216 h demonstrated the greatest yields of extracted PHB, the observations from the TEM images strongly support this argument as large amounts of PHB inclusions (~7) ranging in diameters of 0.1 to 0.3 µm were observed in the majority of cells. The LPA cells yielded 14.6 %w/w compared to 3.34 %w/w from HPA cells. Statistical analysis showed a significant difference ($p = 0.000362$) between the recovered PHB from HPA and LPA *Serratia* cells after 216 h of fermentation.

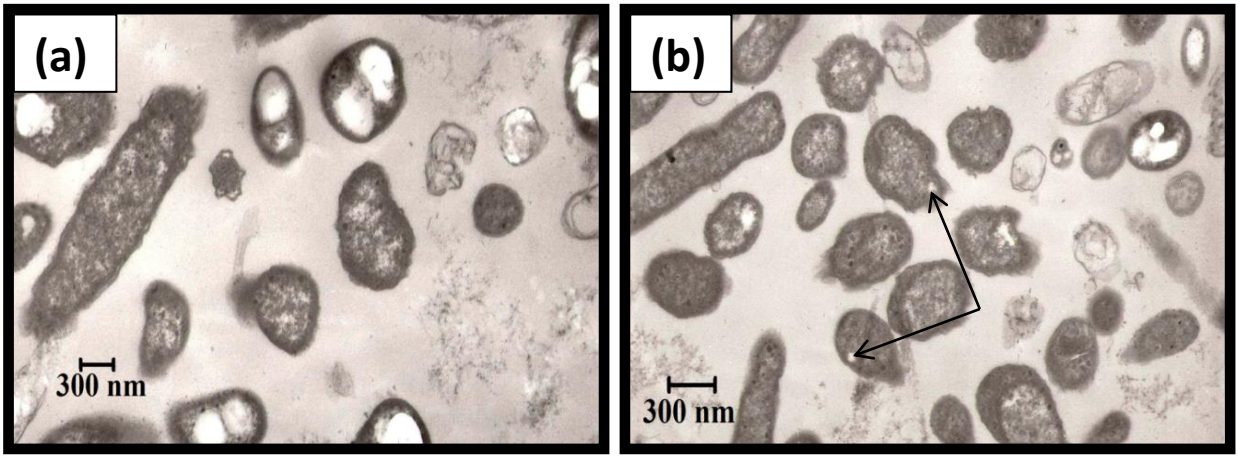

Figure 50: TEM images of inclusion bodies developed within the cells after 360 h fermentation. (a) LPA *Serratia* cells (b) HPA *Serratia* cells.

Figure 50(a) demonstrates LPA cells fermented for 360 h. PHB inclusions were not present in all cells; while the smaller *Serratia* sp. with accumulated PHB did not consist of more than two inclusions per cell. The majority of cells observed consisted of a maximum of four PHB inclusions per cell with an average diameter of ~ 0.2 µm. This decrease in PHB inclusions was expected as the overall mean yield of PHB from LPA cells after 360 h fermentation was 2.2 %w/w.

Figure 50(b) shows HPA cells within a small cluster. PHB inclusions within the cells were similar to those observed from LPA cells. The diameters of the PHB inclusions were ~1 µm and the cells on average consisted of three PHB inclusions per cell. A large proportion of the cells had traces of PHB inclusions within the cell (outlined with arrows), where PHB inclusions may have been degraded by the cell.

In Figure 50(a) and (b) The *Serratia* sp. did not show a large proportion of PHB inclusions. This is as a result of *Serratia* sp. depolymerising the stored PHB for energy (outlined in section 3.4). As the carbon source in the culture solution becomes depleted, the cells will begin to hydrolyse the stored PHB inclusions via intracellular PHB depolymerase, which acts to break down the polymer into monomers and dimers [248]. It is possible that as the concentration of carbon sources in the medium (glycerol and citrate) was not sufficient to sustain the PHB inclusion formation and the cells would begin to breakdown the stored inclusions.

A trend was observed whereby *Serratia* sp. resulted in a greater number of inclusions per cell at longer culture periods. However, at 360 h fermentation period the *Serratia* sp. resulted in the smallest number of inclusions per cell. The cells demonstrating inclusions did so in small numbers, the cells did not appear to be packed in the same manner observed at 216 h of fermentation.

Chapter 4 : Results and Discussion

Development and characterisation of electrospun fibres of PHB from various carbon sources synthesised from *Ralstonia eutropha*

4.1. *Introduction*

The *R. eutropha* species is considered to be the model organism for studying PHB synthesis and accumulation as it is capable of utilizing a wide range of carbon sources [27]. In an attempt to make the process cost effective, two types of oil (rapeseed and olive oil) will be utilised as the carbon source. Oils have been chosen as carbon sources due to the bacterial mechanism involved in the conversion of fatty acids from oil to PHB. As fatty acids are metabolised they are converted into (R)-3-hydroxyacyl-CoA, which is subsequently converted into PHA by the action of PHA synthase. Since plant oils have a greater number of carbon atoms per gram compared to other substrates, they are potentially a better substrate for the production of PHB [205]. Rapeseed oil was chosen for these experiments as a result of its low cost (€ 985.24 per tonne) and high PHA production [27], which made it a viable option for large scale industrial use. In addition, cooking oils disposed of by many restaurants and fast food chains can be a low cost carbon source and can be readily available in large amounts [206]. Glucose was also used as a carbon source due to it being the most traditional and most researched carbon source for the production of PHB from bacterial cells. A substantial increase in PHB production has also been observed when using glucose as a carbon source in the *R. eutropha* strain of bacteria [27]. PHB production from sugars as outlined in Figure 9 follows a different synthesis pathway to fatty acids, as once converted to acetyl-CoA they do not undergo β-oxidation.

PHB synthesised from oil and glucose will be characterised and their thermal and molecular properties will be compared. It has been shown how various carbon sources can affect the properties of bacterial synthesised PHB, which in turn can affect the application of the polymer. It is therefore essential to study not only the effect of the carbon source on the percentage productivity but also its effect on the properties of the synthesised polymer. These properties affect the applicability of the polymer. In order to demonstrate that bacterially

synthesised PHB can be successfully processed for biomedical applications, electrospinning will be carried out in order to produce nanofibres of PHB. Electrospun nanofibres of PHB have a wide range of applications from filtration in the engineering industry to various medical applications such as wound dressing, tissue template, tissue engineering and medical prosthesis [207, 208]. The source and properties of the bacterial PHB, used for nanofibre production, is largely missing in literature. For this reason, the effects of carbon source on the properties of PHB and the consequent effects on the diameter size of electrospun nanofibes will be investigated in this study.

4.2. *Growth of R. eutropha H16*

Growth curves were obtained for all three carbon sources and are presented in Figure 51. The initial viable cell numbers were $\log_{10}$ 7.23 cfu/ml, $\log_{10}$ 7.39 cfu/ml and $\log_{10}$ 7.69 cfu/ml for glucose, rapeseed and olive oil fermentations, respectively. As expected, the viable cell numbers increased after 48 h of fermentation. The cells grown in olive oil and rapeseed oil increased 2 $\log_{10}$ when compared to the initial concentration of viable cells. However, cells fermented in glucose as the primary substrate showed an increase of less than 1 $\log_{10}$. ANOVA analysis was carried out and suggested no significant difference ($P > 0.05$) between the viable cell numbers of olive oil and rapeseed oil during various stages of growth. ANOVA analysis showed that the viable call numbers of rapeseed oil and olive oil fermentations were significantly higher ($P > 0.05$) compared to that of glucose fermentation between 3 and 48 h of cell growth.

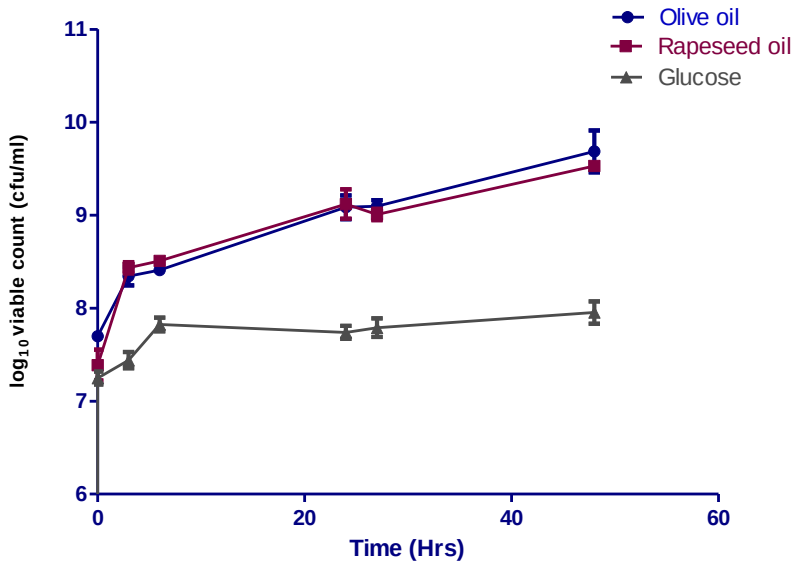

Figure 51: Growth curve of *R. eutropha* NCMBI 10442 grown in BSM at 30 °C using glucose, olive oil and rapeseed oil as the carbon sources.

4.3. *Yields of PHB produced from R. eutropha*

PHB was extracted from *R. eutropha* cells after 48 h of fermentation in all three carbon sources. The CDW, PHB yield and the percentage PHB concentration per cell for each carbon sources is presented in Table 31. The results showed that *R. eutropha* cells inoculated with olive oil and rapeseed oil as substrates produced the greatest PHB yield at 1.26 g/l (36 %w/w) and 1.06 g/l (36 %w/w), respectively. Fermentations with glucose showed the lowest accumulated PHB yield of 0.13 g/l (12 %w/w). ANOVA analysis showed no significant difference between extracted PHB yields produced from rapeseed and olive oil fermentations. The PHB yields obtained from using rapeseed and olive oil as substrates were significantly higher ($P < 0.05$) compared with PHB yields from fermentations with glucose.

Table 31: The CDW, average PHB (n=3) and the PHB produced (%w/w) from the different carbon sources after 48 h fermentation**.**

Oil	Average CDW (g/l)	Average PHB (g/l)	PHB (%w/w)
Rapeseed oil	2.90	1.06 ±(0.1)	36
Olive oil	3.45	1.26 ±(0.2)	36
Glucose	1.07	0.13 ±(0.01)	12

R. eutropha cells were found to grow best in media inoculated with 20 g/l of oils compared with media inoculated with 20 g/l of glucose as shown in Figure 51. The growth of cells in glucose was observed to go into a stationary growth phase after the initial 6 h of incubation. This stationary growth phase is likely a result of the *R. eutropha* cells utilizing all the available glucose present within the media during the initial 6 h of fermentation.

Fermentations of *R. eutropha* cells inoculated with oil yielded 36 %w/w of PHB. Fermentations with glucose produced the lowest PHB yield of 12 %w/w as shown in Table 31. Plant oils are known to possess a greater number of carbon atoms compared with sugars [7, 29], for this reason the higher yield of PHB recovered from both olive and rapeseed oil compared to glucose is possibly a result of the composition of the carbon source as this was the only variable present in the fermentation experiments. The results of the experiments show the recovered yield of PHB from rapeseed and olive oil to be almost three times the yield of PHB recovered from the fermentations with glucose. It has been reported by Akiyama *et al*. that the yield of PHB recovered from oil is twice the amount recovered from glucose [249]. Fernandez *et al.* reported PHB accumulation of 66.1 %w/w using soy bean oil, 29.4 %w/w when using waste frying oil and 16.8 % when using glucose in bacterial cultures of *Pseudonomas resinovorans* [250]. Similar yields of PHB (~30 %w/w) have been reported when inoculating *R. eutropha* cells with 20g/l of rapeseed oil [27].

The use of glucose as a carbon source in this study was for the comparison of PHB yields produced between sugars and oils. The cost of harvesting PHB at industrial level from species of *Alcaligenes eutrophus* has been reported to cost ~$8/Kg [251]. The high cost is primarily due to the carbon source. As a result of its high cost, it is unlikely for glucose to be used as a carbon source for industrial production of PHB. More economical carbon sources such as molasses contain sugars and will produce PHB in an identical manner. The substrate cost of glucose per tonne of PHB is ~ $950 compared to ~$520 from Molasses [252].

The relatively high whole sale cost of olive oil (€ 2,200 a tonne) is an important factor when determining its industrial viability. The price of olive oil also suffers from fluctuations, it was recently reported how the wholesale price jumped 62 % in three months (June-Sept 2012) after a severe drought in Spain, the world's largest producer [253]. Rapeseed oil is commonly used as frying oil within Europe. The popularity of rapeseed oil in Europe has soared as it has become a low cost alternative to olive oil. Rapeseed oil was chosen for these experiments as a result of its low cost (€ 985.24 per tonne) and high PHB production [27], which made it a viable option for large scale industrial use. Waste rapeseed oil has been reported to have been used successfully for the production of PHB and PHAs with valerate monomers [254]. The use of waste rapeseed oils as a carbon source has been reported to be a low cost alternative to the use of pure oils. Waste rapeseed oil (from fast food restaurants) when used as a substrate has been reported to produce 0.98 g/g, compared with 0.48 g/g from glucose [30]. The low cost of waste oils from various fast food chains and restaurants at 20p per Litre, would make the use of waste oils a much more economically viable solution in the production of PHB on an industrial scale. Another benefit of using waste rapeseed oil is that it can be used for the production of PHAs without the need for any filtering. Applications such as the production of soap or biodiesel from waste oil require it to be treated and filtered [27].

4.4. *Morphologies of PHB Fibres*

Three individual samples of PHB were produced and used in order to produce nanofibres of G-PHB (PHB produced from glucose), O-PHB (PHB produced from olive oil) and R-PHB (PHB produced from rapeseed oil). For each PHB sample three separate solutions were electrospun in order to produce nanofibres at 1.5, 2 and 2.5 %w/v and were compared to samples of non-electrospun PHB. To ensure reproducibility, experiments for each concentration were carried out in triplicate using two different preps. The SEM micrographs presented in Figures 52, 54 and 56 shows the successful production of fibres from each of the PHB samples at all three solution concentrations.

4.4.1. *Morphology of G-PHB nanofibres*

In the case of G-PHB nanofibres, an increase in diameter was observed with increasing solution concentrations. The SEM images obtained from electrospun G-PHB are presented along with histograms of diameter distributions in Figure 52. The G-PHB polymer solution with a concentration of 1.5 %w/v resulted in a higher frequency of fibre diameters at ~ 400 nm. The SEM image of the PHB nanofibres clearly showed bead formation. This would suggest the low solution concentration is resulting in a lower solution viscosity and consequently bead formation occurs. The formation of beads have been reported to occur when viscosity of the given sample solution is low [255-257]. A solution concentration of 2 %w/v of G-PHB yielded electrospun nanofibres with a higher frequency of fibre diameters at ~950 nm as shown in Figure 52(1b). An increase in fibre diameter of ~ 550 nm was observed in comparison to nanofibres of G-PHB obtained from 1.5 %w/v solution concentration. As expected the nanofibres produced from G-PHB at a higher solution concentration of 2.5 %w/v resulted in a higher frequency of fibre diameters at ~ 1100 nm as shown in Figure 52(1c). The increase in fibre diameter size was ~225 nm compared to those obtained from 2 % G-PHB. The increase in fibre diameter with increasing solution concentrations can be attributed to the

increased viscosity of the polymer solution, as all other parameters were kept constant. The increased viscosity helps the polymer jet to resist bending instabilities and so will travel in a straight line for a longer period, minimising its travelling distance from the needle tip to the collector [151]. Gomes *at al.* carried out extensive characterisation of the electrospinning process using precursor solutions with various solution concentrations of Polyacrylonitrile (PAN). It was reported that higher solutions concentrations will result in larger average fibre diameters [258]. Dietzel *et al.* reported the presence of larger and more uniform fibre diameters with greater solution concentrations of Poly (ethylene oxide) (PEO) [259].

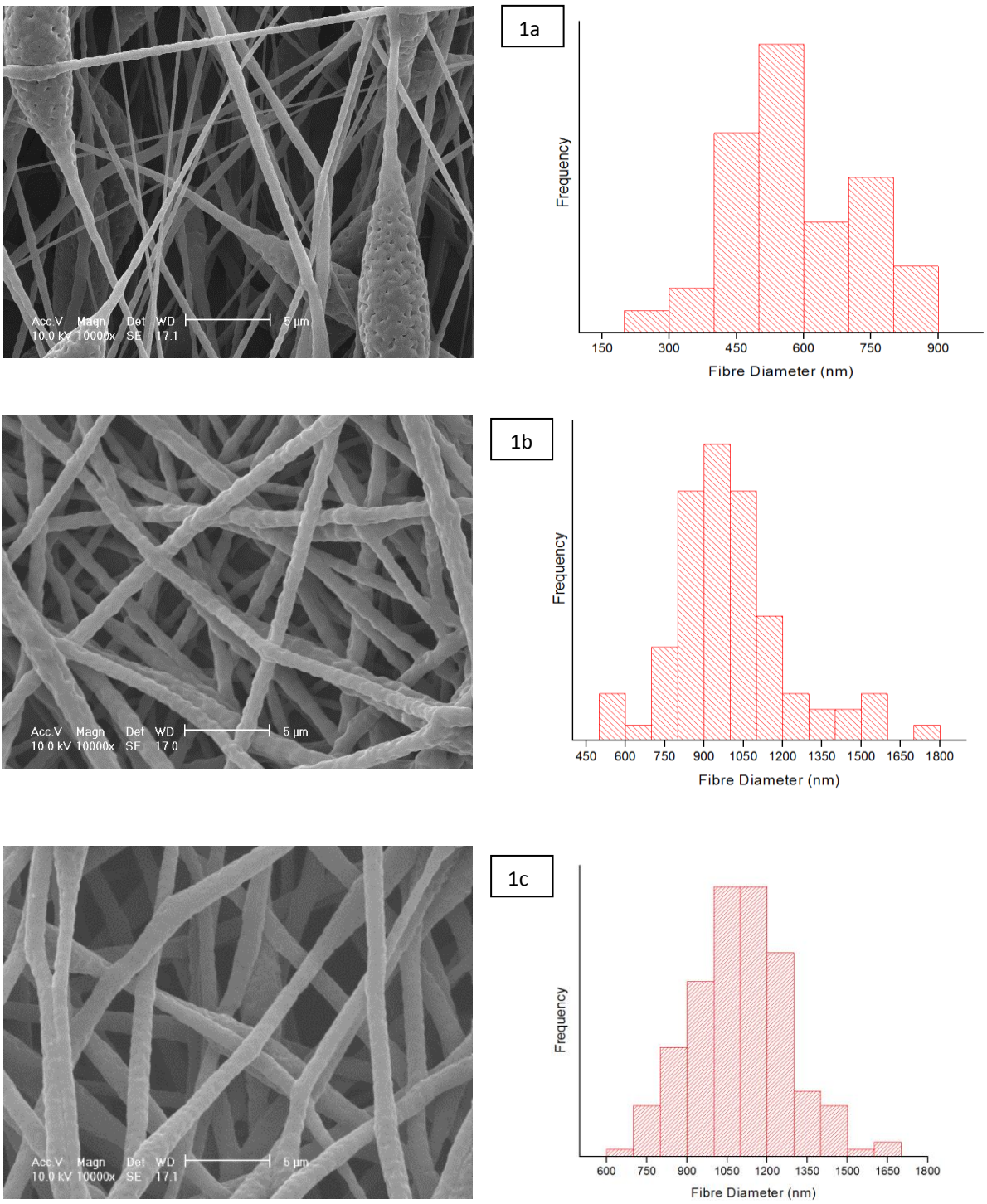

Figure 52: SEM images alongside respective histograms demonstrating the effect of G-PHB solution concentration on the morphology and the fibre diameter distribution of electrospun fibres. (1a) Solution concentration of 1.5 %w/v. (1b) Solution concentration of 2 %w/v. (1c) Solution concentration of 2.5 %w/v.

The histogram showing average diameter distribution for G-PHB at various concentrations is presented in Figure 53. Statistical analysis (T test; $p < 0.05$) confirmed that there is a significant difference ($p = 0.000001$) between the average fibre diameters of G-PHB at 1.5 %w/v compared to 2 %w/v and 2.5 %w/v. No statistical significant difference was observed between the average fibre diameters of G-PHB with a solution concentrations of 2 % compared with that of 2.5 %w/v. As expected the diameter distributions resulted in an increase in fibre diameter with greater solution concentrations. As solution concentration was the only variable in these experiments, it can be deduced that the changes in solution concentration and therefore viscosity account for the increase in average fibre diameters observed.

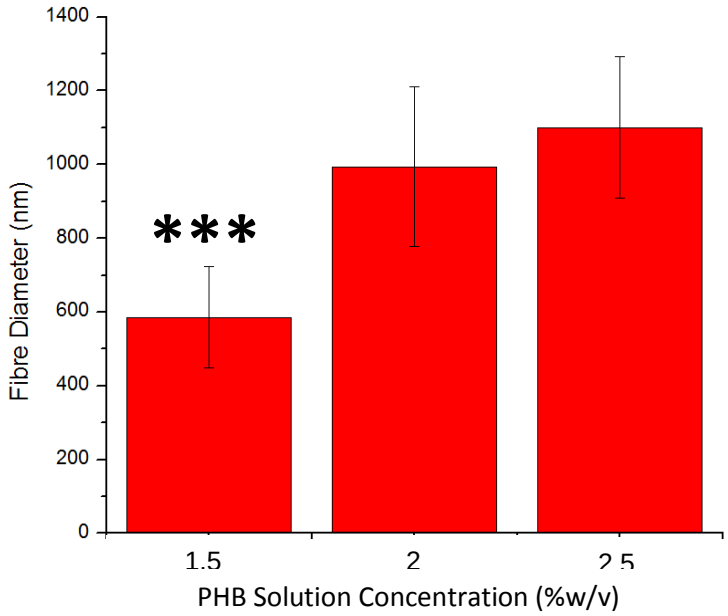

Figure 53: Bar chart of the average fibre diameters for the electrospun samples of G-PHB at solution concentrations of 1.5, 2 and 2.5 %w/v. The values are accompanied by their respective error bars. Level of significance: Three (***) for 0.001 or 0.005.

4.4.2. *Morphology of O-PHB nanofibres*

Electrospun samples of O-PHB resulted in an average increase in fibre diameter with increasing solution concentrations. SEM images obtained from electrospun O-PHB are presented and accompanied with histograms representing the fibre diameter distribution in Figure 54.

The solution concentration of 1.5 %w/v resulted in higher frequency of fibre diameters at ~750 nm. As expected, large amounts of bead formation were observed along the nanofibres. The bead formation can be identified in Figure 54(2a). At low solution concentrations the presence of either electrosprayed beads or beaded fibres were formed [214, 256, 257]. At solution concentrations of 2 %w/v, higher frequency of fibre diameters at~1050 nm was observed as shown from the diameter distribution histogram in Figure 54(2b). The fibre diameters obtained were considerably greater than those obtained from 1.5 %w/v solution concentration. Although, larger fibre diameters were observed, a small amount of bead formation was still present. The formation of beads occurred as a result of the low solution viscosity [151]. As previously mentioned low viscosity has been linked with the formation of beaded fibres [157]. The highest frequency of fibre diameters from 2.5 %w/v solution concentration was ~1100 nm as shown from the diameter distribution histogram in Figure 54(2c). This was expected as the increase in solution concentration and consequent increase in viscosity, resists the bending instability of the jet resulting in more uniform fibres.

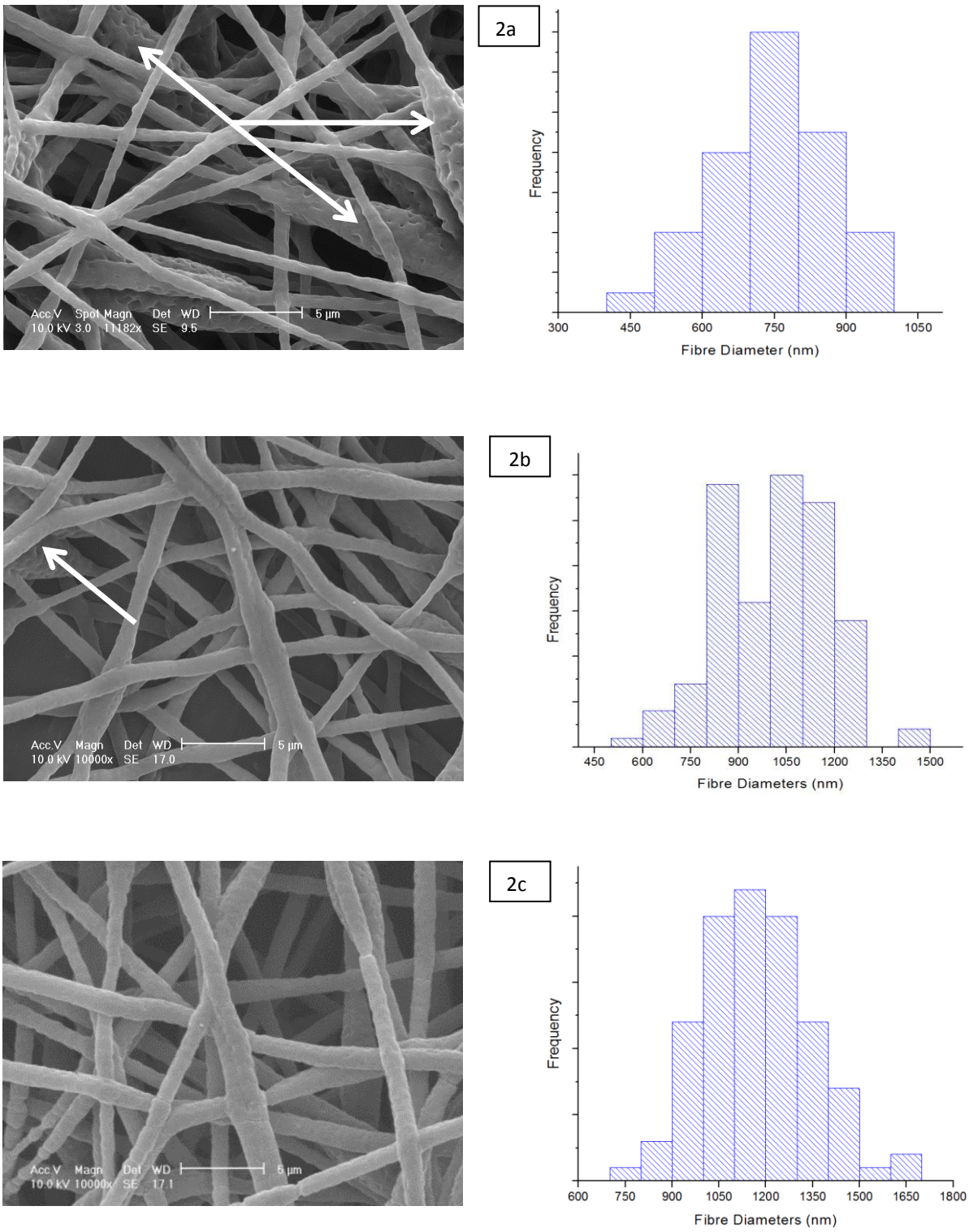

Figure 54: SEM images alongside respective histograms demonstrating the effect of O-PHB solution concentration on the morphology and the fibre diameter distribution of electrospun fibres (2a) Solution concentration of 1.5 %w/v. (2b) Solution concentration of 2 %w/v. (2c) Solution concentration of 2.5 %w/v.

The histogram for the average fibre diameter distribution of O-PHB solution at various concentrations is presented in Figure 55. Statistical analysis (T test; $p < 0.05$) confirmed that there is a significant difference ($p = 0.000001$) between the average fibre diameters of O-PHB at 1.5 %w/v compared to 2 %w/v and 2.5 %w/v. No statistical significant difference was observed between the average fibre diameters of O-PHB with a solution concentrations of 2 % compared with that of 2.5 %w/v.

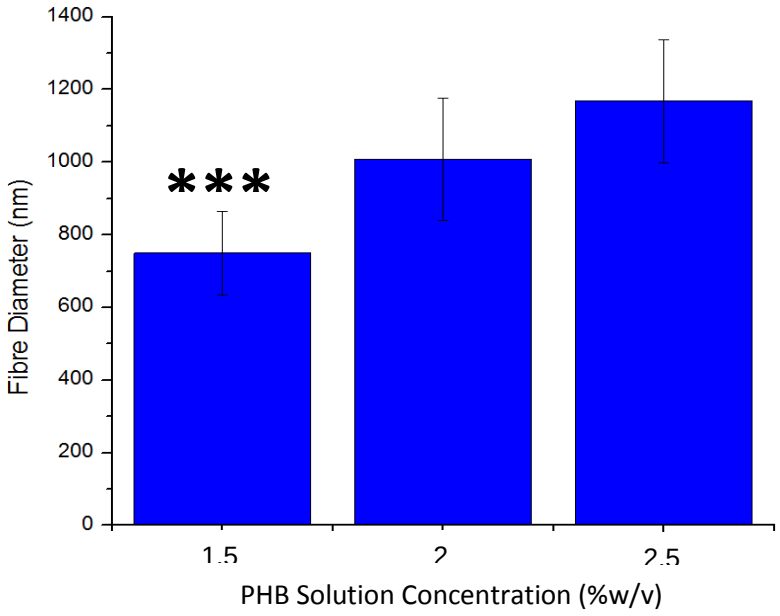

Figure 55: Bar chart of the average fibre diameters for electrospun sample of O-PHB at solution concentrations of 1.5, 2 and 2.5 %w/v. The values are accompanied by their respective error bars. Level of significance: Three (***) for 0.001 or 0.005

4.4.3. *Morphology of R-PHB nanofibres*

SEM images obtained from electrospun R-PHB are presented and accompanied with histograms of fibre diameter distributions for the various solution concentrations (Figure 56). At a solution concentration of 1.5 %w/v a higher frequency of fibre diameters at ~325 nm was observed, which was considerably lower than the values obtained from G-PHB and O-PHB

with 1.5 %w/v solution concentration. As the viscosity of the R-PHB solution was low, it could not resist the bending instability of the jet, which resulted in an increased flight time allowing greater time for the PHB fibres to lengthen and stretch before reaching the collecting plate [260]. However, minimal bead formation was observed in the SEM image for 1.5 %w/v (Figure 56(3a)), as the beads were of a smaller diameter and so were not clearly visible. Electrospun samples of R-PHB at solution concentrations of 2 % resulted in a higher frequency of fibre diameters at ~1050 nm as shown in the diameter distribution histogram in Figure 56(3b). The histogram shows a smaller range of fibre diameters; this is a desirable property for many applications of electrospun nanofibres. Bead formation was not observed in the SEM images for 2 %w/v R-PHB (Figure 56(3b)).

The higher frequency of fibre diameters at 2.5 % solution concentration was ~1050 nm, which was similar to the value obtained from 2 % solution concentration at~1050. However, a greater distribution of electrospun fibres were observed in 2.5 %w/v compared to 2 %w/v solution concentration and consequently a different average fibre diameter values would be observed.Minor bead formation was observed in fibres from solution concentration of 2.5 %w/v, as shown in Figure 56 (3c).

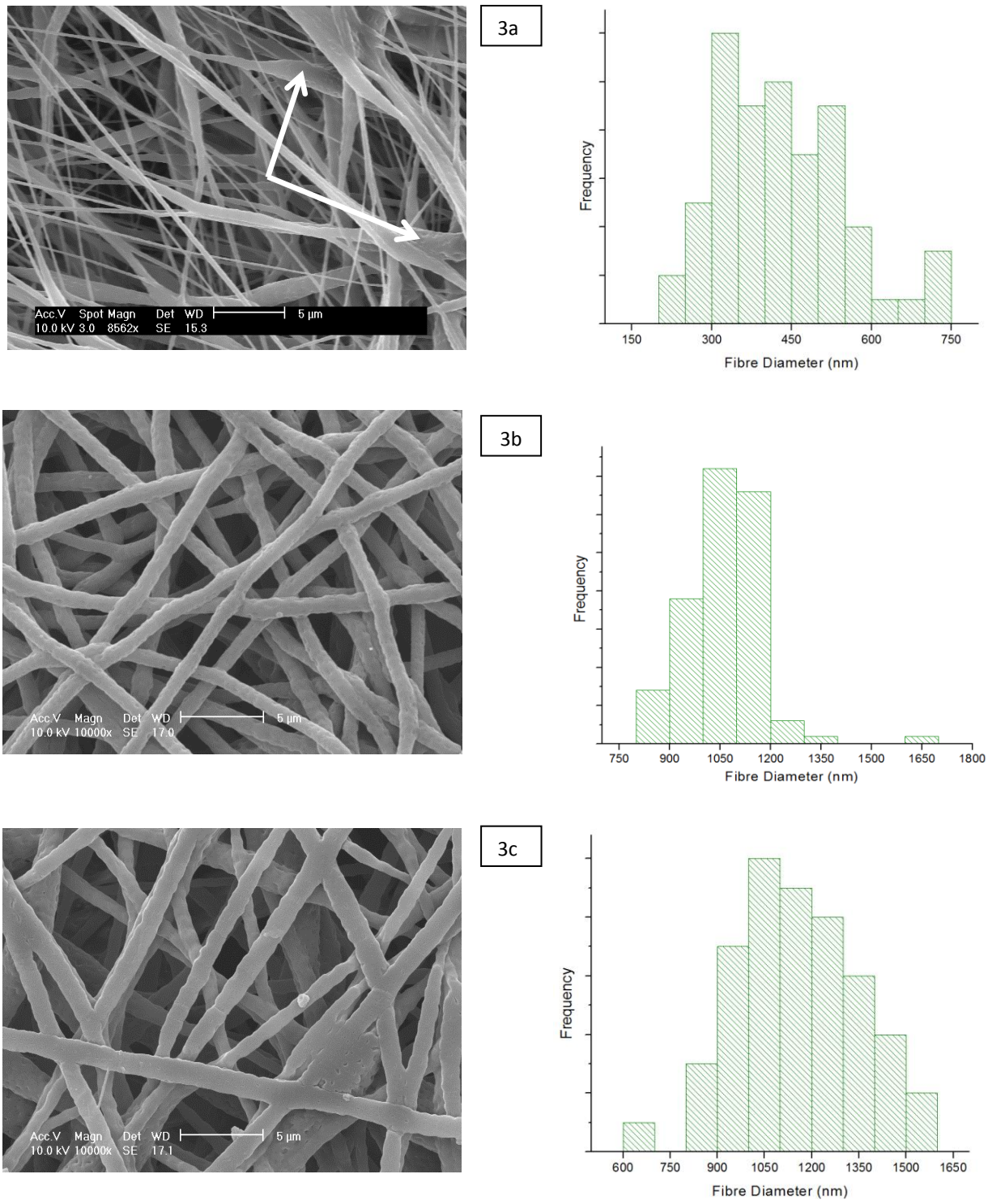

Figure 56: SEM images alongside respective histograms demonstrating the effect of R-PHB solution concentration on the morphology and the fibre diameter distribution of electrospun fibres (3a) Solution concentration of 1.5 %w/v. (3b) Solution concentration of 2 %w/v. (3c) Solution concentration of 2.5 %w/v.

The PHB nanofibres of R-PHB showed an increase in fibre diameter with increasing solution concentrations. Sombatmankhong *et al*. reported in a similar trend in fibre diameters with increasing polymer solution concentrations [214].

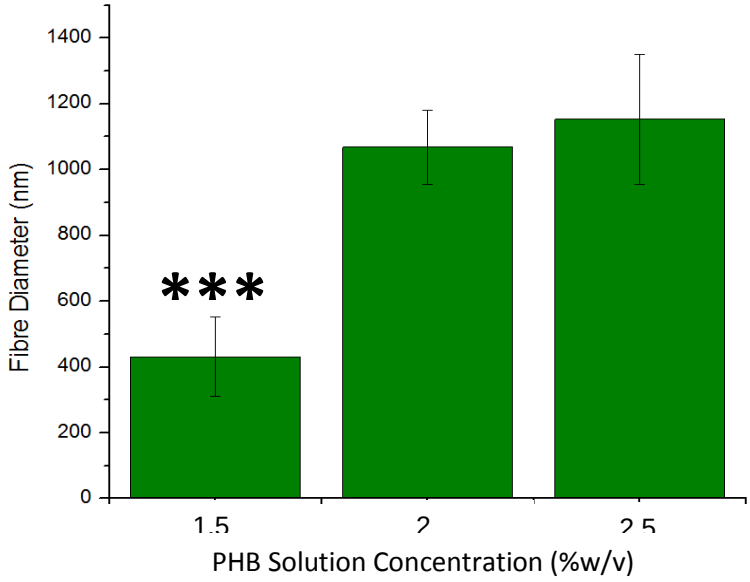

Figure 57: Bar chart of the average fibre diameters for electrospun sample of R-PHB at solution concentrations of 1.5, 2 and 2.5 %w/v. The values are accompanied by their respective error bars.

The average fibre diameters obtained for electrospun G-PHB, O-PHB and R-PHB at solution concentrations of 1.5 %w/v all presented bead formation. The average fibre diameters obtained for R-PHB from 1.5 %w/v solution concentrations were found to be the smallest at ~335. The largest average fibre diameters at 1.5 %w/v were observed from O-PHB at ~750 nm and were similar to the values obtained from G-PHB from 1.5 %w/v solution concentrations at ~600 nm. The fibre diameters from 2 %w/v and 2.5 %w/v solution concentrations from G-PHB, O-PHB and R-PHB were observed to be within the same region. The minor bead formation observed from 2.5 %w/v solution concentrations of R-PHB were

unexpected as an increase in solution concentration and consequent increase in solution viscosity should have eliminated the formation of beads.

The formation of beaded nanofibres was observed at low concentrations of the polymer solutions from G-PHB, O-PHB and R-PHB. In literature a wide range of nanofibres have been reported, produced from various polymer solutions and concentrations. Some of those nanofibres reported are beaded fibres, porous fibres, helical fibres, hollow fibres, branched fibres, flat ribbons, bent ribbons [261-264]. Beaded fibre formation is an undesirable effect when electrospinning polymer solutions. Bead formation has been reported to occur when the solution concentration is low [255]. Bead formation occurs as a result of surface tension, which minimizes the surface area [265]. Low solution concentrations result in a low surface tension, which will cause the jet to be broken down into drops. The disruption of the polymer jet will result in greater bead formation [266]. , therefore a lower surface tension will result in greater bead formation. An increase in polymer solution concentration will produce a greater surface tension resulting in fewer beads forming [267]. It can be concluded that the bead formation observed in the 1.5 %w/v and 2 %w/v (G-PHB and O-PHB) solution concentrations is as a result of the lower surface tension.

The electrospun fibres of G-PHB, O-PHB and R-PHB all demonstrated an increase in fibre diameter with increased solution concentrations. It was reported by Deitzel *et al*. that fibre diameters increased with an increasing polymer solution concentration based on a power law relationship [157, 258, 259]. The PHB solution viscosity is directly linked to the concentration of the PHB solution [151]. Increasing the polymer solution concentration at a set applied voltage can cause the ejected charged jet to travel in a straight line for a longer period of time before giving in to the bending instability and will have a lower tendency to be elongated and thinned before reaching the collector plate [152]

Electrospun G-PHB, O-PHB and R-PHB fibres produced from solution concentrations of 1.5 %w/v consisted of smaller fibre diameters. The thinning of the polymer jet could be attributed to the formation of multiple jets as a result of low solution viscosity. The formation of secondary jets acts to reduce the diameter of the PHB fibres [207]. All the PHB solutions at concentrations of 1.5 %w/v consisted of a lower solution viscosity, which may [259, 268, 269] or may not [161, 256, 270-273] have caused the jet to split into multiple jets during the electrospinning process.

The voltage that is applied to the polymer solution plays an important role in the development of PHB fibres [151]. The voltage used in these studies were consistent at 7 kV; this is as preliminary studies showed that an applied voltage of 7 kV resulted in consistent PHB nanofibres over a range of solution concentrations. The voltage used in this study was comparatively lower than other PHB electrospinning studies [214, 274]. A reduced voltage results in a weakened electric field, which may increase the flight time of the jet due to the reduced columbic forces within the jet. The flight time of the jet is dependent upon the voltage and concentration of the polymer solution [275]. An increased flight time allows greater time for the PHB fibres to lengthen and stretch before reaching the collecting plate producing fibres with a smaller diameter [207, 209, 276, 277]. As the voltage applied to the jet was only 7 kV less stretching of the PHB solution occurred, which resulted in PHB fibres with a greater fibre diameter at lower concentrations. This would suggest how non-beaded PHB nanofibres were obtained from comparatively low concentration of PHB polymer solutions.

The fibre diameters produced in this study were relatively large, with uniform fibres being around 1 µm. These relatively large fibres are thought to be due to the operating parameters used, in particular the low applied voltage of 7 kV. This low voltage was necessary to

produce a stable electrospinning system for all PHB samples in the current work however this parameter could be optimised with the aim to reduce diameters in future work.

The M_w of a polymer is also known to affect its viscosity in solution; a polymer with a high M_w will result in a solution with a higher viscosity. As discussed above it is expected that solutions with higher viscosities would produce fibres with larger diameters [151].

4.5. *Characterisation of PHB from R. eutropha*

4.5.1. *GPC*

GPC was carried out to determine the M_w, M_n and PD for the electrospun and non-electrospun samples of PHB. The GPC results for non-electrospun PHB from all three carbon sources are presented Table 32. The M_w for non-electrospun PHB were highest when glucose was utilised as a carbon source at 7.61 x 10^5 g/mol. The M_w obtained for non-electrospun PHB from rapeseed and olive oil were similar at 7.14 x 10^5 g/mol and 7.1 x 10^5 g/mol respectively. The GPC results presented in Table 32 demonstrate a higher uniformity of M_w distribution of PHB from glucose resulting in a smaller PD of 1.21 when compared with a PD of ~1.4 for PHB from rapeseed and olive oil. Electrospun PHB (2 %w/w) showed a slight decrease in M_w compared to non-electrospun PHB samples. The PD for all samples of PHB remained unchanged after electrospinning.

Table 32: The M_w, M_n and PD of electrospun and non-electrospun PHB from olive oil, rapeseed oil and glucose (M_w = weight average molecular weight, M_n = number average molecular weight and PD = Polydispersity. PD = M_w/M_n.

PHB	M_w (× 10^5 g/mol)	M_n (× 10^5 g/mol)	Polydispersity (PD)
O-PHB(Electrospun)	**5.92**	**4.15**	**1.43**
O-PHB	7.14	4.95	1.42
R-PHB(Electrospun)	**5.79**	**3.94**	**1.47**
R-PHB	7.1	4.89	1.45
G-PHB(Electrospun)	**7.35**	**6.07**	**1.23**
G-PHB	7.61	6.29	1.21

GPC analysis showed small differences in the molecular characteristics of PHB from oils and glucose. No significant differences were observed between the M_w of G-PHB compared to O-PHB and R-PHB. Greater M_w for PHB have previously been reported with fructose as a carbon source compared to virgin oils, soybean oil and waste edible oil [278, 279]. The presence of glycerol in plant oils have been suggested to be problematic as the glycerol is known to terminate PHA chain elongation by acting as a chain transfer agent and therefore reducing the M_w [280].

4.5.2. *DSC of Electrospun and non-electrospun PHB*

The results for the thermal analysis of electrospun PHB obtained using the different carbon sources at concentrations of 1.5, 2 and 2.5 %w/v were compared to non-electrospun samples. DSC traces were obtained from the PHB samples after re-heating and re-cooling. However, these traces were identical to the original heating and cooling traces and so were omitted. The T_g for PHB is known to be ~2 °C and therefore did not appear in any of the traces. The thermal properties for samples of non-electrospun G-PHB, O-PHB and R-PHB are presented in Table 33.

Table 33: Thermal properties of non-electrospurn PHB produced by *R. eutropha* grown in BSM at 30 ^{o}C and 150rpm using olive oil, rapeseed oil or glucose as sources of carbon. T_m = melting temperature and T_c = crystallisation temperature on cooling and C = crystallinity.

Carbon source	T_m (^{o}C)	T_c (^{o}C)	C (%)
Olive oil	173.2	121.6	54.2
Rapeseed oil	172.2	120.8	52.2
Glucose	172.5	118.6	53.5

No significant differences in the T_m, T_c and % crystallinity were observed between the PHB samples obtained from glucose, olive and rapeseed oil. The greatest difference between the % crystallinity were observed between olive and rapeseed oil at 54.2 % and 52.2 % respectively.

4.5.2.1. DSC of G-PHB

The heating and cooling process for samples of electrospun G-PHB at concentrations of 1.5, 2 and 2.5 %w/v are presented in Figure 58. The DSC traces for elctrospun G-PHB were compared to that of non-electrospun G-PHB. The thermal characteristics of electrospun G-PHB are summarised in Table 34 and were compared to those obtained from non-electrospun PHB in Table 33. The T_m and T_c values obtained for electrospun and non-electrospun G-PHB were within the expected regions for PHB.

Table 34: Thermal properties of electrospurn fibres of G-PHB with solution concentrations of 1.5, 2 and 2.5 %, T_m = melting temperature and T_c = crystallisation temperature on cooling and C = cystallinity.

	Polymer solution concentrations (% wt/v) during electrospinning								
Polymer	**1.5**			**2**			**2.5**		
	T_c (°C)	T_m (°C)	C (%)	T_c (°C)	T_m (°C)	C (%)	T_c (°C)	T_m (°C)	C (%)
G-PHB	120.8	173.2	50.2	116.5	171.5	51.1	118.6	166.4	52.6

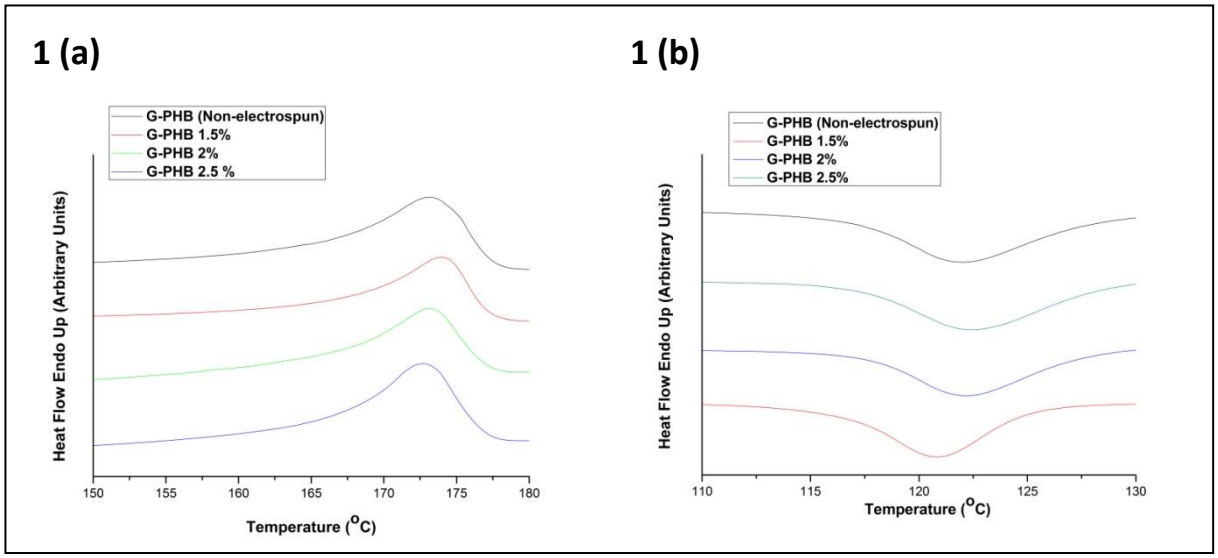

Figure 58: DSC trace for heating 2(a) and cooling 2(b) of electrospun and non-electrospun samples of G-PHB.

The T_m values were all found to be within the same region, with the exception of PHB from 2.5 %w/v, which resulted in a slightly lower T_m at 166.4 °C compared to 173.2 °C for the non-electrospun sample. No differences were observed in the breadth of the melting peaks, the breadth of the endothermic melting peak is dependent on a polymer's PD, a narrow PD will mean a lower distribution of polymer chains exist and consequently will reach melt at approximately similar temperatures [224]. The GPC results presented identical values for the PD of non-electrospun G-PHB compared with 2 %w/v electrospun G-PHB at 1.21 and 1.23,

respectively. The similar endothermic peak breadths observed are as a result of the identical PD.

No crystallisation peak was observed on heating for the DSC traces, this is in agreement with DSC data previously reported [281].It can be attributed to the lack of mobility present in the polymer chains [282]. The areas measured under the melting peaks can give the heat of fusion values for the PHB samples, these values were used to calculate the % crystallinity that are presented in Table 33. The % crystallinity obtained for the electrospun samples were lower compared to non-electrospun G-PHB. The electrospun samples of G-PHB resulted in an increase in crystallinity with decreasing solution concentrations of the electrospun PHB. This loss in crystallinity has been suggested to be as a result of the rapid solvent evaporation and solidification that occurs during the electrospinning process [283]. Yarin *et al.* stated how solvent evaporation is an important factor to consider as it implies solidification and as a result can affect the polymer properties [161]. It has been suggested that in order to increase crystallinity the nanofibres are required to be annealed at high temperatures [284]. Non-electrospun G-PHB presented the greatest crystallinity of 54.2 %. G-PHB at solution concentration of 1.5 % presented the lowest crystallinity at 50.2 %. Increased crystallinity levels result in PHB becoming excessively hard and brittle. This is not a desirable property as it is not well suited for many applications [49].

The peak intensity values and % crystallinity for the various samples of G-PHB obtained from the DSC traces in Figure 59.

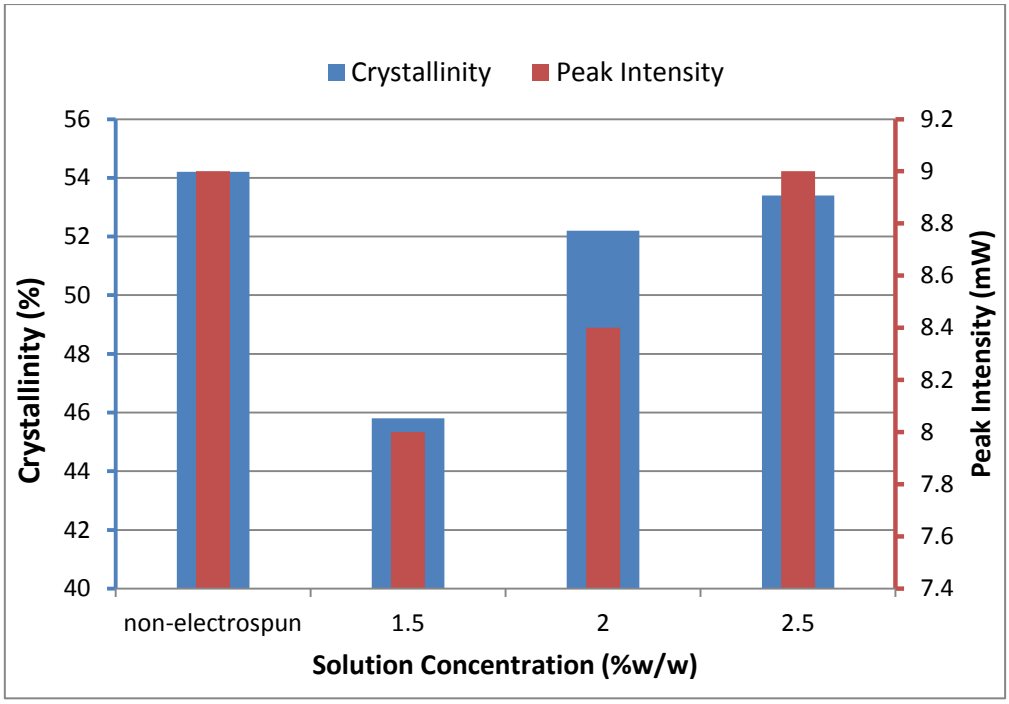

Figure 59: Bar chart representing the peak intensities against the % crystallinity for non-electrospun and electrospun samples of G-PHB.

The 1.5 %w/v sample of electrospun G-PHB showed the smallest peak intensity and also the lowest % crystallinity A clear correlation between the peak intensities and crystallinity can be observed in Figure 59, the smaller the peak intensities the lower the % crystallinity.

4.5.2.2. DSC of O-PHB

The heating and cooling process for samples of electrospun O-PHB at concentrations of 1.5, 2 and 2.5 %w/v are presented in Figure 60. The DSC traces for elctrospun O-PHB were compared to that of non-electrospun O-PHB. The thermal characteristics of electrospun O-PHB are summarised in Table 35 and were compared to those obtained from non-electrospun PHB in Table 33.

Table 35: Thermal properties of electrospurn fibres of O-PHB with solution concentrations of 1.5, 2 and 2.5 %w/v. T_m = melting temperature and T_c = crystallisation temperature on cooling and C = crystallinity.

	Polymer solution concentrations (%w/v) during electrospinning								
Polymer	**1.5**			**2**			**2.5**		
	T_c (^oC)	T_m (^oC)	C (%)	T_c (^oC)	T_m (^oC)	C (%)	T_c (^oC)	T_m (^oC)	C (%)
O-PHB	120.4	173.1	45.8	121.7	173.1	52.2	122.2	174.1	53.4

The T_m and T_c values obtained for electrospun and non-electrospun O-PHB were within the expected region for PHB.

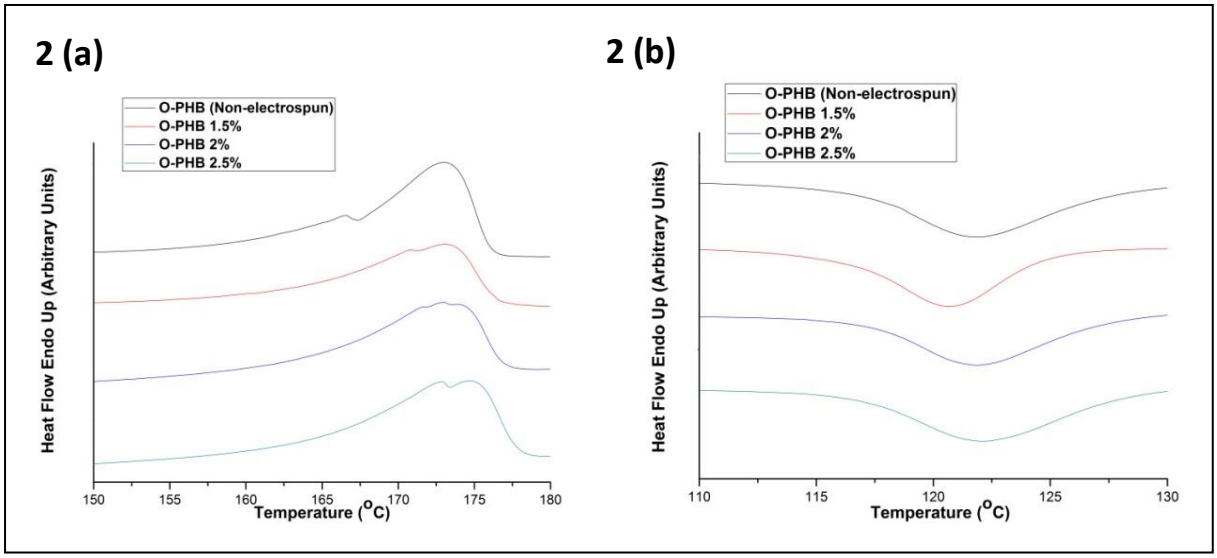

Figure 60: DSC trace for heating 2(a) and cooling 2(b) of electrospun and non-electrospun samples of O-PHB.

The T_m values obtained for electrospun O-PHB were similar to that of non-electrospun PHB. The double melting peaks observed for O-PHB is a result of a greater distribution of lamellar thickness [232]. In principle, samples with multiple melting endothermic peaks reflect a decrease in lamellar thickness or degree of crystalline order [285]. The DSC scans suggest the presence of less perfect crystals that will reach melt at lower temperatures [286]. The

double melting peak is less apparent in the traces for 1.5 % and 2 % compared to 2.5 %w/v electrospun O-PHB, which can be attributed to the higher degree of crystallinity observed at 2.5 %w/v electrospun O-PHB.

No differences in the breadth of the endothermic melting peaks were observed in the DSC traces for O-PHB. The identical breadths of the melting endothermic peaks are as a result of the identical PD for electrospun (2 %w/v) and non-electrospun O-PHB, which were obtained from the GPC analysis.

The peak intensity and % crystallinity for the various samples of G-PHB were plotted against solution concentration in Figure 61.

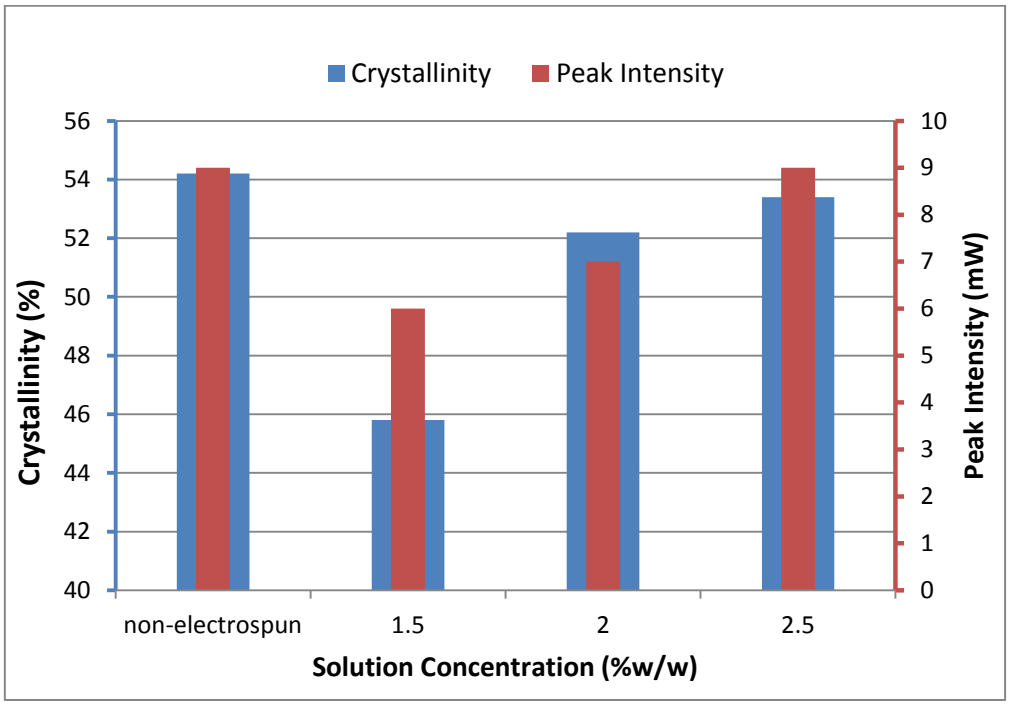

Figure 61: Bar chart representing the peak intensities and % crystallinity for non-electrospun and electrospun samples of O-PHB.

The % crystallinity obtained for electrospun O-PHB appeared to increase in correlation with higher solution concentrations of O-PHB. Non-electrospun PHB resulted in the greatest % crystallinity at 54.2 %. The 1.5 %w/v sample of electrospun O-PHB showed the smallest

peak intensity and also the lowest % crystallinity at 45.8 %. A clear correlation between the peak intensities and crystallinity can be observed in Figure 61, the smaller the peak intensities the lower the % crystallinity. The peak intensity of 2.5 %w/v electrospun G-PHB presented identical peak intensity to that of non-electrospun O-PHB and demonstrated an almost identical % crystallinity.

4.5.2.3. DSC of R-PHB

The heating and cooling process for samples of electrospun R-PHB at concentrations of 1.5, 2 and 2.5 %w/v are presented in Figure 62. The DSC traces for elctrospun R-PHB were compared to that of non-electrospun samples. The thermal characteristics of electrospun and non-electrospun R-PHB samples are summarised in Table 36. The T_m and T_c values obtained for electrospun and non-electrospun R-PHB were within the expected regions for PHB and were almost identical.

Table 36: Thermal properties of electrospurn fibres of PHB from R-PHB with solution concentrations of 1.5, 2 and 2.5 %w/v.

	Polymer solution concentrations (%w/v) during electrospinning								
Polymer	**1.5**			**2**			**2.5**		
	T_c (^{o}C)	T_m (^{o}C)	C (%)	T_c (^{o}C)	T_m (^{o}C)	C (%)	T_c (^{o}C)	T_m (^{o}C)	C (%)
R-PHB	121.4	171.9	41.9	121.9	171.2	42.1	121.9	173.4	47.4

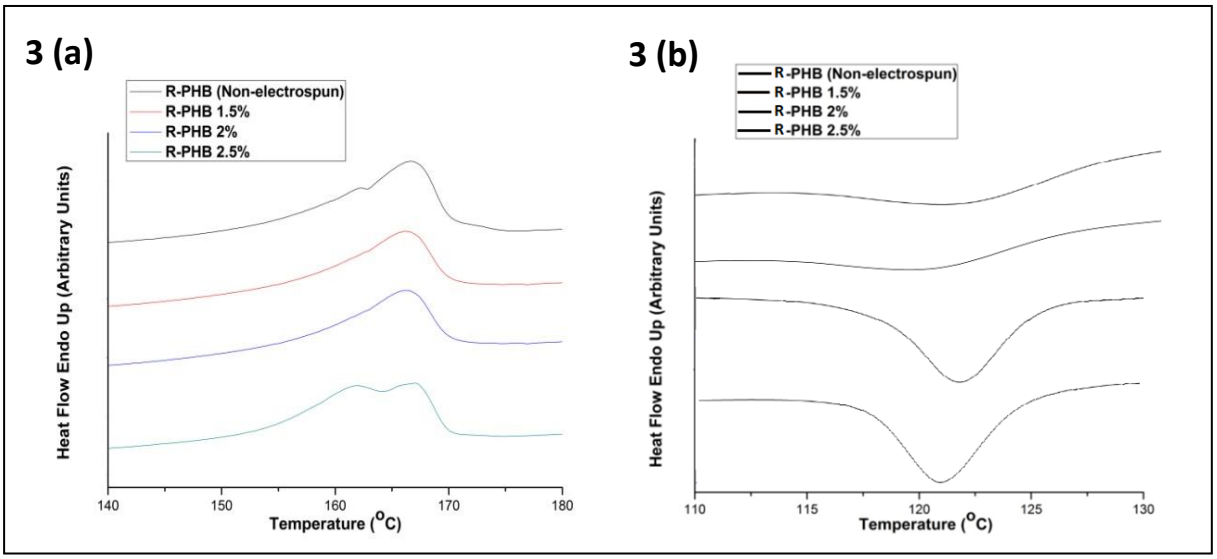

Figure 62: DSC traces for heating 3(a) and cooling 3(b) of electrospun and non-electrospun samples of R-PHB.

The melting peaks obtained for electrospun PHB were found to be within the same region as that of non-electrospun PHB (172 °C). Electrospun PHB at a solution concentration of 2 % and 1.5 %w/v presented the lowest T_m at 171 °C. Solution concentration of 2.5 %w/v for R-PHB presented the highest T_m at 173 °C. No major differences in the breadth of the DSC traces were observed between the different solution concentrations of electrospun R-PHB. Non-electrospun R-PHB and electrospun R-PHB (2 %w/v) showed similar melting peak breadths, this was in agreement with the GPC analysis that showed identical PD values.

The electrospun samples of PHB showed an increase in crystallinity with increasing solution concentrations of R-PHB. The non-electrospun sample of R-PHB showed the greatest % crystallinity at 52.2 %. The lowest % crystallinity obtained for electrospun R-PHB was from 1.5 %w/v at 41.9 % and was much lower compared to the non-electrospun counterpart. The peak intensity and % crystallinity for the different solution concentrations of R-PHB are presented as a line chart in Figure 63.

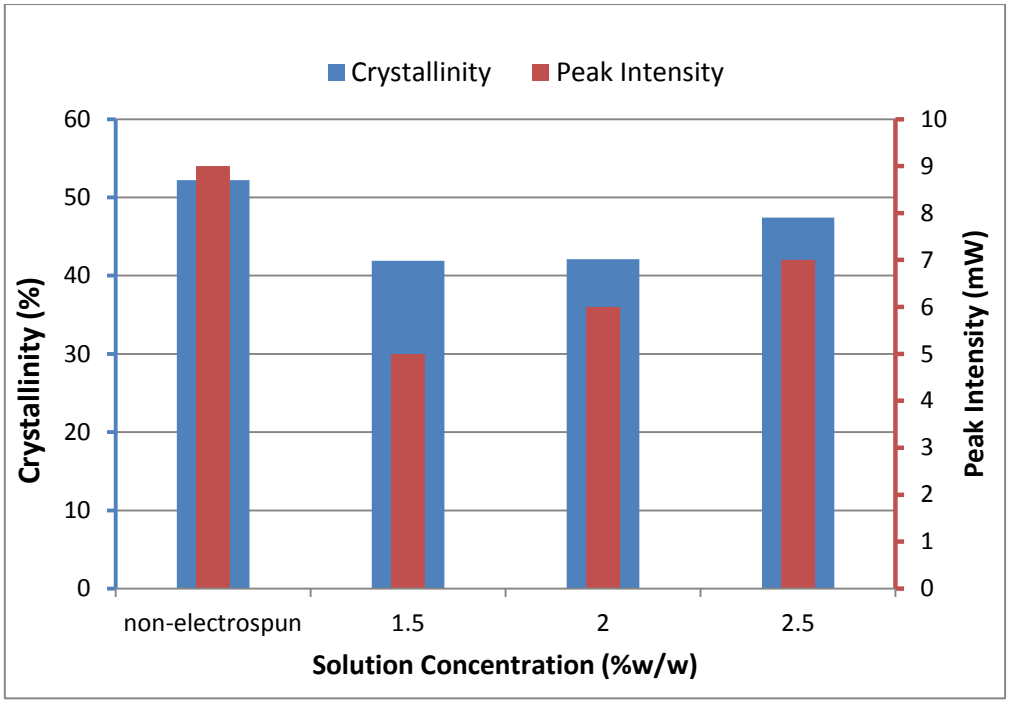

Figure 63: Bar chart representing the peak intensities against the % crystallinity for non-electrospun and electrospun samples of R-PHB.

The peak intensities present in the DSC traces for R-PHB at 2.5 %w/v solution concentrations were greater than those from 1.5 % and 2 %w/v. This can be attributed to the increase in % crystallinity that was observed. A correlation between the peak intensities and crystallinity can be observed in Figure 63, the smaller the peak intensities the lower the % crystallinity.

No major differences in the peak positions for the T_m and T_c values were observed, when comparing the different carbon sources. On average, solution concentrations of 1.5 %w/v G-PHB, O-PHB and R-PHB presented a major difference in crystallinity compared to their non-electrospun counterparts. The differences in % crystallinity observed between the electrospun and non-electrospun samples was much greater compared to the % crystallinity differences observed between samples of non-electrospun G-PHB, O-PHB and R-PHB

4.5.3. *FTIR*

The results obtained for the FTIR spectra of electrospun (2 %w/v) and non-electrospun PHB fibres from all three carbon sources are presented. The FTIR spectra of G-PHB, O-PHB and R-PHB are presented in Figures 64, 65, 67. The characteristic FTIR peaks of PHB are summarised in Table 37 and were obtained from a commercial sample of PHB (Sigma Aldrich).

Table 37: FT-IR peaks assignment of PHB.

Characteristic peaks cm^{-1}	**Assignment**
~2900	C-H Vibration
1720	C=O Stretching
1457	CH_3 Asymmetric deformation
1379	CH Symmetric deformation
1280	C-O-C stretching
1263	C-O-C stretching + CH deformation
1228	C-O-C stretching
1178	C-O-C stretching
1130	CH_3 rocking
1097	C-O-C stretching
1054	C-O stretching
1042	C-CH_3 stretching

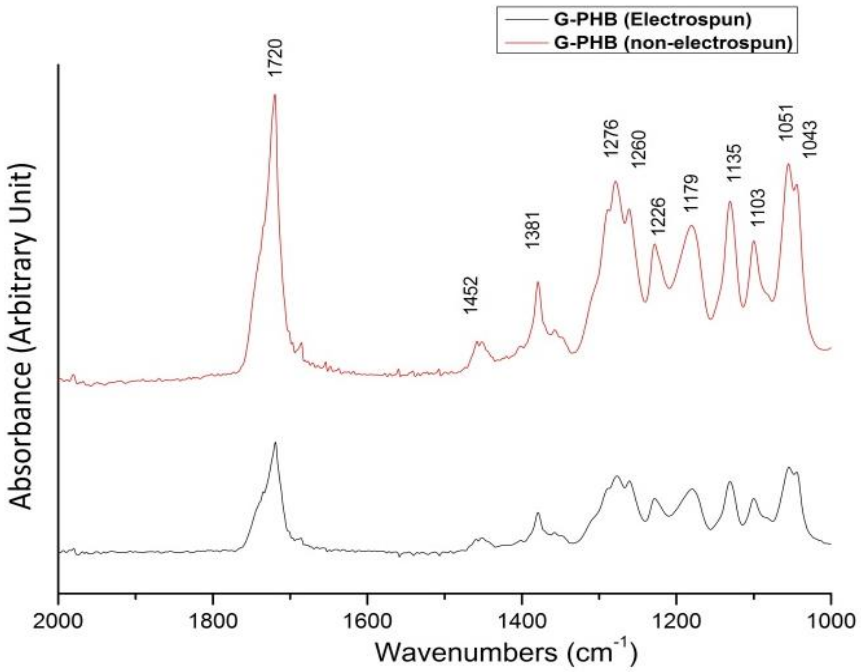

Figure 64: FTIR spectra of electrospun (2 %w/v) and non-electrospun G-PHB.

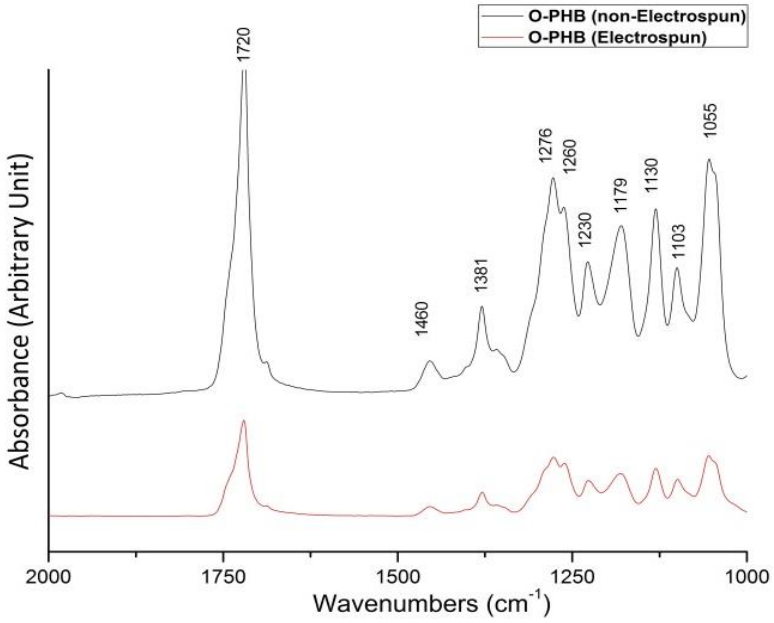

Figure 65: FTIR spectra of electrospun (2 %w/v) and non-electrospun O-PHB.

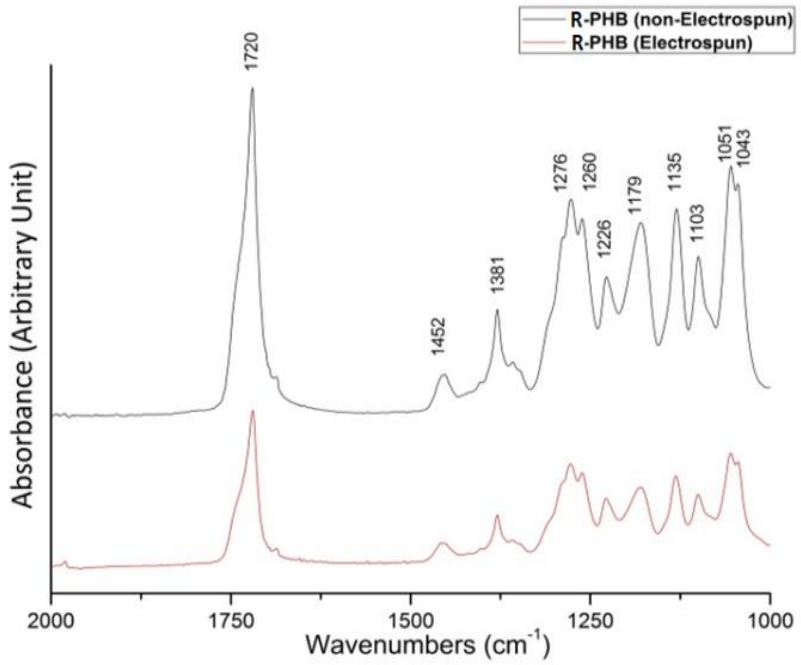

Figure 66: FTIR spectra of electrospun (2 %w/v) and non-electrospun R-PHB.

The most prominent marker band for the identification of PHB is the ester carbonyl group at 1720-1740cm^{-1} and can be seen in all cases for electrospun and non-eletrospun G-PHB, O-PHB and R-PHB. Also, a number of strong bands between wavenumbers 1380 and 1455 cm^{-1} representing methyl (CH_3) and methylene (CH_2) deformations were also visible in the PHB produced from all three carbon sources. The CO-C and C-O stretches at wavenumbers 1224 – 1230 and 1054 cm^{-1} respectively are also clearly visible in all the PHB spectra. The bands present at 1178 cm^{-1}, 1228 cm^{-1} and 1263 cm^{-1} are bands sensitive to crystallinity and are characteristic of C-O-C [287]. The FTIR spectroscopy confirms that PHB from glucose, olive oil and rapeseed oil are chemically identical. The spectra for electrospun samples of PHB were also compared to the FTIR spectrum of PHB nanofibres from other research groups and were found to consist of identical peak positioning [77, 239, 287, 288].

No difference in peak positions was observed between the spectra of electrospun (2 %w/v) and non-electrospun PHB. The peaks were found to be more intense for non-electrospun PHB which was observed in all cases, indicating a possible higher degree of crystallinity [231,

239]. It has been previously reported that crystallinity in electrospun nanofibres is reduced in comparison to non-electrospun bulk of the same polymer [151, 239]. The % crystallinity values that were calculated from DSC analysis (Section 4.4.2) presented slightly higher % crystallinity for non-electrospun PHB samples compared with that of electrospun PHB. Randriamahefa *et al*. reported that FTIR can also be used to evaluate the (CI) of PHB quantitatively [239]. As previously outlined (Section 3.4.3) the relative measure of the degree of crystallinity can be obtained by calculating the CI and can be used to compare the relative crystallinity values from the various FTIR spectra (Equation 6 in section 3.4.3).

The CI obtained for electrospun samples of G-PHB, O-PHB and R-PHB were 0.46, 0.38 and 0.4 respectively and were found to be lower than their non-electrospun counterparts at 0.47, 0.39 and 0.42 respectively. This CI is not to be confused with an absolute degree of crystallinity but is useful as a comparison criterion. Comparisons of the CI and % crystallinity are presented in Figure 67.

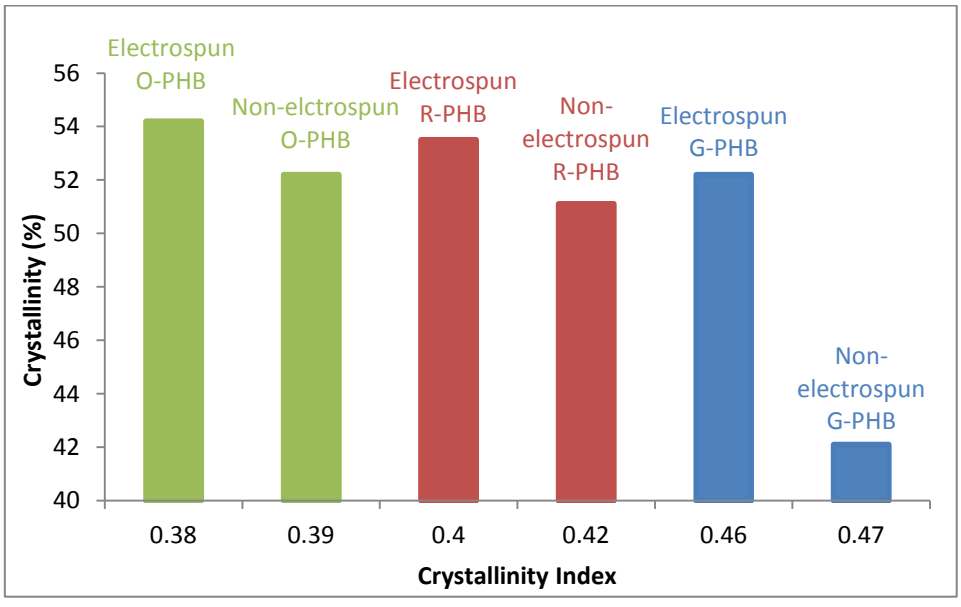

Figure 67: Histogram demonstrating the correlation between the % crystallinity obtaied from DSC traces and the CI obtained from the FTIR spectra of O-PHB, R-PHB and G-PHB (2 %w/v).

The results obtained for the CI in this study complement the % crystallinity values obtained from the DSC traces.

4.5.3.1. Comparison of electrospun and non-electrospun PHB

The metabolism of all three types of carbon source by *R. eutropha* resulted in the production of 3-hydroxybutyrate (3HB) monomers, which are polymerised to PHB via the action of the bacterial cells [7, 217].The T_m, T_c and % crystallinity of PHB obtained from the various carbon sources were in the range of 172.2 °C -173.2 °C, 120.8 °C - 121.6 °C and 52.2 % - 54.2 %, respectively. The thermal characteristics of the produced polymers was not affected by the carbon source as no significant difference was observed in the properties of the polymers obtained from olive oil, rapeseed oil and glucose. The molecular properties were also observed to be within the same region.

The non-electrospun samples of PHB all showed crystallinity values of ~54 %. This was expected as PHB homopolymers are known to consist of a very high crystallinity often well in excess of 50 % [48], which is as a result of the strict molecular stereoregularity of PHB produced from biosynthesis. The % crystallinity obtained for non-electrospun PHB were found to be greater in comparison to electrospun samples. Electrospun G-PHB, O-PHB and R-PHB all presented a decrease in crystallinity when the solution concentration was reduced. The % crystallinity of PHB is a measure of the degree of order in the polymer chains [289].

The electrospinning process involves the polymer jet travelling from the needle tip to the collector, where polymer chain alignment and crystallisation of the polymer takes place [275]. The greater applied voltage during the electrospinning process results in the polymer solution becoming more charged, a greater charge has a greater effect on the stretching of the polymer jet [290]. An increase in the applied voltage will result in a greater alignment of the polymer chains and hence an increase in the crystallinity of the produced fibres [275, 291]. It

has been suggested by Ero-Phillips *et al.* that an optimum voltage for a given polymer solution concentration (%w/v) exists [291]. The crystallinity of the produced nanofibres increases with greater applied voltages, however once the applied voltage reaches its optimum value the degree of crystallinity will begin to decrease. The degree of crystallinity of the electrospun PHB can also be influenced by the flight time of the jet [151]. A higher voltage results in a decrease in the time it takes for the jet to reach the collecting plate after leaving the needle tip and therefore there is less time for the polymer to crystallise [275]. However, increasing the voltage beyond the specific optimum value will result in greater acceleration of the polymer jet therefore, reducing the flight time of the jet. This reduction in flight time will result in a lower crystallinity of the polymer fibres [291].

It was interesting to note a decrease in % crystallinity with decreasing solution concentrations of PHB. As outlined in the previous section the applied voltage above the optimum voltage will result in the production of PHB fibres with lower % crystallinity. This suggests that the optimum voltage for PHB solutions of 2.5 %w/v was close to 7 kV, as it showed a similar degree of crystallinity to that of the non-electrospun sample. Therefore a decrease in the PHB solution concentration with the same applied voltage would result in a lower degree of crystallinity as the optimum voltage would be lower.

The crystallinity of electrospun fibres is a very important property for many potential applications. Biocompatible and biodegradable electrospun polymer fibres are largely used in biomedical applications; therefore the degree of crystallinity is an important property as it can directly affect the rate of degradation [292]. By controlling the degree of crystallinity a polymer scaffold can be produced with a tailored rate of degradation for a specific application and so will be much more desirable for biomedical applications.

Chapter 5 :Conclusions

5.1. *The production of PHB and HA from Serratia sp.*

It can be concluded that *Serratia* sp. NCIMB 40259 were successfully fermented in order to simultaneously biomineralise HA on the surface and to accumulate PHB within the cytoplasm.

This method of PHB accumulation will not reduce the cost of production but will make the fermentation process much more profitable. The production and characterisation of PHB from HPA and LPA *Serratia* sp. was the primary focus of this project. Fermentations were conducted with HPA and LPA *Serratia* sp. in order to accumulate high yields of PHB and HA. The yields of accumulated PHB were generally greater for LPA cells compared to HPA cells after 48, 120, 216 and 360 h fermentations. A significant difference in PHB accumulation between HPA and LPA cells was only observed at 120 h and 216 h fermentations.

The greatest overall average yield of PHB from LPA and HPA cells were observed after 216 h of fermentation with LPA cells. The yields of accumulated PHB from LPA and HPA cells were observed to decrease after 216 h fermentation. The optimum conditions for the accumulation of PHB in this study were found to be 216 h of fermentation and this produced a PHB yield of 14.6 %w/w and 3.3 %w/w for LPA and HPA respectively. The accumulation of PHB by S*erratia* sp. was directly dependant on the fermentation time. An accelerated PHB accumulation was observed between 120 h and 216 h fermentations. However, phosphatase activity appeared to have an indirect effect on the accumulation of PHB. This is as the phosphatase enzyme and its specific activity is localised to the cell surface periplasmic space and has no reported activity within the cytoplasm of the cells. It is possible that the lack of phosphatase enzyme activity has a role in up regulating the activity of specific enzymes within the PHA synthesis pathway resulting in greater accumulation of PHB. Further research

is required in order to investigate the up regulation of specific enzymes within the PHA synthesis pathway in LPA cells compared with HPA cells.

Many strains of bacteria have been reported to accumulate maximal yields of PHB after 48 h fermentation. A fermentation of 48 h is an ideal period for PHB accumulation at an industrial scale, in order to maximise profitability. The *Serratia* sp. under the specific culture conditions in this study requires longer fermentations in order to accumulate greater yields of PHB. Bacterial cells such as *R. eutropha* and *Alcaligenes latus* have been reported to accumulate PHB yields of ~80-90 %w/w after 48 h fermentation. In order for *Serratia* sp. to become a viable option for the industrial production of PHB a greater %w/w yield must be produced. It has been previously suggested that commercial feasibility can only be achieved when 50 %w/w of PHB is produced**.**

The depressed yields of PHB accumulated from *Serratia* sp. can be attributed to the specific culture conditions implemented in this study. The culture conditions were optimised for the mineralisation of HA, as the use of the licensed *Serratia* sp. cells was conditional to maintaining these specific culture conditions throughout. To optimise the accumulation of PHB by *Serratia* sp. the culture conditions must be adjusted to develop a fine balance between HA mineralisation and PHB accumulation.

The accumulated yields of HA mineralisation in this study were greater with increasing fermentation times. This was a result of the daily additions of stock solutions that ensured a constant supply of phosphate ions in solution for the mineralisation of HA.

Fermentations of 360 h resulted in the greatest overall yields of HA. As expected, HPA cells produced greater yields of mineralised HA after the various fermentation periods compared with LPA cells. However, a statistically significant difference between LPA and HPA cells was only observed for 48 h and 120 h fermentations. The high yield accumulation of HA

after 216 h and 360 h from LPA cells requires further investigation as the decrease in phosphatase enzyme activity should have resulted in lower yields of mineralised HA. The increase in HA mineralisation observed after 216 h fermentation for LPA cells is beneficial to the industrial applicability of this process. This is as LPA cells showed greater accumulated yields of PHB compared to HPA cells after 216 h of fermentation. The chemical and thermal properties of PHB were observed to be largely unaffected by the phosphatase activity of the cells and appeared to be dependent on the fermentation time. The FTIR spectra for extracted PHB from HPA and LPA cells showed identical peak positioning and confirmed the extracted polymer as PHB.

A correlation was observed between the fermentation periods, M_w and PD. The GPC analysis of PHB from HPA and LPA *Serratia* sp. showed similar M_w and PD values over the range of fermentation periods. The DSC traces for PHB from LPA and HPA cells showed no major differences in peak positioning after 48, 120, 216 h and 360 h fermentations. The breadth of the melting endothermic peaks for PHB from LPA and HPA showed the same pattern of peak broadening with increasing fermentation time. This was attributed to the increase in PD and the presence of smaller polymer chain lengths that reach complete melt at varying temperatures. The % crystallinity of PHB from HPA and LPA were highest after 216 h fermentation and correlated with the peak intensities of the endothermic melting peak of the DSC traces. The % crystallinity was in the expected region for PHB, as PHB homopolymers are known to consist of a very high crystallinity often well in excess of 50 %, this is as a result of the strict molecular stereoregularity of PHB produced from biosynthesis. The increase in crystallinity is not a desirable polymer property. A high degree of crystallinity results in an excessively stiff and brittle polymer and may not be well suited for many applications [50].

The FTIR spectra for HA from HPA and LPA were found to be identical. The position of absorption peaks at wavelengths of 1090, 1026 and 963 cm^{-1}, indicated the presence of P-O-H bonds and were identical to those observed in commercial HA as reported by Sammons *et al.* [169] [169] [169] [169] [169] and Yong *et al.* The use of analytical techniques (XRD, NMR) confirmed the mineralised material on the surface of *Serratia* sp. as HA.

The production of HA alongside PHB by *Serratia* sp. will make the process more economically viable. However, at present it is not a viable option considering the low yields of PHB that are accumulated and the high fermentation times required for optimum PHB accumulation. The greatest yields of PHB were accumulated after 216 h of fermentation with LPA cells and represented on average 14.6 %w/w. Considering that many species of bacteria are capable of accumulating up to ~90 %w/w PHB after 48 h fermentation, more research is required in order to optimise the fermentation conditions for the accumulation of PHB whilst maintaining the high yields of HA mineralisation.

5.2. *Development and characterisation of electrospun fibres of PHB from various carbon source synthesised from R eutropha.*

Nanofibres of PHB were produced by electrospinning using 1.5, 2 and 2.5 %w/v of PHB synthesized from 20 g/l of glucose, olive oil and rapeseed oil fermentations. The greatest yield of PHB produced from *R. eutropha* was when using olive oil and rapeseed oil as a carbon source compared with glucose. Overall 36 %w/w of O-PHB and R-PHB was extracted compared to 12 %w/w for G-PHB. This study showed that the chemical and thermal properties of the polymer were unaffected by the carbon substrate utilised in the fermentation process and only minor differences in molecular properties of the produced polymers were observed. This suggests that PHB produced from oils is a viable replacement for the use of sugars as substrates. As previously discussed, the use of pure glucose and olive oil would not be suited for large industrial fermentations of PHB, due to the high cost of the substrates. Rapeseed oil has been presented as a low cost alternative to other conventional oils and in this study it showed an almost identical yield of produced PHB compared with the more expensive olive oil. The low cost and high production yields of PHB make rapeseed oil a viable option for the production of PHB at an industrial scale. The use of waste rapeseed oil has attracted much research as a means of further reducing the cost of PHB production and has shown to be an effective substrate capable of accumulating high yields of PHB (0.98 g/g).

The diameter of the electrospun nanofibres from G-PHB, O-PHB and R-PHB were found to be similar. This study shows that the source of carbon used did not have a significant effect on the diameters of electrospun nanofibres, this was attributed to the similar M_w properties of each carbon source.

As previously mentioned, the thermal characteristics of the various polymers were not affected by the carbon source, no significant difference was observed in the properties of the polymers obtained from olive oil, rapeseed oil and glucose. The FTIR spectra for electrospun

and non-electrospun PHB for samples of G-PHB, R-PHB and O-PHB were found to have identical peak positioning. The most prominent marker band for the identification of PHB was the ester carbonyl band at 1720-1740cm^{-1} and was seen in all cases for electrospun and non-eletrospun G-PHB, O-PHB and R-PHB. The peak intensities were greater for samples of non-electrospun PHB compared to electrospun samples indicating a possible higher degree of crystallinity for the non-electrospun samples. The results of the FTIR spectra were in agreement with the findings of the DSC traces. The % crystallinity obtained for non-electrospun PHB were overall greater compared to the electrospun samples of PHB. The non-electrospun samples of PHB had a crystallinity of ~54 %. This was expected as PHB homopolymers are known to consist of a very high crystallinity often well in excess of 50 %. By adjusting the electrospinning parameters it may be possible to control the crystallinity of PHB fibres. Controlling the crystallinity of the PHB fibres is essential if they are to be used in biomedical applications. A higher degree of crystallinity will result in a lower degradation rate. By controlling the crystallinity the degradation rate of the PHB fibres can also be controlled, allowing fibres with a tailored degradation rate to be produced.

Future work

The depressed yields of PHB accumulated from *Serratia* sp. can be attributed to the specific culture conditions implemented in this study. The culture conditions were optimised for the mineralisation of HA. The use of licensed *Serratia* sp. cells was conditional to maintaining these specific culture conditions throughout. To optimise the accumulation of PHB by *Serratia* sp. the culture conditions must be adjusted to develop a fine balance between HA mineralisation and PHB accumulation.

Many species of bacteria have been reported to accumulate high yields of PHB when fermented with glucose as a sole carbon source [30, 31]. The addition of glucose to the fermentation media may improve the yields of PHB accumulated by *Serratia* sp. It would also be beneficial to investigate a wide range of low cost carbon sources in order to determine the carbon source that provides optimal PHB accumulation.

The results of this study indicate a possible correlation between phosphatase activity and PHB accumulation by *Serratia* sp. Further research is required to investigate whether up-regulation of specific enzymes within the PHA synthesis pathway, in LPA cells, is occurring, which may result in greater accumulated yields of PHB.

It would be beneficial to investigating the addition of chemicals to the bacterial fermentation medium. The addition of specific chemicals can induce the organism into a stress situation, in which they may accumulate greater yields of PHB. It has been reported that strains of resistant *Pseudonomas* can accumulate greater yields of PHB with the addition of polymyxin to the fermentation media [293].

Raman spectroscopy has been suggested as a powerful tool for the classification of species and strains of bacteria. Previous studies reported the use of micro Raman as a suitable tool for single cell microbial identification. The use of Raman spectroscopy could provide

information on intracellular components of bacterial cells. It could also provide information regarding the intracellular polymer structure and whether it is predominantly amorphous or crystalline at different stages. It would be beneficial to conduct Raman spectroscopy in order to compare the intracellular polymer structure of LPA and HPA cells at different fermentation times.

The fibre diameters produced in this study were relatively large, with uniform fibres of approximately 1 μm. These relatively large fibres are potentially due to the operating parameters used, in particular the low applied voltage of 7 kV. This low voltage was necessary to produce a stable electrospinning system for all PHB samples in the current work, however this parameter could be optimised with the aim to reduce diameters in future work. The addition of a salt to the electrospinning solution has also been reported to reduce fibre diameters by marginally decreasing surface tension and increasing solution conductivity; this may also be investigated in subsequent work [267].

A significant challenge with current electrospinning techniques is achieving the production of uniform polymer fibres, as fibre diameters are rarely uniform. Much of the reported electrospinning research has not addressed this problem. However, it has been recently reported that the production of fibre diameters from polymer solutions at higher temperatures were much more uniform than those produced from solutions at ambient temperatures [294]. Optimising production of uniform fibres is an area that requires more investigation.

Curriculum Vitae

Soroosh Bagheriasl, born in 1986, studied Medical Science at The University of Birmingham from 2004 to 2007. In 2008 he achieved a Masters of Research in Biomaterials, focusing on the production of PHB from bacteria. In the same year he acepted a PhD studentship at The University of Birmingham.

Scientific Publications

Handley-Sidhu S, Renshaw JC, Moriyama S, Stolpe B, Mennan C, Bagheriasl S, Yong P, Stamboulis A. Removal of Sr^{2+} and Co^{2+} into Biogenic Hydroxyapatite: Implications for Biomineral Ion Exchange Synthesis. Environmental Science 2011.

Bagheriasl S, Irorere V, Blevins M, Radecka I, Stamboulis A. Development and characterisation of electrospun fibres of Polyhydroxybutyrate synthesized by *Ralstonia eutropha* from different carbon sources. Journal of Applied Polymer Science. 2012. (Awaiting Publication).

Conference Poster Presentations

- **Poster Presentation 'The production of PHB and HA from *Serratia* sp' – UK Society for Biomaterials, Glasgow (2010).**
- **Poster presentation 'The production of PHB co-polymers from *Ralstonia eutrophaI*- International Symposium on Biopolymers, Stuttgart, Germany (2010).**
- **Oral Presentation- 'The production of PHB from various bacterial species'-4th International Conference on Tissue Engineering, Crete, Greece (2011).**

References

1. **Poirier.Y, Nawrath.C, and Somerville.C, Production of polyhydroxyalkanoates, a family of biodegradable plastics and elastomers, in bacteria and plants. Biotechnology (N Y), 1995. 13(2): p. 142-50.**

2. **Braunegg, G., G. Lefebvre, and K.F. Genser, Polyhydroxyalkanoates, biopolyesters from renewable resources: physiological and engineering aspects. J . Biotechnol, 1998. 65(2-3): p. 127-61.**

3. **Salehizadeh, H. and M.C. Van Loosdrecht, Production of polyhydroxyalkanoates by mixed culture: recent trends and biotechnological importance. Biotechnology Advances, 2004. 22(3): p. 261-79.**

4. **Lemoigne, M., Produit de déshydratation et de polymérisation de l'acide β-oxybutyrique. Bull Soc Chim Biol, 1926. 8: p. 770-782.**

5. **Whitman, W.B., D.C. Coleman, and W.J. Wiebe, Prokaryotes: the unseen majority. Proc Natl Acad Sci U S A, 1998. 95(12): p. 6578-83.**

6. **Lemos, P.C., L.S. Serafim, and M.A. Reis, Synthesis of polyhydroxyalkanoates from different short-chain fatty acids by mixed cultures submitted to aerobic dynamic feeding. J Biotechnol, 2006. 122(2): p. 226-38.**

7. **Verlinden, R.A., et al., Bacterial synthesis of biodegradable polyhydroxyalkanoates. J Appl Microbiol, 2007. 102(6): p. 1437-49.**

8. **WasteOnline. Plastic recycling information sheet. 2011 [cited 2011 10/02]; Available from: www.wasteonline.org.**

9. **Bioplastic24. Bioplastic market – an overview. 2011 [cited 2011 10/02].**

10. **Reuters. China launches suprise crackdown on plastic bags. 2008 [cited 2011 10/02]; Available from: http://uk.reuters.com/article/environmentNews/idUKPEC25589820080108.**

11. **Independent, T. Billions fewer plastic bags handed out. 2009; Available from: http://www.independent.co.uk/environment/green-living/billions-fewer-plastic-bags-handed-out-1632392.html.**

12. **Smithers, R. Plastic bag use up for second year running. 2012; Available from: http://www.guardian.co.uk/environment/2012/jul/05/plastic-bag-use-rise-supermarkets.**

13. **Mergaert, J., et al., Biodegradation of polyhydroxyalkanoates. FEMS Microbiol Rev, 1992. 9(2-4): p. 317-21.**

14. **Jendrossek, D. and R. Handrick, Microbial degradation of polyhydroxyalkanoates. Annu Rev Microbiol, 2002. 56: p. 403-32.**

15. Beijerinck, M.W., Cultur des Bacillus radicicola aus den Kno¨llchen. Bot Ztg, 1888. 46: p. 740-750.

16. Rehm, B.H. and A. Steinbuchel, Biochemical and genetic analysis of PHA synthases and other proteins required for PHA synthesis. Int J Biol Macromol, 1999. 25(1-3): p. 3-19.

17. Reddy, C.S.K., R. Ghai, and V.C. Rhami, Polyhydroxyalkanoates: an overview. Bioresource Technology, 2003. 87: p. 707-709.

18. Holmes, P.A., ed. Developments of Crystalline Polymers. ed. D.C. Basset. Vol. 2. 1988, Elsevier Applied Science: London. 1-65.

19. Griffin, J.L., Chemistry and technology of biodegradable polymers (POD). 1993, Kluwer Academic publishing group: Netherlands. p. 48-96.

20. Taguchi, S., et al., Production of polyhydroxyalkanoates (PHA) from renewable carbon sources in recombinant Ralstonia eutropha using mutants of original PHA synthase. Biochemical Engineering, 2003. 16: p. 107-113.

21. Kahar, P., et al., Effective production and kinetic characterisation of ultra-high-molecular-weight poly (R)-3-hydroxybutyrate in recombinant Escherichia. Polymer Degradation and Stability, 2005. 87: p. 161-169.

22. Nikel, P.I., et al., Poly(3-hydroxybutyrate) synthesis by recombinant Escherichia coli arcA mutants in microaerobiosis. Appl Environ Microbiol, 2006. 72(4): p. 2614-20.

23. Sujatha, K. and R. Shenbagarathai, A study on medium chain length-polyhydroxyalkanoate accumulation in Escherichia coli harbouring phaC1 gene of indigenous Pseudomonas sp. LDC-5. Lett Appl Microbiol, 2006. 43(6): p. 607-14.

24. Grothe, E., M. Moo-Young, and Y. Chisti, Fermentation optimization for the production of poly(beta-hydroxybutyric acid) microbial thermoplastic. Enzyme and Microbial Technology, 1999. 25: p. 132-141.

25. Patwardham, P.R. and A.K. Srivastava, Model-based fed-batch cultivation of R.eutropha for enhanced bio polymer production. Biochemical Engineering, 2004. 20: p. 21-28.

26. Yang, S., ed. Bioprocessing for value-added products from renewable resources. 2007, Elsevier: Amsterdam.

27. Verlinden, R.A.J., Biodegradable polyhydroxyalkanoates from waste frying oil, in School of Applied Sciences. 2009, Univesity of Wolverhampton: Wolverhampton.

28. Lugg, H., et al., Polyhydroxybutyrate accumulation by a Serratia sp. Biotechnol Lett, 2008. 30(3): p. 481-91.

29. Kahar, P., et al., High yield production of polyhydroxyalkanoates from soy bean oil by Ralstonia eutropha and its recommbinant strain. Polymer Degradation and Stability, 2004. 83: p. 70-86.

30. Yamane, T., Cultivation engineering of microbial bioplastic production. FEMS Microbiology Letters, 1992. 103: p. 257-264.

31. Madison, L.L. and G.W. Huisman, Metabolic engineering of poly (3-hydroxyalkanoates): from DNA to plastic. Microbiol Mol Biol R, 1999. 63: p. 21-53.

32. Alias, Z. and I.K. Tan, Isolation of palm oil-utilising, polyhydroxyalkanoate (PHA)-producing bacteria by an enrichment technique. Bioresour Technol, 2005. 96(11): p. 1229-34.

33. Fernandez, D., et al., Agro-industrial oily wastes as substrates for PHA production by the new strain Psedmonas aeruginosa NCIMB 40045: effect of culture conditions. Biochemical Engineering, 2005. 26: p. 159-167.

34. van Beilen, J.B. and Y. Poirier, Production of renewable polymers from crop plants. Plant J, 2008. 54(4): p. 684-701.

35. Bohmert, K., et al., Constitutive expression of the beta-ketothiolase gene in transgenic plants. A major obstacle for obtaining polyhydroxybutyrate-producing plants. Plant Physiology, 2002. 128(4): p. 1282-90.

36. Lee, S.Y., Bacterial polyhydroxyalkanoates. Biotechnology and Bioengineering, 1996. 49(1): p. 1-14.

37. Doi, Y., Microbial Polyesters. 1990, New York: VCH Publisher.

38. Poirier, Y., C. Nawrath, and C. Somerville, Production of polyhydroxyalkanoates, a family of biodegradable plastics and elastomers, in bacteria and plants. Biotechnology (N Y), 1995. 13(2): p. 142-50.

39. Bayari, S. and F. Severcan, FTIR studyof biodegradable biopolymers:P(3HB),P(3HB-co-4HB) and P(3HB-co-3HV). Journal of Molecular Structure, 2005. 744: p. 529-534.

40. Wong, M.S., et al., Engineering poly(3-hydroxybutyrate-co-3-hydroxyvalerate) copolymer composition in E. coli. Biotechnology and Bioengineering, 2008. 99(4): p. 919-28.

41. Yan, Q., et al., Biosynthesis of short-chain-length-polyhydroxyalkanoates during the dual-nutrient-limited zone by Ralstonia eutropha World Journal of Microbiology & Biotechnology, 2005. 21: p. 17-21.

42. Xu, J., et al., A mathematical model for regulating monomer composition of the microbially synthesized polyhydroxyalkanoate copolymers. Biotechnology and Bioengineering, 2005. 90(7): p. 821-9.

43. Pederson, E.N., C.W. McChalicher, and F. Srienc, Bacterial synthesis of PHA block copolymers. Biomacromolecules, 2006. 7(6): p. 1904-11.

44. Farreh, W. What is PHA. 2011 [cited 2011 2nd May]; Available from: http://naturalplastics.blogspot.co.uk/2011/05/what-is-pha.html.

45. Labuzek, S. and I. Radecka, Biosynthesis of PHB tercopolymer by Bacillus cereus UW85. J Appl Microbiol, 2001. 90(3): p. 353-7.

46. Nicholson, J.W., The Chemistry of Polymers. Third ed. 2006: RSC Publishing.

47. Kensiz, M., H. Billman-Jacobe, and D. McNaughton, Quantitative determination of the biodegradable polymer Poly(Beta-hydroxybutyrate) in a recombinant Escherichia coli strain by use of Mid-infrared spectroscopy and multivariative. Applied and Environmental Microbiology, 2000. 66(3415-3420).

48. Padermshoke, A., et al., Melting behavior of poly(3-hydroxybutyrate) investigated by two-dimensional infrared correlation spectroscopy. Spectrochim Acta A Mol Biomol Spectrosc, 2005. 61(4): p. 541-50.

49. Antipov, E.M., et al., Strain-induced mesophase and hard-elastic behaviour of biodegradable polyhydroxyalkanoates fibres. Polymer, 2006. 47(5678-5690).

50. Agus, J., et al., Molecular wieght characterisation of poly[(R)-3-hydroxybutyrate] synthesised by genetically engineered strains of Escherichia coli. . Polymer Degradation and Stability, 2006. 91: p. 1645-1650.

51. Akhtar, S., C.W. Pouton, and L.J. Notarianni, Crystallization Behavior and Drug Release from Bacterial Polyhydroxyalkanoates. Polymer, 1992. 33(1): p. 117-126.

52. Bloembergen, S. and D.A. Holden, Studies of Composition and Crystallinity of Bacterial Poly(Beta-hydroxybutyrate-co-Beta-hydroxyvalerate). Macromolecules, 1986(19): p. 2856-2871.

53. Noda, I., et al., Polymer alloys of Nodax copolymers and poly(lactic acid). Macromol Biosci, 2004. 4(3): p. 269-75.

54. Noda, I., et al., Preparation and properties of a novel class of polyhydroxyalkanoate copolymers. Biomacromolecules, 2005. 6(2): p. 580-6.

55. Tsuge, T., Metabolic improvements and use of inexpensive carbon sources in microbial production of polyhydroxyalkanoates. J Biosci Bioeng, 2002. 94(6): p. 579-84.

56. Asenjo, J.A., P.R. Anderson, and B.A. Andrews, Effect of single nutrient limitation of poly--hydroxybutyrate molecular weight distribution in alcaligens europhus. Biotechnology and Bioengineering, 2004. 46(5): p. 497-502.

57. Chen, G., ed. Plastics from Bacteria:Natural Functions and Applications. ed. A. Steinbuchel. 2010, Springer: Berlin.

58. Steinbuchel, A. and H.G. Schlegel, Physiology and molecular genetics of poly(beta-hydroxy-alkanoic acid) synthesis in Alcaligenes eutrophus. Mol Microbiol, 1991. 5(3): p. 535-42.

59. Barber, M. and S.W. Kuper, Identification of Staphylococcus pyogenes by the phosphatase reaction. J Pathol Bacteriol, 1951. 63(1): p. 65-8.

60. Marchessault, R.H., et al., Chiral poly(beta-hydroxyalkanoates): an adaptable helix influenced by the alkane side-chain. Int J Biol Macromol, 1990. 12(2): p. 158-65.

61. Debenedetti, P.G. and F.H. Stillinger, Supercooled liquids and the glass transition. Nature, 2001. 410(6825): p. 259-67.

62. Carrasco, F., et al., Thermal stability of polyhydroxyalkanoates. Journal of Applied Polymer Science, 2006. 100(3): p. 2111-2121.

63. Erceg, M., Y. Doi, and H. Abe, Dynamic thermogravimetric degradation of poly(3-hydroxybutyrate)/aliphatic-aromatic copolyester blends. Polym.Deg.Stab, 2005. 90.

64. Belgacem, M.N. and A. Gandini, eds. Monomers, Polymers and Composites from Renewable Resources. 2008, Elsevier: Amsterdam.

65. Gu, J.D., et al., Microbial degradation and deterrioration of polymeric materials. The Uhlig Corrosion Handbook. 2000, New York: Wiley.

66. Choi, G.G., H.W. Kim, and Y.H. Rhee, Enzymatic and non-enzymatic degradation of poly (3-hydroxybutyrate-co-3-hydroxyvalerate) copolyesters produced by Alcaligenes sp. MT-16. J Microbiol, 2004. 42(4): p. 346-52.

67. Scott, G., ed. Biodegradable polymers. Polymers and the environment. 1999, Royal Society of Chemistry: London. 93-125.

68. Sun, Z., et al., Fermentation process development for the production of medium-chain-length poly-3-hyroxyalkanoates. Appl Microbiol Biotechnol, 2007. 75(3): p. 475-85.

69. Sridewi, N., K. Bhubalan, and K. Sudesh, Degradation of commercially important polyhydroxyalkanoates in tropical mangrove ecosystem. Polymer Degradation and Stability, 2006. 91: p. 2931-2940.

70. Majid, M.I.A., et al., The degradation kinetics of poly(3-hydroxybutyrate) under non-aqueous and aqeous conditions. European Polymer Journal, 2002. 38(837-839).

71. Bonartsev, A.P., et al., Biosynthesis, biodegradation, and application of poly(3-hydroxybutyrate) and its copolymers - natural polyestersproduced by diazotrophic bacteria. Formatex, 2007: p. 295-307.

72. Spyros, A., et al., 1H NMR imaging study of enzymatic degradation in poly(3-hydroxybutyrate) and poly(3-hydroxybutyrate-co-3-hydroxyvalerate). Evidence for preferential degradation of the amorphous phase by PHB depolymerase B from Pseudomonas lemoignei. Macromolecules, 1997. 30: p. 327-329.

73. Shangguan, Y.Y., et al., The mechanical properties and in vitro biodegradation and biocompatibility of UV-treated poly(3-hydroxybutyrate-co-3-hydroxyhexanoate). Biomaterials, 2006. 27(11): p. 2349-57.

74. Lindsay, K.F., Truly degradable resins are now truly commercial. Modern Plastics, 1992. 2: p. 62-64.

75. Volova, T.G., et al., Results of biomedical investigation of PHB and PHB/PHV fibres. Biochemical Engineering, 2003. 16: p. 125-133.

76. Rychter, P., et al., Environmental degradation of polyester blends containing atactic poly(3-hydroxybutyrate). Biodegradation in soil and ecotoxicological impact. Biomacromolecules, 2006. 7(11): p. 3125-31.

77. Kashani, M., Production and Characterisation of Polyhydroxybutyrate by Serratia sp., in Mettalurgy and Materials. 2007, Birmingham Birmingham.

78. Peters, V. and B.H. Rehm, In vivo monitoring of PHA granule formation using GFP-labeled PHA synthases. FEMS Microbiol Lett, 2005. 248(1): p. 93-100.

79. Pouton, C.W. and S. Akhtar, Biosynthetic polyhydroxyalkanoates and their potential in drug delivery. Advanced Drug Delivery Reviews, 1996. 18(2): p. 133-162.

80. Larsen, T. and N.I. Nielsen, Fluorometric determination of beta-hydroxybutyrate in milk and blood plasma. J Dairy Sci, 2005. 88(6): p. 2004-9.

81. Ratledge, C. and B. Kristiansen, Basic Biotechnology (second edition). 2001, Cambridge: Cambridge University Press.

82. Doi, Y., S. Kitamura, and H. Abe, Microbial synthesis and characterization of poly(3-hydroxybutyrate-co-3hydroxyhexanoate). Macromolecules, 1995. 28: p. 4822-4828.

83. Kamnev, A.A., N. Sadovnikova Iu, and L.P. Antoniuk, [Effects of nitrogen deficiency and wheat lectin on the composition and structure of some biopolymers of Azospirillum brasilense Sp245]. Mikrobiologiia, 2008. 77(2): p. 278-81.

84. Cho, K., et al., Utilization of swine waste water as a feedstock for the production of polyhydroxyalkanoates by Aztobacter vinelandii UWD. J Biosci Bioeng, 2001. 91: p. 129-133.

85. Valappil, S.P., et al., Polyhydroxyalkanoate (PHA) biosynthesis from structurally unrelated carbon sources by a newly characterized Bacillus spp. J Biotechnol, 2007. 127(3): p. 475-87.

86. Valappil, S.P., et al., Polyhydroxyalkanoates in Gram-positive bacteria: insights from the genera Bacillus and Streptomyces. Antonie Van Leeuwenhoek, 2007. 91(1): p. 1-17.

87. Loo, C.Y. and K. Sudesh, Biosynthesis and native granule characteristics of poly(3-hydroxybutyrate-co-3-hydroxyvalerate) in Delftia acidovorans. Int J Biol Macromol, 2007. 40(5): p. 466-71.

88. Li, R., H. Zhang, and Q. Qi, The production of polyhydroxyalkanoates in recombinant Escherichia coli. Bioresour Technol, 2007. 98(12): p. 2313-20.

89. Yezza, A., et al., Bioconversion of industrial wastewater and wastewater sludge into Bacillus thuringiensis based biopesticides in pilot fermentor. Bioresour Technol, 2006. 97(15): p. 1850-7.

90. Yezza, A., et al., Production of polyhydroxyalkanoates from methanol by a new methylotrophic bacterium Methylobacterium sp. GW2. Appl Microbiol Biotechnol, 2006. 73(1): p. 211-8.

91. Sujatha, K., A. Mahalakshmi, and R. Shenbagarathai, Molecular characterization of Pseudomonas sp. LDC-5 involved in accumulation of poly 3-hydroxybutyrate and medium-chain-length poly 3-hydroxyalkanoates. Arch Microbiol, 2007. 188(5): p. 451-62.

92. Huisman, G.W., et al., Synthesis of poly-3-hydroxyalkanoates is a common feature of fluorescent pseudomonads. Appl Environ Microbiol, 1989. 55(8): p. 1949-54.

93. Simon-Colin, C., et al., A novel mcl PHA-producing bacterium, Pseudomonas guezennei sp. nov., isolated from a 'kopara' mat located in Rangiroa, an atoll of French Polynesia. J Appl Microbiol, 2008. 104(2): p. 581-6.

94. Simon-Colin, C., et al., A novel mcl-PHA produced on coprah oil by Pseudomonas guezennei biovar. tikehau, isolated from a "kopara" mat of French Polynesia. Int J Biol Macromol, 2008. 43(2): p. 176-81.

95. Volova, T.G., P.V. Mironov, and A.D. Vasil'ev, [Physicochemical properties of multicomponent polyhydroxyalkanoates]. Biofizika, 2007. 52(3): p. 460-5.

96. Kichise, T., et al., Biosynthesis of polyhydroxyalkanoates (PHA) by recombinant Ralstonia eutropha and effects of PHA synthase activity on in vivo PHA biosynthesis. Int J Biol Macromol, 1999. 25(1-3): p. 69-77.

97. Lakshman, K. and T.R. Shamala, Extraction of polyhydroxyalkanoates from Sinorhizobium meliloti cells using Microbispora sp. culture and its enzymes. Enzyme and Microbial Technology, 2006. 39: p. 1471-1475.

98. Sangkharak, K. and P. Prasertsan, Optimization of polyhydroxybutyrate production from a wild type and two mutant strains of Rhodobacter sphaeroides using statistical method. J Biotechnol, 2007. 132(3): p. 331-40.

99. Jau, M.H., et al., Biosynthesis and mobilization of poly(3-hydroxybutyrate) [P(3HB)] by Spirulina platensis. Int J Biol Macromol, 2005. 36(3): p. 144-51.

100. Wong, P.A.L., et al., Investigation of the effects of the types of food waste utilized as carbon source on the molecular weight distributions and thermal properties of polyhydroxy-butyrateproduced by two strains of microorganisms. Materials Research Innovations, 2004. 9: p. 4-5.

101. Chien, C.C., et al., Production of poly-beta-hydroxybutyrate (PHB) by Vibrio spp. isolated from marine environment. J Biotechnol, 2007. 132(3): p. 259-63.

102. Arshad, M.U., et al., Analysis of bacterial strains from contaminated and non-contaminated sites for the production of biopolymers. African Journal of Biotechnology, 2007. 6: p. 1115-1121.

103. Kleerebezem, R. and M.C. van Loosdrecht, Mixed culture biotechnology for bioenergy production. Curr Opin Biotechnol, 2007. 18(3): p. 207-12.

104. Slater, S.C., W.H. Voige, and D.E. Dennis, Cloning and expression in Escherichia coli of the Alcaligenes eutrophus H16 poly-beta-hydroxybutyrate biosynthetic pathway. J Bacteriol, 1988. 170(10): p. 4431-6.

105. Schubert, P., A. Steinbuchel, and H.G. Schlegel, Cloning of the Alcaligenes eutrophus genes for synthesis of poly-beta-hydroxybutyric acid (PHB) and synthesis of PHB in Escherichia coli. J Bacteriol, 1988. 170(12): p. 5837-47.

106. Metabolix, Mirel Bio-Plastic Resins, in Bioplastics Conference Cologne 2007, Diether Hesse: Germany.

107. Schaferjohann, J., R. Bednarski, and B. Bowien, Regulation of CO2 assimilation in Ralstonia eutropha: premature transcription termination within the cbb operon. J Bacteriol, 1996. 178(23): p. 6714-9.

108. Pohlmann, A., et al., Genome sequence of the bioplastic-producing "Knallgas" bacterium Ralstonia eutropha H16. Nat Biotechnol, 2006. 24(10): p. 1257-62.

109. Hejazi, A. and F.R. Falkiner, Serratia marcescens. J Med Microbiol, 1997. 46(11): p. 903-912.

110. Clark, D.P., Molecular Biology: Understanding the Genetic Revolution. 2005, USA: Academic Press. 500.

111. Pompei.R, et al., Use of a novel phosphatase test for simplified identification of species of the tribe Proteeae. J . Clin. Microbiol, 1990. 28(6): p. 1214-8.

112. Jeong, B.C. and L.E. Macaskie, Production of two phosphatases by a Citrobacter sp. grown in batch and continuous culture. Enzyme and Microbial Technology, 1999. 24(3-4): p. 218-224.

113. Thackray, A.C., et al., Bacterial biosynthesis of a calcium phosphate bone-substitute material. Journal of Materials Science-Materials in Medicine, 2004. 15(4): p. 403-406.

114. Thackray, A.C., et al., Bacterial biosynthesis of calcium bone-substitute material. . J Mater Sci Mater Med, 2004. 15: p. 403-406.

115. Yong, P., et al., Synthesis of nanophase hydroxyapatite by a Serratia sp. from waste-water containing inorganic phosphate. Biotechnol Lett, 2004. 26(22): p. 1723-30.

116. Ledo, H.M., et al., Microstructure and composition of biosynthetically synthesised hydroxyapatite. Journal of Materials Science-Materials in Medicine, 2008. 19(11): p. 3419-3427.

117. Ellar, D.J., et al., The internal structure of poly-beta-hydroxybutyrate granules from Bacillus megaterium. J Gen Microbiol, 1968. 50(3): p. Suppl:i-ii.

118. Bonthrone, K.M., et al., Biological and physical chemistry of polyhydroxyalkanoates as seen by NMR spectroscopy. Microbiology reviews, 1992. 103: p. 269-277.

119. Sudesh, K., H. Abe, and Y. Doi, Synthesis, structure and properties of polyhydroxyalkanoates:biological polyesters. Progress in Polymer Science, 2000. 25: p. 1503-1555.

120. **Tian, J., et al., Analysis of transient polyhydroxybutyrate production in Wautersia eutropha H16 by quantitative Western analysis and transmission electron microscopy. J Bacteriol, 2005. 187(11): p. 3825-32.**

121. **Okamura, K. and R.H. Marchessaultm, X-Ray Structure of Poly-b-hydroxybutyrate, in: Conformation of Biopolymers. Academic Press, 1967: p. 709**

122. **Bonthrone, K.M., et al., The biological and physical chemistry of polyalkanoates as seen by NMR spectroscopy. FEMS Microbiol Rev, 1992. 103: p. 269-278.**

123. **Aldor, I.S. and J.D. Keasling, Process design for microbial plastic factories: metabolic engineering of polyhydroxyalkanoates. Curr Opin Biotechnol, 2003. 14(5): p. 475-83.**

124. **MBEL. Production of Chiral Compounds. 2003; Available from: mbel.kaist.ac.kr/lab/research/mcl-phas.htm.**

125. **Leader, E. Bioplastics market to reach 1.2 B ibs by 2010, but improvements needed. 2009 [cited 2010 11/11]; Available from: http://www.environmentalleader.com/2008/11/24/bioplastics-market-to-reach-12-b-lbs-by-2012-but-improvements-needed/.**

126. **Franchetti, S.M. and J.C. Marconato, Biodegradable polymers- A partial way of decreasing the plastic waste. Quimica Nova, 2006. 29: p. 811-816.**

127. **plastics, H.p. Italy set to ban non-biodegradable bags. 2006 [cited 2010 11/11]; Available from: http://www.allbusiness.com/government/government-bodies-offices/8251908-1.html.**

128. **Chronicle, A. San Francisco passes plastic-bag ban. 2007 [cited 2010 11/11]; Available from: http://americanchronicle.com/articles/view/22966.**

129. **CNBC. Consumers Push Plastics Industry to Find Bio-Based Solutions. 2011 [cited 2011 20th April]; Available from: http://www.cnbc.com/id/42194558.**

130. **PaperMate. Biodegradable ballpoint pen. 2011 [cited 2011 20th of April]; Available from: http://papermate.com/pages/products/biodegradable-pens.aspx.**

131. **Packaging, B.I. No Biodegradable, Compostable Packaging for Coca-Cola and Heinz. 2011 [cited 2011 20th of April].**

132. **Cola, C. Brand Fact Sheet. 2011; Available from: http://www.virtualvender.coca-cola.com/ft/index.jsp.**

133. **Basnett, P. and I. Roy, Microbial production of biodegradable polymers and their role in cardiac stent development. Formatex, 2010: p. 8.**

134. **Araujo, M.A., et al., In-vitro degradation behaviour of starch/EVOH biomaterials. Polymer Degradation and Stability, 2001. 73(2): p. 237-244.**

135. **Choi.J and Lee.S.Y, Process analysis and economical evaluation for poly(3-hydroxybutyrate) production from fermentation. . Bioprocess Eng, 1997. 17: p. 335-342.**

136. **Lee, K.M. and D.F. Gilmore, Modeling and optimization of biopolymer (polyhydroxyalkanoates) production from ice cream residue by novel statistical experimental design. Applied Biochemistry and Biotechnology, 2006. 133(2): p. 113-148.**

137. **Koller, M., et al., Production of polyhydroxyalkanoates from agricultural waste and surplus materials. Biomacromolecules, 2005. 6(2): p. 561-565.**

138. **Ojumu, T.V., J. Yu, and B.O. Solomon, Production of polyhydroxyalkanoates,a bacterial biodegradable polymer. Afr J Biotechnol Lett, 2004. 3(1): p. 18-24.**

139. **Galbraikh, L., et al., Modeling of surface modification of sewing thread. Fibre Chemistry, 2005. 37(6): p. 441-446.**

140. **Rebrov, V., et al., Vysokomol. Soedin, 2002. 44(2): p. 347.**

141. **Grage, K., et al., Bacterial polyhydroxyalkanoate granules: biogenesis, structure, and potential use as nano-/micro-beads in biotechnological and biomedical applications. Biomacromolecules, 2009. 10(4): p. 660-9.**

142. **Moldes, C., et al., In vivo immobilization of fusion proteins on bioplastics by the novel tag BioF. Appl Environ Microbiol, 2004. 70(6): p. 3205-12.**

143. **Bucci, D.Z., L.B.B. Tavares, and I. Sell, Biodegradable and physical evaluation of PHB packaging. Polymer testing, 2007. 26: p. 908-915.**

144. **A Bianco, I.C., M Lombardi, L Montanaro and G Gusmano, Thermal Stability and Sintering Behaviour of Hydroxyapatite Nanopowders. Journal of Thermal Analysis and Calorimetry, 2007. 88(1): p. 237-243.**

145. **Nec. A bioplastic with biomass ratio of more than 75%. 2011 [cited 2010 11th November]; Available from: http://www.nec.com/global/environment/featured/bioplastics/index.html.**

146. **Hubbell, J.A., Biomaterials in tissue engineering. Biotechnology (N Y), 1995. 13(6): p. 565-76.**

147. **Barnes, C.P., et al., Nanofiber technology: designing the next generation of tissue engineering scaffolds. Adv Drug Deliv Rev, 2007. 59(14): p. 1413-33.**

148. **Theron, S.A., E. Zussman, and A.L. Yarin, Experimental investigation of the governing parameters in the electrospinning of polymer solutions. Polymer, 2004. 45(6): p. 2017-2030.**

149. Piras, A.M., et al., A new biocompatible nanoparticle delivery system for the release of fibrinolytic drugs. International Journal of Pharmaceutics, 2008. 357(1-2): p. 260-71.

150. Piras, A.M., et al., Polymeric nanoparticles for hemoglobin-based oxygen carriers. Biochimica Et Biophysica Acta, 2008. 1784(10): p. 1454-61.

151. Ramakrishna, S., et al., An Introduction to Electrospinning and Nanofibers. 2005, USA: World Scientific Publishing Co.

152. Ramakrishna, S., et al., Electrospun nanofibers: solving global issues. Materials Today, 2006. 9(3).

153. Doshi, J. and D.H. Reneker, Electrospinning Process and Applications of Electrospun Fibers. Journal of Electrostatics, 1995. 35(2-3): p. 151-160.

154. Agarwal, S., J.H. Wendorff, and A. Greiner, Use of electrospinning technique for biomedical applications. Polymer, 2008. 49(26): p. 5603-5621.

155. Dalton, P.D., et al., Electrospinning of polymer melts: Phenomenological observations. Polymer, 2007. 48(23): p. 6823-6833.

156. Lyons, J., C. Li, and F. Ko, Melt-electrospinning part I: processing parameters and geometric properties. Polymer, 2004. 45(22): p. 7597-7603.

157. Ramakrishna, S. and W.E. Teo, A review on electrospinning design and nanofibre assemblies. Nanotechnology, 2006. 17(14): p. R89-R106.

158. Reneker, D.H. and A.L. Yarin, Electrospinning jets and polymer nanofibers. Polymer, 2008. 49(10): p. 2387-2425.

159. Yarin, A.L., S. Koombhongse, and D.H. Reneker, Taylor cone and jetting from liquid droplets in electrospinning of nanofibers. Journal of Applied Physics, 2001. 90(9): p. 4836-4846.

160. Reneker, D.H. and H. Fong, Polymeric Nanofibers. 2005.

161. Yarin, A.L., S. Koombhongse, and D.H. Reneker, Bending instability in electrospinning of nanofibers. Journal of Applied Physics, 2001. 89(5): p. 3018-3026.

162. Bowlin, G.L., et al., Nanofiber technology: Designing the next generation of tissue engineering scaffolds. Advanced Drug Delivery Reviews, 2007. 59(14): p. 1413-1433.

163. Vaz, C.M., et al., Design of scaffolds for blood vessel tissue engineering using a multi-layering electrospinning technique. Acta Biomaterialia, 2005. 1(5): p. 575-582.

164. Zeng, J., et al., Biodegradable electrospun fibers for drug delivery. J Control Release, 2003. 92(3): p. 227-31.

165. Hsieh, Y.L. and Y. Wang, Immobilization of lipase enzyme in polyvinyl alcohol (PVA) nanofibrous membranes. Journal of Membrane Science, 2008. 309(1-2): p. 73-81.

166. Boland, E.D., et al., Electrospinning of bioresorbable polymers for tissue engineering scaffolds. Polymeric Nanofibers, 2006. 918: p. 188-204.

167. Shishatskaya, E.I., et al., Resorbable polyhydroxyalkanoates as a carrier of anti-tumor drugs. Journal of biotechnology, 2007: p. 131.

168. Naveen, N., et al., Synthesis of Nonwoven Nanofibers by Electrospinning - A Promising Biomaterial for Tissue Engineering and Drug Delivery. Advanced Engineering Materials, 2010. 12(8): p. B380-B387.

169. Sammons, R.L., et al., Characterisation and sintering of nanophase hydroxyapatite synthesised by a species of Serratia. J . Phys:Conference series, 2007(93).

170. Vallet-Regi, M. and J.M. Gonzalez-Calbet, Calcium phosphate as substitution of bone tissues. Progress in Solid State Chemistry, 2004. 32: p. 1-31.

171. Suchanek, W. and M. Yoshimura, Processing and properties of hydroxyapatite-based biomaterials for use as hard tissue replacement implants. Journal of Materials Research, 1998. 13(1): p. 94-117.

172. Kuo, M.C. and S.K. Yen, The process of electrochemical deposited hydroxyapatite coatings on biomedical titanium at room temperature. Materials Science & Engineering C-Biomimetic and Supramolecular Systems, 2002. 20(1-2): p. 153-160.

173. Webster, T.J., et al., Enhanced functions of osteoblasts on nanophase ceramics. Biomaterials, 2000. 21(17): p. 1803-10.

174. Handley-Sidhu, S., et al., Nano-crystalline hydroxyapatite bio-mineral for the treatment of strontium from aqueous solutions. Biotechnol Lett, 2011. 33(1): p. 79-87.

175. Webster, T.J., et al., Enhanced osteoclast-like cell functions on nanophase ceramics. Biomaterials, 2001. 22(11): p. 1327-33.

176. Xu, J.L., et al., Preparation and characterization of nano-sized hydroxyapatite powders produced in a radio frequency (rf) thermal plasma. Materials Science and Engineering a-Structural Materials Properties Microstructure and Processing, 2004. 374(1-2): p. 101-108.

177. Nilen, R.W. and P.W. Richter, The thermal stability of hydroxyapatite in biphasic calcium phosphate ceramics. J Mater Sci Mater Med, 2008. 19(4): p. 1693-702.

178. O. Gauthier, J.-M.B., P. Weiss, J. Bosco, E. Aguado and G. Daculsi, Short-term effects of mineral particle sizes on cellular degradation activity after implantation of injectable calcium phosphate biomaterials and the consequences for bone substitution Bone, 1999. 25(2): p. 71s-74s.

179. Posner, A.S., A. Perloff, and A.F. Diorio, Refinement of the Hydroxyapatite Structure. Acta Crystallographica, 1958. 11(4): p. 308-309.

180. Shi, D.L. and X.J. Wen, eds. Bioactive ceramics: structure, synthesis, and mechanical properties. Introduction to biomaterials, ed. D.L. Shi. 2006, Tsinghua University Press. 16-17.

181. Ikoma, T., et al., Preparation and structure refinement of monoclinic hydroxyapatite. Journal of Solid State Chemistry, 1999. 144(272-276).

182. Arcos, D., J. Rodriguez, and M. Vallet-Regi, Neutron scattering for the study of improved bone implants. Physica B: Condensed Matter, 2004. 350: p. E607-E610.

183. Suda, H., et al., Monoclinic hexagonal phase transition in hydroxyapatite studied by X-ray powder diffraction and differential scanning calorimeter techniques. The Journal of Physical Chemistry, 2002. 99(6752-6754).

184. Kay, M.I., R.A. Young, and A.S. Posner, Crystal Structure of Hydroxyapatite. Nature, 1964. 204: p. 1050-2.

185. Heise, U., J.F. Osborn, and F. Duwe, Hydroxyapatite ceramic as a bone substitute. Int Orthop, 1990. 14(3): p. 329-38.

186. Ioana Baltag , K.W., Haruka Kusakari , Naoyuki Taguchi , Osamu Miyakawa , Masayoshi Kobayashi , Naoko Ito Long-term changes of hydroxyapatite-coated dental implantsJournal of Biomedical Materials Research Part B: Applied Biomaterials 2000. 53(1): p. 76-85.

187. Khairoun, I., et al., Limited compliance of some apatitic calcium phosphate bone cements with clinical requirements. J Mater Sci Mater Med, 1998. 9(11): p. 667-71.

188. Low, D. and M.V. Swain, Mechanical properties of dental investment materials. J Mater Sci Mater Med, 2000. 11(7): p. 399-405.

189. Yeong KCB, W.J., Ng SC, Mechanical synthesis of nanocrystalline hydroxyapatite from CaO and CaHP04. Biomaterials, 2001. 22: p. 2705-2712.

190. Li, J., Structural Characterisation of Apatite-Like Materials, in Metallurgy and Materials. 2009, University of Birmingham: Birmingham.

191. Monmaturapoj, N. and C. Yatongchai, Effect of Sintering on Microstructure and Properties of Hydroxyapatite Produced by Different Synthesizing Methods. Journal of Metals, 2010. 20(2): p. 53-61.

192. Junqueira, L.C. and J. Carneiro, Basic Histology:Text and Atlas. 10th Edition ed, ed. J. Foltin, H. Lebowitz, and P.J. Boyle. 2003: McGraw-Hill Companies.

193. Geesink, R.G., Experimental and clinical experience with hydroxyapatite-coated hip implants. Orthopedics, 1989. 12(9): p. 1239-42.

194. Zhu, S.H., et al., Hydroxyapatite nanoparticles as a novel gene carrier. Journal of nanoparticles as a novel gene carrier, 2004. 6: p. 307-311.

195. Riccio, P., et al., bc1-complex from beef heart, one-step purification by hydroxyapatite chromatography in triton X-100, polypeptide pattern and respiratory chain characteristics. Biochimica et Biophysica Acta (BBA) - Bioenergetics, 1977. 459(2): p. 250-262.

196. Liao, D., et al., Removal of lead(II) from aqueous solutions using carbonate hydroxyapatite extracted from eggshell waste. J Hazard Mater, 2010. 177(1-3): p. 126-30.

197. Mucalo, M.R., et al., The novel use of waste animal bone from New Zealand agricultural sources as a feedstock for forming plasma sprayed hydroxyapatite coatings on biomedical implant materials. J Appl Biomater Biomech, 2004. 2(2): p. 96-104.

198. Zupančiča, M., et al., Critical evaluation of the use of the hydroxyapatite as a stabilizing agent to reduce the mobility of Zn and Ni in sewage sludge amended soils. Waste Managment, 2006. 26(12): p. 1392-1399.

199. Siva Rama Krishna, D., et al., A novel route for synthesis of nanocrystalline hydroxyapatite from eggshell waste. J Mater Sci Mater Med, 2007. 18(9): p. 1735-43.

200. Ryan, J.A., Formation of Chloropyromorphite in a Lead-Contaminated Soil Amended with Hydroxyapatite. Environmental Science Technology, 2001. 35(18): p. 3798-3803.

201. Arey, J.S., J.S. Seaman, and P.M. Bertsch, Immobilization of Uranium in Contaminated Sediments by Hydroxyapatite Addition. Environmental Science, 1999. 33: p. 337-342.

202. Reichert, J. and J.G.P. Binner, An evaluation of hydroxyapatite-based filters for removal of heavy metal ions from aqueous solutions. Journal of Material Science, 1996. 31(5): p. 1231-1241.

203. Handley-Sidhu, S., et al., Removal of Sr2+ and Co2+ into Biogenic Hydroxyapatite: Implications for Biomineral Ion Exchange Synthesis. Environmental Science, 2011.

204. Ozawa, M., K. Satake, and R. Suzuki, Removal of aqueous chromium by fish bone waste originated hydroxyapatite. Journal of Materials Science Letters, 2003. 22(7): p. 513-514.

205. Kahar, P., et al., High yield production of polyhydroxyalkanoates from soybean oil by Ralstonia eutropha and its recombinant strain. Polym Degradation Stab, 2004. 81: p. 79-86.

206. Solaiman, D.K., et al., Conversion of agricultural feedstock and coproducts into poly(hydroxyalkanoates). Appl Microbiol Biotechnol, 2006. 71(6): p. 783-9.

207. Huang, Z.-M., et al., A review on polymer nanofibers by electrospinning and their applications in nanocomposites. Compostes Science and Technology, 2003. 63: p. 2223-2253.

208. Yoshida, H., et al., Disulfide-Crosslinked Electrospun Poly(γ-glutamic acid) Nonwovens as Reduction-Responsive Scaffolds. Macromolecular Bioscience, 2009. 9(6): p. 568–574.

209. Lee, J.S., et al., Role of molecular weight of atactic poly(vinyl alcohol) (pva) in the structure and properties of pva nanofabric prepared by electrospinning. Journal of Applied Polymer Science, 2004. 93: p. 1638-1646.

210. Baji, A., et al., Electrospinning of polymer nanofibers: Effects on oriented morphology, structures and tensile properties. Composites Science and Technology, 2010. 70(5): p. 703-718.

211. Ero-Phillips, O., A. Stamboulis, and M. Jenkins, Tailoring Crystallinity of Electrospun Plla Fibres by Control of Electrospinning Parameters. Polymers, 2012. 4(3): p. 1331-1348.

212. Yong.P, et al., Synthesis of nanophase hydroxyapatite by a Serratia sp. from waste-water containing inorganic phosphate. Biotechnol Lett, 2004. 26(22): p. 1723-30.

213. Macaskie, L.E., et al., A novel non line of-sight method for coating HA onto thesurfaces of support materials by biomineralization. J Biotechnol Lett, 2005(118): p. 187-200.

214. Sombatmankhong, K., et al., Electrospun fiber mats of poly(3-hydroxybutyrate), poly(3-hydroxybutyrate-co-3-hydroxyvalerate), and their blends. Journal of Polymer Science Part B-Polymer Physics, 2006. 44(19): p. 2923-2933.

215. Duan, B., et al., Electrospinning of chitosan solutions in acetic acid with poly(ethylene oxide). J Biomater Sci Polym Ed, 2004. 15(6): p. 797-811.

216. Barham, P.G., et al., Crystallization and morphology of a bacterial thermoplastic: poly-B-hydroxybutyrate. J . Mater. Sci., 1984. 19: p. 2781-2794.

217. Chaijamrus, S. and N. Upday, Production and characterization of polyhydroxybutyrate from molasses and corn steep liquor produced by Bacillus megaterium ATCC 6748. Agricultural Engineering International: the CIGR Ejournal. Manuscript FP 07 030, 2008. X.

218. Macaskie, L.E., et al., A novel non line-of-sight method for coating hydroxyapatite onto the surfaces of support materials by biomineralization. J Biotechnol, 2005. 118(2): p. 187-200.

219. Chen, G.-Q., A microbial polyhydroxyalkanoates (PHA) based bio- and materials industry. Chem Soc Rev, 2009. 38: p. 2434-2446.

220. Chen, G.Q., Production von Poly-D(-)-3-Hydroxybuttersaure und Poly-D(-)-3-hydroxyvaleriansaure mit Einzel und Mischpopulation von Alcaligenes latus DSM 112, 113 bzw.1124. 1989, Graz University of Technology: Graz/Australia.

221. Kim, H.Y., et al., Isolation of glucose utilizing mutants of Alcaligenes eutrophus, its substrate selectivity and accumulation of PHB. Journal of Microbiology, 1995. 22: p. 51-58.

222. Miyake, M., et al., Control of poly beta hydroxybutyrate synthase mediated byacetyl phosphate in cyanobacteria. J.Bacteriol, 1997. 179: p. 5009-5013.

223. Scrutton, M.C. and M.F. Utter, Pyruvate carboxylase. IX. Some properties of the activation by certain acyl derivatives of coenzyme A. J Biol Chem, 1967. 242(8): p. 1723-35.

224. Taidi, B., et al., Effect of carbon source and concentration on the molecular mass of poly (3-hydroxybutyrate) produced by Methylobacterium extorquens and Alcaligenes eutrophus. Appl Microbiol Biotechnol, 1994. 40: p. 786-790.

225. Mergaert, J., et al., Microbial degradation of poly(3-hydroxybutyrate) and poly(3-hydroxybutyrate-co-3-hydroxyvalerate) in soils. Appl Environ Microbiol, 1993. 59(10): p. 3233-8.

226. Waters, B.R., Molecular weight modulation in polyhydroxybutyrate fermentations, in Massachusetts institute of technology. 2007, Texas A&M University: Texas.

227. Handrick, R., et al., The "intracellular" poly(3-hydroxybutyrate) (PHB) depolymerase of Rhodospirillum rubrum is a periplasm-located protein with

specificity for native PHB and with structural similarity to extracellular PHB depolymerases. J Bacteriol, 2004. 186(21): p. 7243-53.

228. Taidi, B., D. Mansfield, and J. Anderson, Turnover of poly(3-hydroxybutyrate) (PHB) and its influence on the molecular mass of the polymer accumulated by Alcaligenes eutrophus during batch culture. FEMS Microbiology Letters, 1995. 129(2-3): p. 201-205.

229. Sung, H.Y. and J.Y. Young, Effect of pH on the Mw of Poly-3-hydroxybutyric Acid Produced by Alcaligenes sp. Biotechnol. Lett, 1995. 17: p. 389-394.

230. Xin, J., et al., An experimental study on molecular weight of poly-3-hydroxybutyrate (PHB) accumulated in Methylosinus trichosporium IMV 3011. African Journal of Biotechnology, 2011. 10(36): p. 7078-7087.

231. Furukawa, T., et al., Structure, dispersibility, and crystallinity of poly(hydroxybutyrate)/poly(L-lactic acid) blends studied by FT-IR microspectroscopy and differential scanning calorimetry. Macromolecules, 2005. 38(15): p. 6445-6454.

232. Barham, P.G., et al., Crystallization and morphology of a bacterial thermoplastic: poly-3-hydroxybutyrate. J . Mater. Sci., 1984(19): p. 2781-2794.

233. Callister, W.D.J., Materials Science and Engineering: An Introduction,. 2003, Hoboken: John Wiley & Sons, Inc.

234. Gunaratne, L.M.W.K., R.A. Shanks, and G. Amarasingheinghe, Thermal History Effects on Crystallisation and Melting of Poly(3-Hydroxybutyrate). Thermochimica Acta, 2004. 423(1-2): p. 127-135.

235. Padermshoke, A., et al., Melting Behavior of Poly(3-Hydroxybutyrate) Investigated by Two Dimensional Infrared Correlation Spectroscopy. spectrochim Acta A, 2005. 61(4): p. 541-550.

236. Porter, M. and J. Yu, Crystallization Kinetics of Poly(3-Hydroxybutyrate) Granules in Different Environmental Conditions. Journal of Biomaterials and Nanobiotechnology, 2011. 2: p. 301-310.

237. Sato, H., et al., Infrared Spectroscopy Studies of CH···O Hydrogen Bondings and Thermal Behavior of Biodegradable Poly(Hydroxyalkanoate). Macromolecules, 2004. 37(19): p. 7203-7213.

238. Barham, P.J., Nucleation Behaviour of Poly-3-Hydroxy-Butyrate. Journal of Material Science, 1984. 19(12): p. 3826-3834.

239. Randriamahefa, S., et al., Fourier transform infrared spectroscopy for screening and quantifying production of PHAs by Pseudomonas grown on sodium octanoate. Biomacromolecules, 2003. 4(4): p. 1092-1097.

240. Palard, M., E. Champion, and S. Foucaud, Synthesis of silicated hydroxyapatite Ca-10(PO4)(6-x)(SiO4)(x)(OH)(2-x). Journal of Solid State Chemistry, 2008. 181(8): p. 1950-1960.

241. Tjahjono, M., et al., Self-association of acetic acid in dilute deuterated chloroform. Wide-range spectral reconstructions and analysis using FTIR spectroscopy, BTEM, and DFT. J Phys Chem A, 2010. 114(46): p. 12168-75.

242. Prakash, K.H., et al., Effect of super saturation level on the size and morphology of hydroxyapatite precipitate. 2006 IEEE Conference on Emerging Technologies - Nanoelectronics, 2006: p. 345-349.

243. Macaskie, L.E., et al., Enzymically mediated bioprecipitation of uranium by a Citrobacter sp. : a concerted role for exocellular lipopolysaccharide and associated phosphatase in biomineral formation. Microbiology, 2000. 146 (Pt 8): p. 1855-67.

244. Patterson, A.L., The Scherrer formula for X-ray particle size determination. Phys Rev, 1939. 56: p. 978-982.

245. Posner, A.S., Crystal Chemistry of Bone Mineral. Physiological Reviews, 1969. 49(4): p. 760-&.

246. Harper, R.A. and A.S. Posner, Measurment of non-crystalline calcium phosphate in bone mineral. Proceedings of the Society for Experimental Biology and Medicine, 1966. 122: p. 137-142.

247. Fathi, M.H. and A. Hanifi, Evaluation and characterisation of nanostructure hydroxyapatite powderprepared by simple sol-gel method. Materials Letters, 2007. 61: p. 3978-3983.

248. Tan, I.K.P., Polyhydroxyalkanoates. Kirk-Othmer Encyclopedia of Chemical Technology. 2003, Malaya: Institute of Biological Sciences.

249. Akiyama, M., T. Tsuge, and Y. Doi, Polymer Degradation and Stability. 2003(80): p. 183.

250. Fernández, D., et al., Agro-industrial oily wastes as substrates for PHA production by the new strain Pseudomonas aeruginosa Effect of culture conditions. bej.2005.04.022. Biochem Eng J, 2005(26): p. 159-167.

251. Beom Soo, K., S. Byung-Seob, and T.H. Ching, Production of Lipase and Oxygenated Fatty Acids from Vegetable Oils. Biocatalysis and Bioenergy, ed. T.H. Ching. 2008, Chungbuk: Wiley.

252. Choi, J.L. and S.Y. Lee, Process analysis and economic evaluation for poly(3-hydroxybutyrate) production by fermentation. Bioprocess Eng, 1997. 17: p. 335-342.

253. Neate, R. Olive oil prices to soar after Spanish drought devastates crop. 2012 [cited 2012.

254. Obruca, S., et al., Production of poly(3-hydroxybutyrate-co-3-hydroxyvalerate) by Cupriavidus necator from waste rapeseed oil using propanol as a precursor of 3-hydroxyvalerate. Biotechnol Lett, 2010. 32(12): p. 1925-32.

255. Megelski, S., et al., Micro- and nanostructured surface morphology on electrospun polymer fibers. Macromolecules, 2002. 35(22): p. 8456-8466.

256. Reneker, D.H., et al., Bending instability of electrically charged liquid jets of polymer solutions in electrospinning. Journal of Applied Physics, 2000. 87: p. 4531.

257. Mit-uppatham, C., M. Nithitanakul, and P. Supaphol, Ultrafine Electrospun Polyamide-6 Fibers: Effect of Solution Condition on Morphology and Average Fiber Diameter. Macromolecular Chemistry and Physics, 2004. 205(17): p. 2327-2338.

258. Gomes, D.S., et al., Characterisation of an electrospinning process using different PAN/DMF concentrations. Polimeros, 2007. 17: p. 206-211.

259. Deitzel, J.M., et al., The effect of processing variables on the morphology of electrospun nanofibers and textiles. Polymer, 2001. 42: p. 261-272.

260. Reneker, D.H., et al., Bending instability of electrically charged liquid jets of polymer solutions in electrospinning. Journal of Applied Physics, 2000. 87(9): p. 4531-4547.

261. Bognitzki, M., et al., Nanostructured fibers via electrospinning. Advanced Materials, 2001. 13(1): p. 70-+.

262. Koombhongse, S., W.X. Liu, and D.H. Reneker, Flat polymer ribbons and other shapes by electrospinning. Journal of Polymer Science Part B-Polymer Physics, 2001. 39(21): p. 2598-2606.

263. Zhang, C., et al., Study on morphology of electrospun poly(vinyl alcohol) mats. European Polymer Journal, 2005. 41: p. 423-432.

264. Kessick, R. and G. Tepper, Microscale polymeric helical structures produced by electrospinning. Applied Physics Letters, 2004. 84(23): p. 4807-4809.

265. Huebner, A.L. and H.N. Chu, Instability and Breakup of Charged Liquid Jets. Journal of Fluid Mechanics, 1971. 49(Sep29): p. 361-&.

266. Roth, D.G. and A.J. Kelly, Analysis of the Disruption of Evaporating Charged Droplets. Ieee Transactions on Industry Applications, 1983. 19(5): p. 771-775.

267. Yong, L., et al., Controlling numbers and sizes of beads in electrospun nanofibers.Polym Int, 2008. 57: p. 632-636.

268. Bergshoef, M.M. and G.J. Vancso, Transparent nanocomposites with ultrathin, electrospun Nylon-4,6 fiber reinforcement. Advanced Materials, 1999. 11(16): p. 1362-1365.

269. Koombhongse, S., W.X. Liu, and D.H. Reneker, Flat polymer ribbons and other shapes by electrospinning. Journal Polymer Science: Part B: Polymer physics, 2001. 39: p. 2598-2606.

270. Yarin, A.L., S. Koombhongse, and D.H. Reneker, Taylor cone and jetting from liquid droplets in electrospinning of nanofibers. Appl Phys, 2001. 89(9)(48): p. 36-46.

271. Shin, Y.M., et al., Electrospinning: A whipping fluid jet generates submicron polymer

fibers. Applied Physics Letters, 2001. 78: p. 1149-1151.

272. Hohman, M.M., et al., Electrospinning and electrically forced jets. I. Stability theory. Physics of Fluids, 2001. 13: p. 2201-2220.

273. Hohman, M.M., et al., Electrospinningand electrically forced jets. II. Applications. Physics of Fluids, 2001. 13: p. 2221-2236.

274. Ndreu, A., et al., Electrospun biodegradable nanofibrous mats for tissue engineering. Nanomedicine (Lond), 2008. 3(1): p. 45-60.

275. Zhao, S., et al., Electrospinning of ethylcyanoethyl cellulose/tetrahydrofuran solutions. Journal of Applied Polym Sci, 2004. 91: p. 242-246.

276. Buchko, C.J., et al., Processing and microstructural characterization of porous biocompatible protein polymer thin films. Polymer, 1999. 40: p. 7397–7407.

277. Megelski, S., et al., Micro- and nanostructured surface morphology on electrospun polymer fibers. Macomolecules, 2002. 35: p. 8456-8466.

278. Ikuo Taniguchi, K.K.a.Y.K., Microbial production of poly(hydroxyalkanoate)s from waste edible oils. Green Chemistry, 2003. 5: p. 545-548.

279. Hyakutake, M., et al., Polyhydroxyalkanoate (PHA) Synthesis by Class IV PHA Synthases Employing Ralstonia eutropha PHB(-)4 as Host Strain. Bioscience Biotechnology and Biochemistry, 2011. 75(8): p. 1615-1617.

280. Wu, Q., Y. Wang, and G. Guo-Qiang, Medical application of microbial biopolyesters polyhydroxyalkanoates. Artificial cells blood substitute and immobilization biotechnology, 2009. 37(1): p. 1-12.

281. Buzarovska, A., et al., Crystallization Behavior of Polyhydroxybutyrate in Model Composites with Kenaf Fibers. Wiley Interscience, 2006.

282. Wang, W., et al., Effective reinforcement in carbon nanotube-polymer composites. Philos Trans R Soc, 2008. 366: p. 1613-1626.

283. Srikar, R., et al., Nanofiber coating of surfaces for intensification of drop or spray impact cooling. International Journal of Heat and Mass Transfer, 2009. 52: p. 5814-5826.

284. Wong, S.C., A. Baji, and S. Leng, Effect of fiber diameter on tensile properties of electrospun poly(epsilon-caprolactone),. Polymer, 2008. 49(21): p. 4713-4722.

285. Gunaratne, L., R. Shanks, and G. Amarasinghe, Thermal history effects on crystallisation and melting of poly(3-hydroxybutyrate) Thermochimica Acta, 2004. 423: p. 127-135.

286. Chen, C., et al., Nonisothermal crystallization and melting behaviour of poly(3-hydroxybutyrate) and maleated poly(3-hydroxybutyrate). European Polymer Journal, 2002. 38: p. 1663-1670.

287. Xu, J., et al., In situ FTIR study on melting and crystallization of polyhydroxyalkanoates. Polymer, 2002. 43: p. 6893-6899.

288. Misra, A.K., et al., Screening of poly-B-hydroxybutyrate-producing microorganisms using Fourier transform infrared spectroscopy. Biotechnology letters, 2000. 22: p. 1217-1219.

289. de Koning, G.J.M. and P.J. Lemstra, Crystallization phenomena in bacterial poly[(R)-3- hyd roxybutyrate]: 2. Embrittlement and rejuvenation. Polymer, 1993. 34(19): p. 4089-4093.

290. Tong, H.W. and M. Wang, An investigation into the influence of electrospinning parameters on the diameter and alignment of poly(hydroxybutyrate-co-hydroxyvalerate) fibers. J Appl Polym Sci, 2011. 120: p. 1694-1706.

291. Ero-Phillips, O., M. Jenkins, and A. Stamboulis, Tailoring Crystallinity of Electrospun Plla Fibres by Control of Electrospinning Parameters. Polymers, 2012. 4: p. 1331-1348.

292. Zhang, Y.Z., et al., Biomimetic and bioactive nanofibrous scaffolds from electrospun composite nanofibers. Int. J. Nanomed, 2007. 2: p. 623-638.

293. Brown, M.R.W. and W.M. Watkins, Low Magnesium and phospholipid content of cell walls of pseudonomas aeruginosa resistant to Polymyxin Nature 1970. 227: p. 1360-1361.

294. Huang, Z.M., et al., A review on polymer nanofibers by electrospinning and their applications in nanocomposites. Composites Science and Technology, 2003. 63: p. 2223–2253.

Appendix